Tecnologías de la Telecomunicación e Ingeniería Computacional

Study and design of electrode arrays of cochlear implants to improve the discrimination of the electrical stimulus

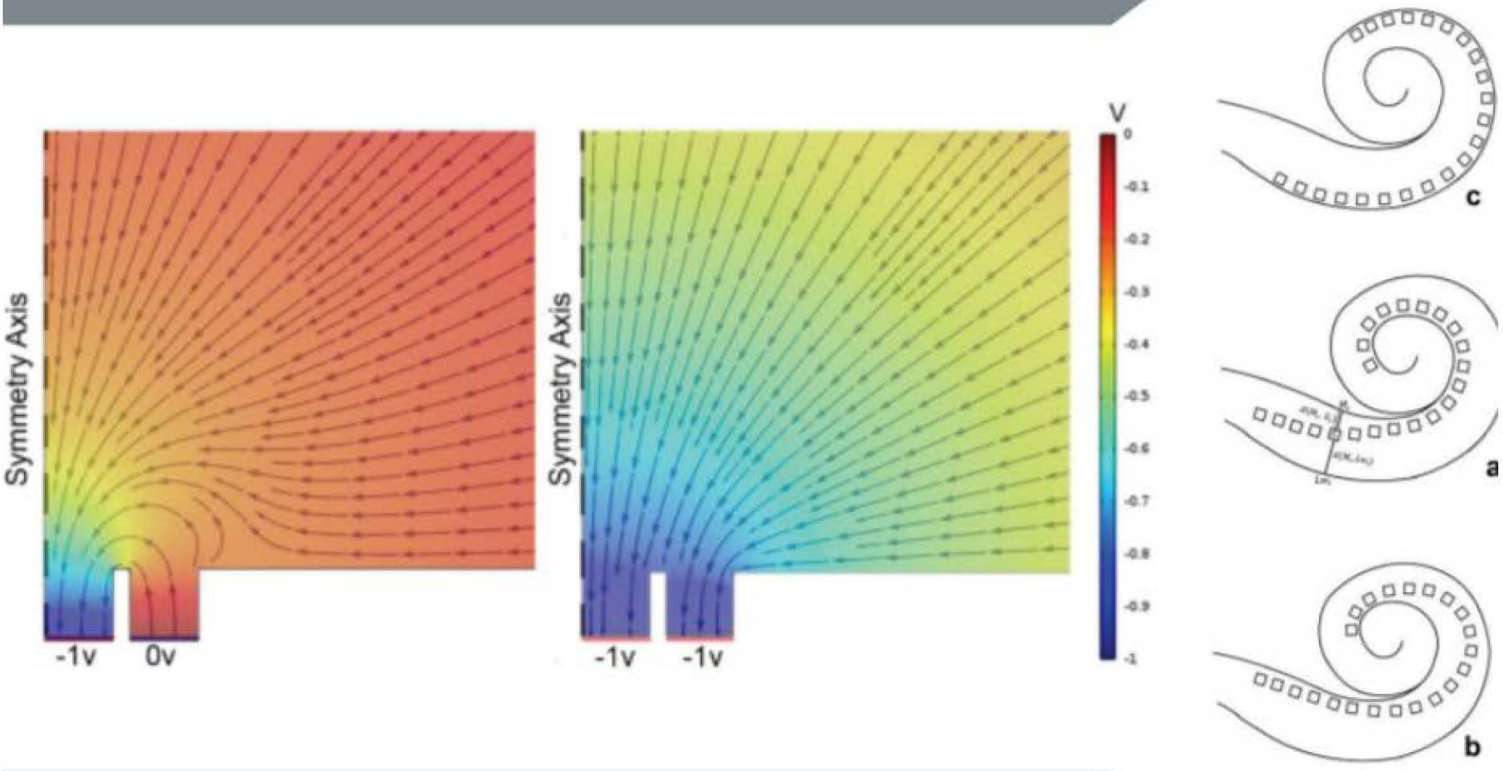

Ángel Ramos de Miguel

PhD Thesis

Discretization and Applications Division

Las Palmas de Gran Canaria . Septiembre 2018

INSTITUTO UNIVERSITARIO SIANI INGENIERÍA COMPUTACIONAL

UNIVERSIDAD DE LAS PALMAS DE GRAN CANARIA

Universidad de Las Palmas de Gran Canaria
Doctorado en Tecnologías de Telecomunicación e Ingeniería Computacional

Study and design of electrode arrays of cochlear implants to improve the discrimination of the electrical stimulus.

Ángel Ramos de Miguel

Directors:
José María Escobar Sánchez
David Juan Greiner Sánchez

Las Palmas de Gran Canaria
4 de Junio de 2018

Agradecimientos

Gracias a mis tutores, José María Escobar y David Greiner por la paciencia, la dedicación y las ganas ante un tema tan multidisciplinar. Han conseguido que fuera posible lo que al principio no parecia tener solución. Ha sido un verdadero placer contar con su ayuda y guía.

Agradecer a todo el personal del Instituto Universitario de Sistemas Inteligentes y Aplicaciones Numericas en la Ingeniería el apoyo recibido en todo momento.

No pueden faltar Juan Carlos Falcón y Silvia Borkoski de la Unidad de Hipoacusia del Complejo Hospitalario Universitario Insular Materno Infantil por todas las horas que le dedicamos a la investigación del oído y el implante coclear que sin ellos todo esto hubiera sido imposible.

Tambien agradecer a todas la personas que han sido claves en mi vida profesional, y por extensión, en la personal. A mis padres por haberme formado y educado como la persona que soy. Son ellos los que han estado siempre para ayudarnos a mirar hacia delante y conseguir cada uno de nuestros objetivos. Mis hermanos que siempre estan a mi lado y a mis amigos por ser como son.

Por último y en especial a mi mujer por estar siempre a mi lado en los buenos y malos ratos y conseguir que todo lo que hago tenga sentido.

¡Gracias! ¡Gracias a todos!

Contents

Chapter 1

Resumen en español

Contents

La cóclea, se encuentra en el oído interno, y es el órgano donde el sonido se transforma en un pulso eléctrico para ser transmitido por las neuronas a la corteza auditiva. El daño de las células ciliadas en la cóclea produce una pérdida auditiva neurosensorial. Dependiendo de la gravedad de la pérdida auditiva, se pueden adoptar diferentes tratamientos para corregirla.

Durante los últimos 40 años se ha utilizado la estimulación eléctrica del nervio auditivo para el tratamiento de la pérdida auditiva severo-profunda de tipo neurosensorial [8].

Los implantes cocleares (IC) modernos se han diseñado para imitar la tonotópica natural de la cóclea mediante el uso de unas guías de electrodos multicanal. Para aprovechar la organización tonotópica de las neuronas de esta cóclea, cada electrodo estimula diferentes subpoblaciones del nervio auditivo (NA) en el oído interno y, por lo tanto, proporciona una percepción psicoacústica diferente. La percepción del tono resultante al estimular esta subpoblación depende de la ubicación del electrodo dentro de la cóclea. El tejido entre los electrodos y el NA produce una propagación de la corriente de estimulación, excitando una amplia población del NA, reduciendo la selectividad, el número de electrodos efectivos y la eficacia de los estímulos eléctricos. En algunos casos, la mejor solución para reducir la interacción entre canales y aumentar la calidad del sonido es desconectar los electrodos problemáticos [35].

En esta tesis se aborda el estudio de la distribución espacial de la corriente de estimulación bajo diferentes posiciones de la guía de electrodos y el diseño de los contactos para optimizar la discriminación de los electrodos.

En la primera sección, se hará una breve introducción sobre la anatomía y la fisiología del oído humano y los principios de funcionamiento de los implantes cocleares multicanal. En el segundo capítulo, se explican los objetivos y el procedimiento seguido. El tercer capítulo es la colección de las tres publicaciones de la tesis. En el cuarto capítulo, se presentarán las conclusiónes obtenidas. Y finalmente, los trabajos futuros que surgen a raíz de los estudios realizados.

1.1 El oído humano

1.1.1 Anatomía

El oído humano es el órgano sensorial del sistema auditivo. Puede convertir la energía de la presión sonora en movimiento mecánico y esto en impulsos nerviosos eléctricos que viajan hasta el cerebro. La capacidad del oído para llevar a cabo este proceso nos permite percibir los detalles de un sonido complejo.

El oído se divide en tres partes principales: oído externo, medio e interno (Figura 1.1). Cada parte tiene una función específica en el proceso de detección de sonido. El primero sirve para recoger el sonido y lo prepara para transferir la energía al oído medio de la manera más

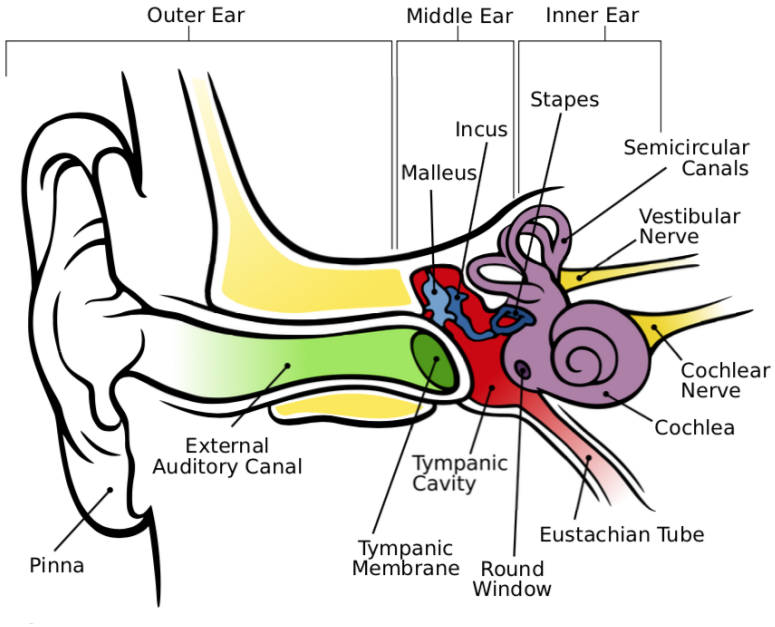

Figure 1.1: Anatomía del oído humano. [6]

eficiente. La segunda parte es responsable de transformar la energía de la onda de sonido en desplazamientos mecánicos de la cadena osicular, lo que crea una onda de compresión dentro del oído interno. El oído interno se encuentra lleno de líquido, lo que hace que las células ciliadas se doblen a medida que se mueven y transforman este desplazamiento mecánico en un pulso neuro-eléctrico para ser transmitido por las neuronas a la corteza auditiva.

Oído externo

El oído externo está compuesto por el pabellón auditivo y el canal auditivo. Su función general es conducir el sonido a la membrana timpánica y actúa como un preamplificador para mejorar la sensibilidad al sonido. [32]

Oído medio

Las partes principales del oído medio son la membrana timpánica y la cadena osicular (martillo, yunque y estribo) que conectan la superficie interna de la membrana timpánica con la membrana de la ventana oval del hueso temporal. Juntos amplifican la onda de sonido y realizan la importante función de igualación de impedancias. Esto mejora la eficiencia de la transferencia de las vibraciones mecánicas de la membrana timpánica (baja impedancia mecánica) a la ventana oval (20 veces mayor impedancia). [27]

La membrana timpánica es una membrana circular de aproximadamente 8-9 mm de diámetro, 0.1 mm de espesor, con un área de 65 a 80 mm^2 y un peso de 14 mg. Tiene una forma cónica y está unida al hueso del martillo. Establece el límite entre el oído externo y el oído medio, actuando como la membrana de un micrófono. Convierte las ondas de presión de aire en vibraciones mecánicas que se transmiten a la cadena osicular.

La cadena osicular funciona como una palanca compuesta que logra una multiplicación de la fuerza entre la membrana timpánica y la ventana oval. Esta cadena transfiere la fuerza proveniente de la membrana timpánica (área efectiva de 65 mm^2) a la ventana oval (área efectiva de 3.2 mm^2), aumentando así la presión con la cual se aplica esta fuerza.

Oído interno

El oído interno consiste en un laberinto óseo, compuesto por el sistema vestibular y la cóclea. La cóclea está compuesta por Scala Vestibuli, Scala Media y Scala Tympani, que están separadas por la membrana de Reissner (entre Scala Vestibuli y Scala Media) y la membrana basilar (entre Scala Media y Scala Tympani), Figura 1.2. En la membrana basilar, se encuentra el órgano de Corti, donde las células ciliadas internas transforman la vibración de la membrana basilar en un estímulo nervioso que se envía a la corteza auditiva a través de la NA.

La cóclea humana es una espiral ovalada con dos vueltas y media con una longitud de aproximadamente 30 mm [36, 23]. El diámetro principal promedio de la cóclea es de alrededor de 7 - 8 mm y el eje menor es de alrededor de 5.5 mm [19]

La cóclea actúa como un filtro mecánico de paso de banda. A esto se le llama organización tonotópica de la cóclea, donde cada parte de la membrana basilar sintoniza a una frecuencia para producir la máxima vibración sobre sí misma, Figure 1.3. Las frecuencias se distribuyen en la cóclea de la siguiente manera: las frecuencias bajas en el apex y las frecuencias altas en la base. En la práctica, se asume que la distribución de las frecuencia sigue la función Greenwood [24], que asigna una frecuencia característica a una fibra nerviosa auditiva (ANF) en función de la posición en la membrana basilar [31].

El estribo contacta con la ventana oval. Al otro lado de la ventana oval encontramos la Scala Vestibuli rellena de perilinfa. El movimiento del estribo produce una vibración de la perilinfa que produce un desplazamiento de la membrana basilar. Cuatro filas de células ciliadas se encuentran en la membrana basilar. Hay dos tipos de células ciliadas: las células ciliadas internas, más cercanas al núcleo central de la cóclea (modiolo) con un abundante nervio aferente que transmite el estímo al cerebro, y las células ciliadas externas que reciben principalmente un suministro de nervio eferente.

Los movimientos de deflexión en las células ciliadas provocan reacciones de hiperpolarización y depolarización en las mismas, que producen la activación de las neuronas ganglionares [40].

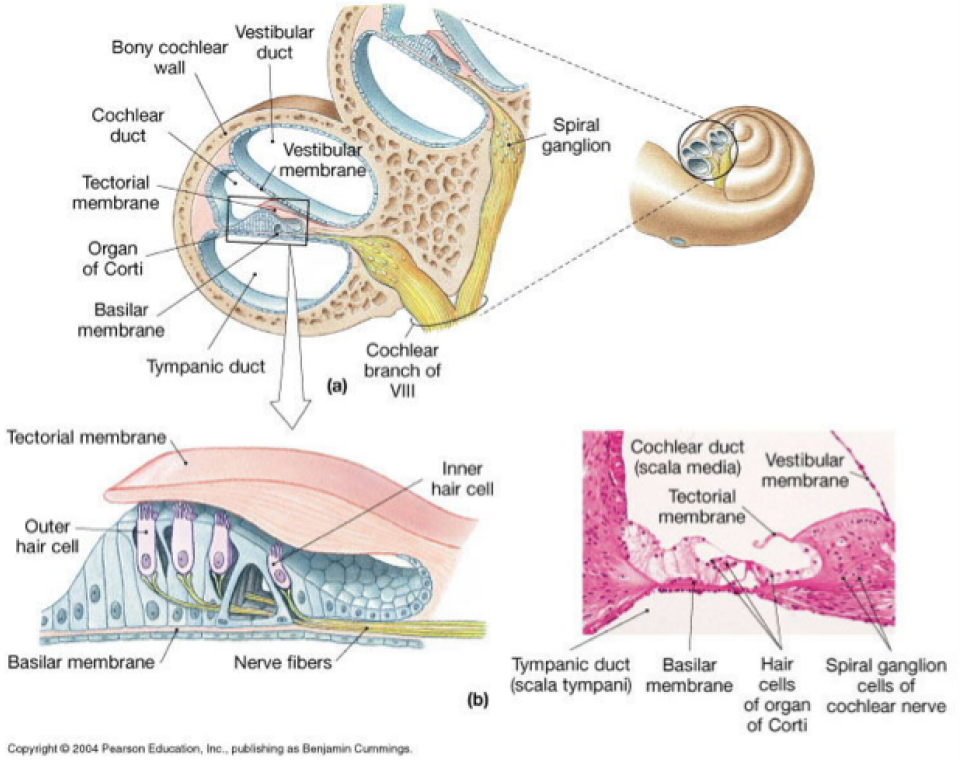

Figure 1.2: Anatomía de la cóclea. a) diagrama de una sección de la cóclea. b) diagrama e histología del órgano de Corti. [34].

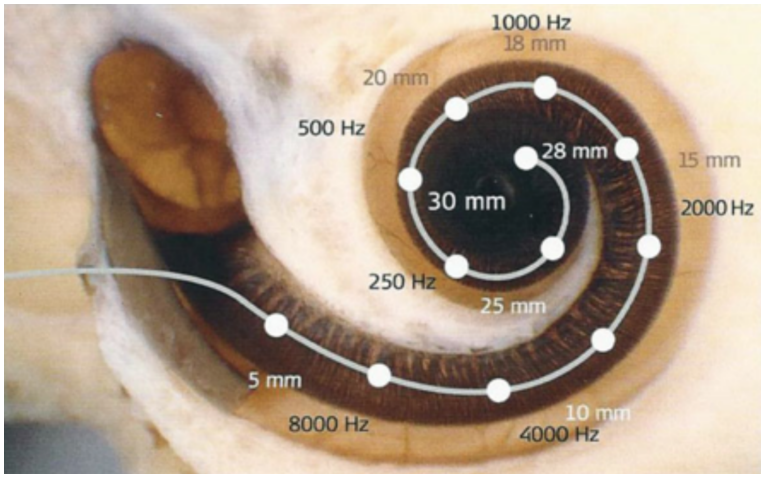

Figure 1.3: Tonotopía del oído interno. [45]

El ganglio espiral está formado por los cuerpos neuronales y que gira a lo largo del modiolo durante aproximadamente dos vueltas [41].

En la cóclea, se extraen los diferentes componentes frecuenciales del sonido. La cóclea usa dos formas de codificar la información de frecuencia: tonotopía y el phase locking.

1.1.2 Tonotopía

George Von Bekesy (ganador del premio Nobel de fisiología y medicina de 1961) describió por primera vez el mecanismo por el cual la cóclea descompone los sonidos complejos en sus componentes frecuenciales. Utilizando cócleas de cadáveres humanos y modelos hidráulicos, demostró que cuando la cóclea era estimulada por una onda de sonido, el movimiento de la membrana basilar era una onda que viajaba desde la base de la cóclea hasta el apex. En su "Teoría de la tonotopía", descubrió que la amplitud de esta onda aumenta con la distancia recorrida, alcanzando una amplitud máxima y luego cayendo rápidamente. El punto de máxima amplitud de la onda que viaja depende de la frecuencia del sonido, Figura 1.4. Este efecto es producido por las propiedades físicas de la membrana basilar. La rigidez, la anchura y la altura de la membrana basilar cambian gradualmente de la base al ápice de la cóclea. Cada punto de la membrana basilar tiene una frecuencia característica asociada que es la que produce el desplazamiento máximo de esta membrana y, por lo tanto, la deflexión máxima de las células ciliadas.

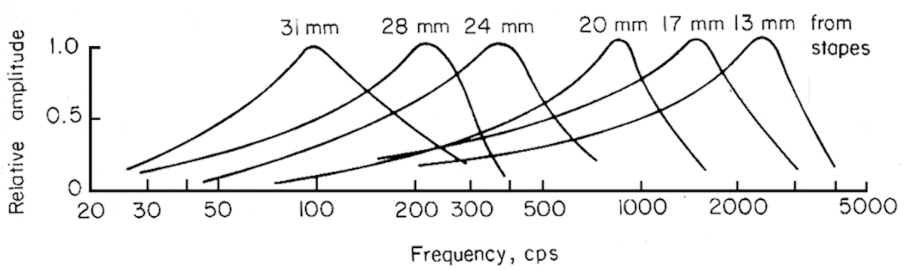

Figure 1.4: Movimiento de la membrana basilar dependiendo de la frecuencia del estímmulo sonoro. [5]

Así, Bekesy llegó a la conclusión de que cada punto de la membrana basilar responde a una determinada frecuencia. En consecuencia, las altas frecuencias se detectan en el extremo basal y las bajas frecuencias en el extremo apical, lo que hace que la cóclea sea un analizador de frecuencia muy eficiente [5]. Como resultado, el sonido de entrada se codifica en las posiciones del ANF activado en la cóclea.

1.1.3 Phase locking

"Phase locking" define la capacidad del ANF para sincronizarse con un estímulo. Para las frecuencias inferiores a 4 kHz se observó que la velocidad de descarga del nervio y el estímulo permanecen en la misma fase [30, 15]. En frecuencias superiores a 4 kHz no se observa esta sincronia. "Phase locking", en combinación con la tonotopía, proporcionan al cerebro información sobre el tono del estímulo [2]. Algunos fabricantes de IC están empezando a hacer uso de esta propiedad para adaptar la tasa de estimulación eléctrica del IC al estímulo.

1.2 Pérdida auditiva

1.2.1 Tipos de pérdidas auditivas

La discapacidad auditiva es una incapacidad parcial o total para oir. Existen tres clases de pérdida de audición: neurosensorial, conductiva o mixta. La pérdida auditiva neurosensorial se produce debido a un problema en el oído interno, particularmente en el funcionamiento de las células ciliadas o el NA. Este daño puede ser producido por varias razones como exposición al ruido, ototoxicidad, genética o envejecimiento entre otros muchos factores.

Por otro lado, la pérdida auditiva conductiva se produce por un mal funcionamiento del oído externo o medio (por ejemplo, procesos inflamatorios, colesteatoma u otoesclerosis) que produce una mala transmisión del sonido a través del oído hacia el órgano sensorial, la cóclea. Este daño produce una reducción de la intensidad del sonido percibido por el paciente.

Finalmente, la pérdida auditiva mixta es una combinación de los dos anteriores, una pérdida conductiva y una pérdida neurosensorial.

1.2.2 Nivel de pérdida auditiva

Otra característica importante de la discapacidad auditiva es el nivel de pérdida auditiva. Este nivel indica el umbral de audición de un paciente. Existen cuatro grados definidos: leve (25-40dB HL), moderado (40-70dB HL), severo (70-90dB HL) y profundo (90-120dB HL).

1.2.3 Tratamiento

La pérdida auditiva conductiva generalmente es reversible quirúrgicamente restaurando el funcionamiento conductivo del oído medio y externo con una mejoría parcial o completa en la audición. Otras alternativas son los audífonos, los sistemas osteointegrados o el implante del oído medio. Los audífonos básicamente amplifican la señal acústica, el implante del oído medio reemplaza la función de la cadena de osicular y los sistemas osteointegrados producen una vibración del hueso temporal que se transmite directamente a la cóclea.

Para la pérdida auditiva neurosensorial, el uso de audífonos depende del grado de deterioro auditivo y también del desempeño del habla del paciente. Es importante considerar que este tipo de pérdida de audición se debe a una pérdida o mal funcionamiento de las células ciliadas o del nervio auditivo. Si el receptor acústico se pierde, no hay posibilidad de estimularlo acústicamente mediante amplificación. El IC está indicado para pacientes que tienen una pérdida auditiva severa profunda en las frecuencias bajas y profundas, en las frecuencias medias y altas en aquellos con un beneficio limitado de amplificación en el reconocimiento de frases en contecto abierto.

Actualmente, las indicaciones para los IC se están ampliando. Varios estudios han demostrado el beneficio del IC en los siguientes casos:

- Audición binaural
  - Sordera unilateral: condición en la cual una persona es candidata para un IC en un oído y no en el oído contralateral [1, 37],
  - Estimulación bimodal: condición en la que una persona es candidata para un IC en un oído y en el oído contralateral necesita un audífono, sistema osteointegrados o implante del oído medio.
  - Implantación bilateral: cuando un paciente tiene una sordera neurosensorial profunda bilateral en ambos oídos.
- Tinnitus es una sensación de sonido sin una fuente de sonido externa. Esta patología tiene un gran impacto en la calidad de vida y es difícil de tratar. Varios estudios han demostrado el beneficio del IC como tratamiento de supresión del tinnitus [1, 37].
- La estimulación electroacústica es una combinación de un IC y un audífono para tratar pacientes con sordera neurosensorial severo-profunda en altas frecuencias y de moderada a grave en bajas frecuencias.

1.3 Implante coclear multi-canal

Hace solo 50 años, no existian tratamientos efectivos para la sordera y pérdidas severas en la audición. El desarrollo del implante coclear (IC) cambió por completo el tratamiento de la patólogía [20].

En 1961, William House, de Los Ángeles, y John Doyle, desarrollaron un electrodo monocanal que colocaron en la ventana redonda en dos pacientes. Estos pacientes refirieron sensacion auditiva, cambios de volumen cuando el nivel de estimulación variaba y, el cambio del tono con la variación en la velocidad de la estimulación [29].

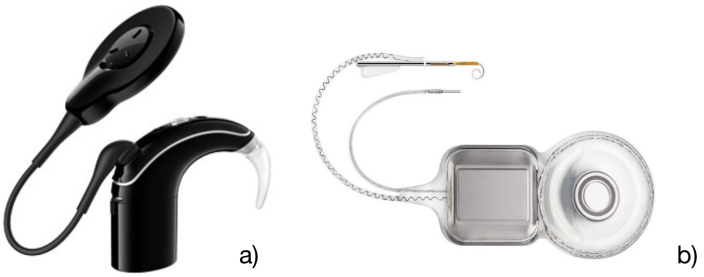

Figure 1.5: Sistema de implante coclear. a) Parte externa del sistema compuesto por la batería, los micrófonos, el procesador y la antena; b) parte interna compuesta por la antena / decodificador y el conjunto de electrodos. Images adapted from Cochlear.

En 1967, Graeme Clark, un profesor de otorrinolaringología de Melbourne, estudió la fisiopatología de la sordera profunda en animales y la tolerabilidad de los materiales implantados. Esto permitió el desarrollo del primer sistema de implante coclear multicanal en 1984, dando lugar a la compañia Cochlear [7].

Al mismo tiempo, en Europa, Kurt Burian, desarrollo en 1975 un dispositivo multicanal. Su trabajo fue continuado por su alumna, Ingeborg Hochmair y su marido Erwin Hochmair, en Innsbruck. Su trabajo culminó en 1982 con el lanzamiento de los implantes MedEl [3].

Estos trabajos previos demostraron la eficacia del sistema de implante coclear para tratar la sordera profunda, y también, que las prótesis multicanal son mejores que los dispositivos monocanales [43].

Los IC modernos están compuestos por dos partes: un procesador de sonido externo portátil y un receptor/estimulador implantado con un conjunto de electrodos intracocleares y extracocleares. Figura 1.5. El procesador de sonido consiste en un micrófono que recoge el sonido; un procesador electrónico digital, que codifica el sonido en impulsos eléctricos y un transmisor de radiofrecuencia, que envía los parámetros de estimulación al receptor/estimulador a través de una bobina transmisora. Esta transmisión se realiza a través de la inductancia (variaciones de campo magnético), que induce pulsos de corriente alterna en la bobina receptora. El receptor/estimulador es un dispositivo electrónico implantado quirúrgicamente. Recibe y decodifica señales del procesador de sonido y genera señales eléctricas para activar selectivamente los electrodos intracocleares. Los pequeños pulsos de corriente eléctrica se envían a estos electrodos para estimular las fibras nerviosas auditivas en el sistema auditivo periférico, causando sensaciones auditivas.

Los IC imitan la codificación tonotópica natural utilizando una guía de electrodos multicanal. Para aprovechar la organización tonotópica de las neuronas de la cóclea, cada electrodo estimula diferentes subpoblaciones del ANF en el oído interno y, por lo tanto, proporciona una percepción

psicoacústica diferente. La percepción del tono se produce al estimular distintas subpoblaciones del ANF en la cóclea. Estudios previos indican que se pueden estimular hasta 7 u 8 electrodos independientes [28, 14, 21, 22]. Esto se debe a la interacción del canal donde la corriente eléctrica se extiende a lo largo de la cóclea, excitando así una amplia población de las ANF y, en consecuencia, disminuyendo la selectividad y el número de electrodos efectivos. En algunos casos, la mejor solución para reducir la interacción del canal y aumentar la calidad del sonido es desconectar algunos electrodos con una interacción de canal alta [35].

Los procesadores del IC filtran la señal entrada en un número de canales de frecuencia contiguos utilizando un banco de filtros de paso de banda. La salida de cada filtro se pasa a través de un detector de envolvente, que consiste en un rectificador de onda completa y un filtro de paso bajo. De esta forma, se obtiene una estimación de la energía para cada banda. El rango dinámico (RD), definida como la amplitud de intensidades que va del umbral auditivo al nivel máximo confortable, se obtiene transformando el RD acústico al RD eléctrico para cada electrodo. Esta transformación es específica para cada paciente y es diferente para cada electrodo. Finalmente, según la tasa de estimulación, el procesador genera impulsos eléctricos que se enviará a cada electrodo en cada instante de tiempo. En la mayoría de las estrategias, los impulsos se generan de tal manera que, en cada momento, solo hay un canal activo, para evitar interacciones entre electrodos.

1.3.1 Inserción quirúrgica

El proceso quirúrgico del implante coclear consiste en hacer una incisión detrás de la oreja, seguido de una mastoidectomía; la cavidad de la mastoidectomía debe permitir la colocacion del electrodo. Luego, siguiendo el canal horizontal y la rama corta del yunque, se visualiza y abre el receso facial. En este punto, el nicho del promontorio y la ventana redonda debe identificarse claramente. Luego, se fresa una cama para el receptor/estimulador en la superficie del hueso temporal y también un canal para la guía del electrodo en la dirección del receso facial.

Dependiendo de la anatomía del paciente, se debe decidir la apertura de la cóclea. Las dos principales opciones son la cocleostomía o la apertura de ventana redonda. En caso de apertura de ventana redonda se garantiza que la inserción del electrodo comienza en Scala Tympani. Si no hay posibilidad de abrir la ventana redonda, se realizará una cocleostomía perforando anteroinferiormente el nicho de la ventana redonda para insertar el implante en la Scala Tympani.

Para terminar, el receptor/estimulador del implante se coloca sobre el lecho previamente perforado y el conjunto de electrodos se inserta manualmente a través de la cocleostomía o la abertura de la ventana redonda, Figure 1.6.

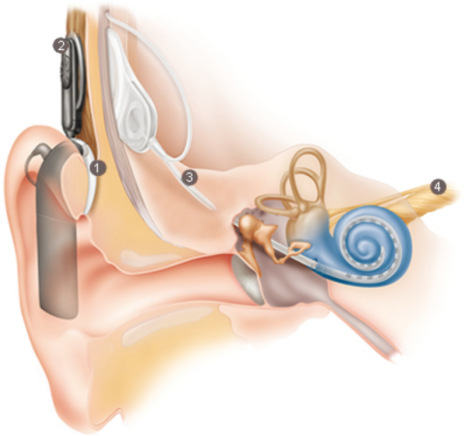

Figure 1.6: Posición del implante coclear después de la cirugía. 1) Procesador externo, 2) Antena, 3) Conjunto de electrodos, 4) Nervio auditivo. Cochlear.

1.3.2 Diseño de guías de electrodos

En la actualidad existen muchos tipos de guías de electrodos, que difieren entre sí en longitud, rigidez, diámetro, número de electrodos, forma del electrodo, forma de la guía de electrodos.

Posición de la guía de electrodos

La posición de la guía de electrodos dentro de Scala Tympani se divide en dos categorías principales: electrodos perimodiolares y rectos. El perimodiolar tiene una forma precurvada para envolver el modiolo de tal manera que, idealmente, los electrodos están tocando la pared del modiolo. Los electrodos rectos se apoyan en la pared lateral del Scala Tympani y, por lo tanto, los electrodos están en la posición más alejada con respecto al modiolo, Figure 1.7.

Longitud y rigidez

La longitud del conjunto de electrodos depende de la fabricación y del modelo de CI. Esta variación se ha creado para abarcar diferentes tamaños de cóclea y para lograr diferentes profundidades de inserción (por ejemplo, inserción parcial para estimulación electroacústica). El rango de longitud de las guías de electrodos disponibles varia de 15 a 31.5 mm

La rigidez del IC depende de dos aspectos principales: el procedimiento de fabricación/material y el uso de estilete. La rigidez del implante se elige según la patología del paciente. Los pacientes con osificaciones (por ejemplo, meningitis) necesitan electrodos más rígidos. Por otro lado, los electrodos flexibles se usan para pacientes con audición residual.

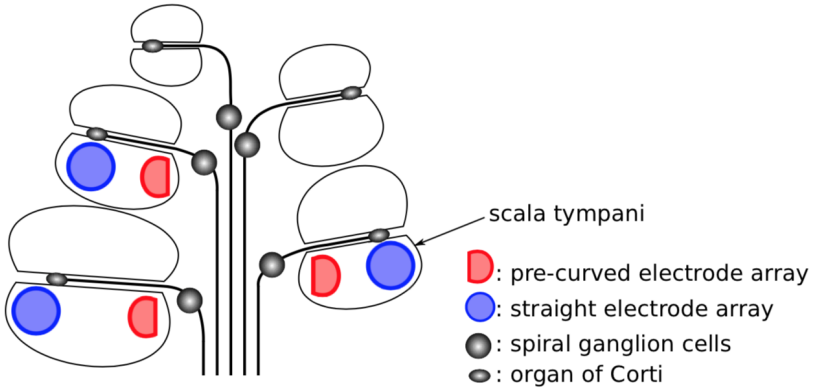

Figure 1.7: Posición de la guía de electrodos en la Scala Tympani [11]

Contactos

Hay dos tipos de contacto de electrodo: media banda y banda completa. Los de media banda cubren la mitad de la guía y los de banda completa cubren la totalidad de la guía, Figure 1.8.

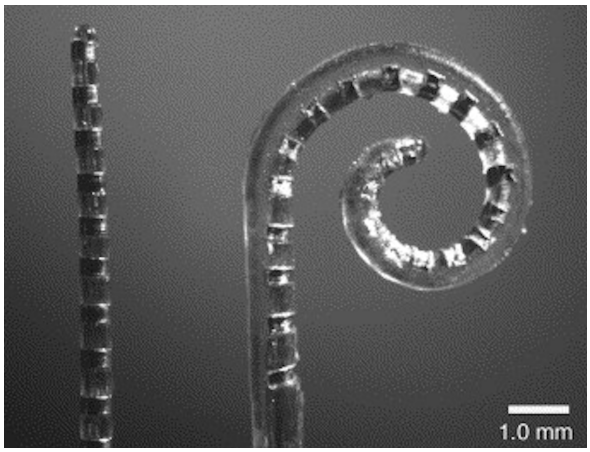

Figure 1.8: Contactos: Izquierda) Electrodos banda completa. Derecha) Electrodos media banda. [44]

Otras guías de electrodos

En algunos casos, cuando hay alguna malformación en la anatomía de la cóclea, no es posible insertar un IC. Para esos casos se plantea:

- El electrodo de guía doble, cuando se ha osificado una parte de la cóclea, Figura 1.9.

Figure 1.9: Electrodo de guía doble. Cochlear

- El implante auditivo del tronco, cuando un paciente no puede utilizar un implante coclear porque la cóclea no es accesible, o no existe o porque el nervio auditivo no existe. Este implante se coloca en el núcleo coclear, Figura 1.10.

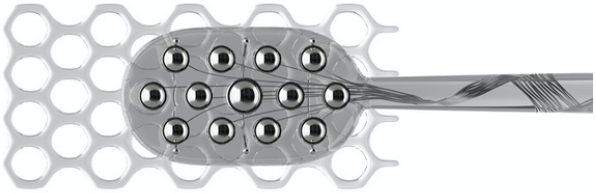

Figure 1.10: Implante auditivo del tronco. Medel

1.3.3 Modos de estimulación

Los IC pueden definir las conexiones internas para proporcionar diferentes modos de estimulación. Esta opción de aumentar la focalización del estímulo para obtener una mejor discriminación de electrodos, lo que ha producido diferentes modos de estimulación.

La estimulación monopolar (MP) es la más utilizada porque es relativamente simple y tiene un rendimiento aceptable en el consumo de energía. En el modo monopolar, la corriente fluye desde un electrodo intracoclear a un electrodo de referencia que es un electrodo extracoclear. El resto de los electrodos no están activos y actúan como un potencial flotante (electrodos aislados). La mejor característica de este modo de estimulación es que alcanza el mismo nivel de activación neuronal con menor intensidad que con otros modos de estimulación [4, 46]. Por otro lado, el costo de esta reducción de potencia conduce a una amplia dispersión de corriente que produce una peor discriminación de electrodos [10], Figura 1.11.

El modo de estimulación bipolar (BP) está diseñado para focalizar la estimulación en un

área estrecha del tejido neural. En este caso el electrodo de referencia no es extracoclear, sino que es un electrodo intracoclear. La elección de ese electrodo de referencia depende de cuán lejos queramos tener el electrodo de referencia, por tanto BP + 1 significa que el electrodo de referencia es el electrodo más cercano al activo y BP + n significa que el electrodo de referencia está n electrodos del electrodo intracoclear activo. En la evaluación de la estimulación bipolar se ha observado un alto consumo y poco beneficio en la focalización del estímulo eléctrico, Figura 1.11. El modo de estimulación multipolar es una generalización de la estimulación bipolar donde tenemos un electrodo intracoclear activo y m electrodos intracocleares como referencia.

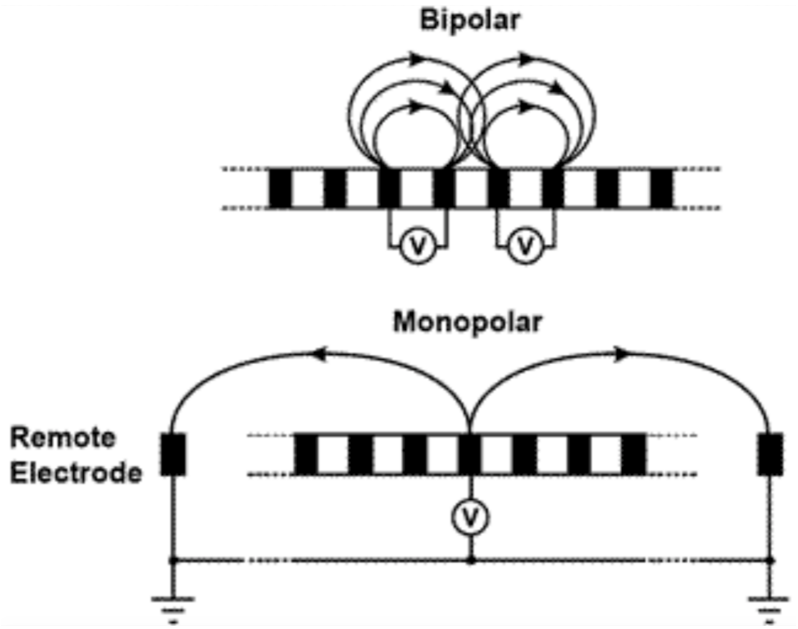

Figure 1.11: Tipos de estimulación. Arriba, estimulación bipolar. Abajo estimulación monopolar. [16]

1.4 Objetivos de la tesis

El primer objetivo es evaluar la mejor posición de un implante coclear en el Scala Tympani, de acuerdo con la discriminación de electrodos. El segundo objetivo es encontrar el mejor contacto para optimizar la focalización y el consumo de energía.

A continuación se describen los objetivos principales de cada publicación y su justificacion de la unidad tematica de tesis.

El primer estudio tiene como objetivo correlacionar la telemetría de respuesta neural (NRT), el umbral electrico (T), la impedancia y la distancia de electrodo a modiolo con la prueba de discriminación de electrodos. Observamos que los electrodos perimodiolares proporcionan beneficios estadísticamente significativos respecto a la posición de los electrodos rectos.

La segunda publicación evalúa la discriminación de electrodos de diferentes tipos de conjuntos de electrodos. Para eso, hemos utilizado una guía de eletrodo lateral (CI522), un electrodo perimodiolar clásico (CI512) y una guía perimodiolar nueva generación (CI532). De este estudio se concluye que la posición perimodiolar es la que ofrece mejores resultados para la discriminación de electrodos y se traduce en mejores resultados de la calidad auditiva.

Atendiendo a los resultados previos, se realizó la tercera publicación para estudiar la forma óptima de los electrodos para lograr la máxima focalización y el consumo mínimo. Para esa propuesta, y basado en nuestra experiencia previa, utilizamos algoritmo genético [9, 26, 12, 13, 25, 42] para la optimización de los electrodos. El potencial electrostático se calcula utilizando el método de elementos finitos (FEM). Debido a que en este problema aparecen fronteras móviles, y después, se deforma la malla FEM, es fundamental aplicar un procedimiento de adaptación de malla para mantener constantes las conectividades de la malla [18, 17].

1.5 Conclusiones

Entre los dos tipos electrodos, perimodiolares y laterales, las características de los electrodos perimodiolares ofrecen un mejor rendimiento en la discriminación de electrodos y un umbral de NRT y niveles T más bajos. Estas mejoras producen un beneficio en la calidad auditiva, la discriminación del habla, la duración de la batería y la calidad de vida.

Otro factor que mejora la discriminación de los electrodos es mantener una distancia constante de los electrodos con respecto al modiolo. Se ha observado que el nuevo electrodo Slim Modiolar CI532 tiene una mejor discriminación de electrodos en comparación con los electrodos perimodiolares previos debido a la mejor colocación de los electrodos.

Por último hemos diseñado un nuevo tipo de electrodo formado por dos anillos conductores separados por un material dieléctrico. Además, hemos desarrollado un procedimiento para optimizar la forma del electrodo propuesto en términos de focalización y consumo, lo que permite la inclusión de más electrodos con la misma interacción entre electrodos. Aumentar la cantidad de electrodos intracocleares podría mejorar la resolución frecuencial y, en consecuencia, la calidad de la audición.

Chapter 2

Introduction

Contents

The cochlea, located in the anterior part of the inner ear, is the organ where the sound, as a pressure wave, is transformed into an electrical pulse to be transmitted by the neurons to the auditory cortex. Damage of the hair cells in the cochlea leads to sensorineural hearing loss. Depending on the severity of the hearing loss, different treatments can be adopted.

Electrical stimulation of the auditory nerve has been used for more than 40 years [8] for the restoration of severe-to-profound hearing loss due to a sensorineural inner ear problem.

Modern cochlear implants (CIs) try to imitate the natural tonotopic encoding by using a multichannel electrode array. To take advantage of this cochlea's tonotopical organization of neurons, each electrode stimulates different subpopulations of the auditory nerve (AN) in the inner ear and, thus, provides a different psycho-acoustic perception. The pitch perception resulting from stimulating this subpopulation depends on the electrode's location in the cochlea. Previous studies indicate that up to 7 or 8 independent electrodes can be stimulated [28, 14, 21, 22]. The diffusive tissue between the electrodes and the AN causes the spread of the stimulation current, exciting a wide population of AN, and reducing the selectivity and the number of effective electrodes and the efficiency of the artificial stimuli. In some cases the best solution to reduce the channel interaction and to increase the sound quality is to disconnect some electrodes with a high channel interaction [35].

This thesis is concerned with the spatial distribution of the stimulation current under different electrode array position and electrode contact design to optimize the electrode discrimination.

In the first section, a brief introduction will be given about the anatomy and physiology of the human ear and the working principles of multi-channel cochlear implants. In the second chapter the objectives and procedure are explained. The third chapter is related to the collection of the three publications of the thesis. In the fourth chapter, the main conclusion will be presented. Finally, the future works that arise from the present work will end the complete research.

2.1 The human ear

2.1.1 Anatomy

The human ear is the sensory organ of the auditory system. It is able to convert energy from sound pressure into mechanical movement and this into electrical nerve impulses that travel all the way to the brain. The ear's ability to carry out this process allows us to perceive the details of a complex sound.

The ear is divided in three main parts: outer, middle and inner ear (Figure 2.1). Each part has a specific function in the process of detection of sound. The first serves to collect the sound and prepares it to transfer the energy to the middle ear in the most efficient way, by matching

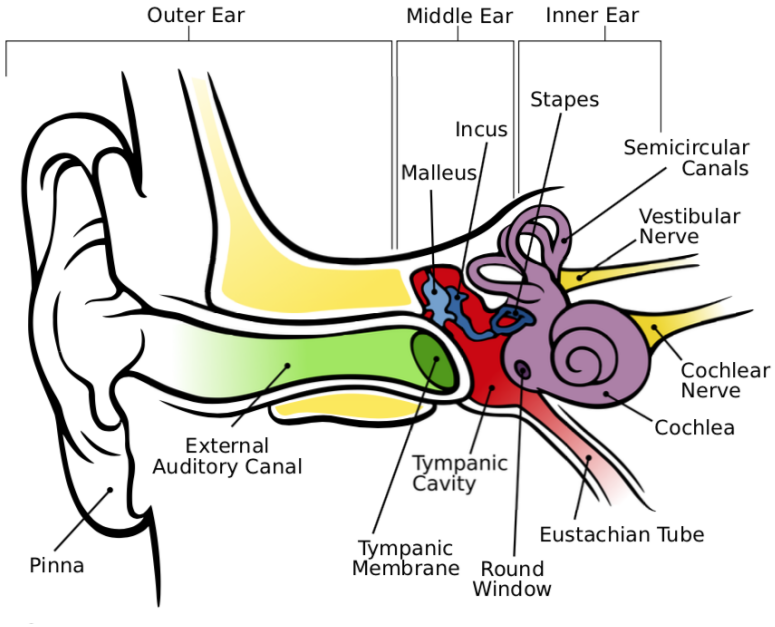

Figure 2.1: Anatomy of the human ear. [6]

air and bone impedance. The second part is responsible for transforming the energy of the sound wave into mechanical displacements of the ossicles, which creates a compressive wave within the inner ear. The inner ear is filled with fluid, which bends hair cells cilia as it moves and transforms this mechanical displacement into neuro-electrical pulse to be transmitted by the neurons to the auditory cortex.

External ear

The outer ear has two main parts: the pinna and the external auditory canal. Its overall function is to conduct the sound to the tympanic membrane and acts as a pre-amplifier to improve the sensitivity of the organ. [32]

Middle ear

The main parts of the middle ear are the tympanic membrane, the tympanic space and the three ossicles (malleus, incus and stapes) that connects the inner surface of the tympanic membrane to the membrane on the oval window of the temporal bone to continue the mechanical vibrations. Together they amplify the sound wave and perform the important function of impedance matching. This improves the efficiency of the transfer of the mechanical vibrations of the tympanic membrane (low mechanical impedance) to the oval window (20 times higher impedance). [27]

The tympanic membrane is a circular membrane of about 8-9 mm in diameter, 0.1 mm in thickness, with an area of 65 to 80 mm^2 and a weight of 14 mg. It has a conical shape and is attached to the malleus. It establishes the boundary between the outer and middle ear, acting just like the membrane of a microphone. It converts the air pressure waves into mechanical vibrations that are transmitted to the ossicles.

Ossicles work like a composite lever that achieves a multiplication of force between the tympanic membrane and the oval window. When these three bones work together in combination with two small muscles, they form the ossicle chain. This chain transfers the force coming from the tympanic membrane (effective area of of 65 mm^2) to the oval window (effective area of 3.2 mm^2), thus increasing the pressure with which this force is applied.

Inner ear

The inner ear consists of a bonny labyrinth, divided into the vestibular system and the cochlea. The cochlea is composed of the Scala Vestibuli, Scala Media and the Scala Tympani , which are separated by the Reissner's membrane (between Scala Vestibuli and Scala Media), and the basilar membrane (between Scala Media and Scala Tympani), Figure 2.2. On the basilar membrane, it is located the organ of Corti, where the inner hair cells transform the vibration of the basilar membrane into a nerve stimulus to be sent to the auditory cortex through the AN, while the external inner ear cells modulate the signal.

The human cochlea is an oval spiral with two and half turns with a length of about 30 mm [36, 23]. The average major diameter of the cochlea is around 7 to 8 mm and the minor axis is around 5.5 mm [19].

The cochlea acts like a mechanical band-pass filter. This is called the tonotopic organization of the cochlea, where each part of the Basilar Membrane is tuned to one frequency to produce the maximum vibration on itself. The frequencies are distributed in the cochlea with the low frequencies on the apex and the high frequencies on the base of the cochlea, Figure 2.3. In practice, it is presumed that the frequency alignment follows the Greenwood function [24], which assigns a characteristic frequency to an auditory nerve fiber (ANF) based on the position of its peripheral tip along the basilar membrane [31].

The stapes is attached to the membrane on the oval window. On the other side of the oval window we found the Scala Vestibuli fill-in with perilymph. The movement of the stapes produce a vibration of the perilymph that produce a displacement of the Basilar Membrane. Four rows of hair cells lie on the Basilar Membrane, together with supporting cells. There are two types of hair cells: inner hair cells, closest to the central core of the cochlea (modiolus) with an abundant nerve afferent carrying messages to the brain. The three outer rows receive mainly an efferent nerve supply. Any natural displacement of the cochlear partition leads into

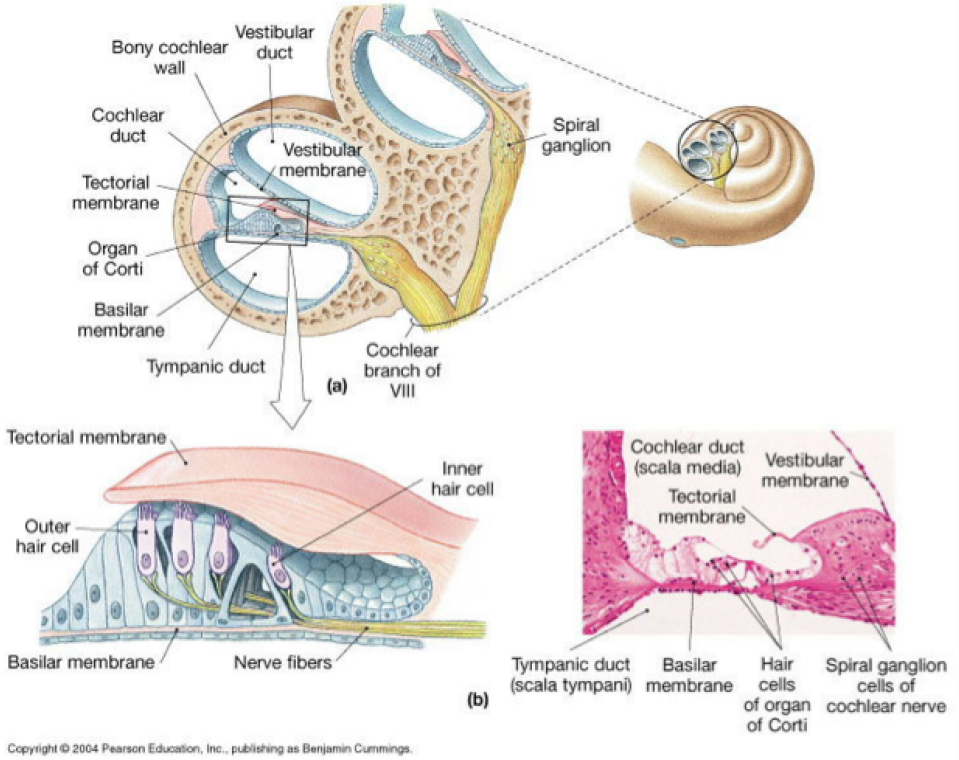

Figure 2.2: Anatomy of the cochlea. a) diagram of a section of the cochlea. b) diagram and histology of the organ of Corti. [34].

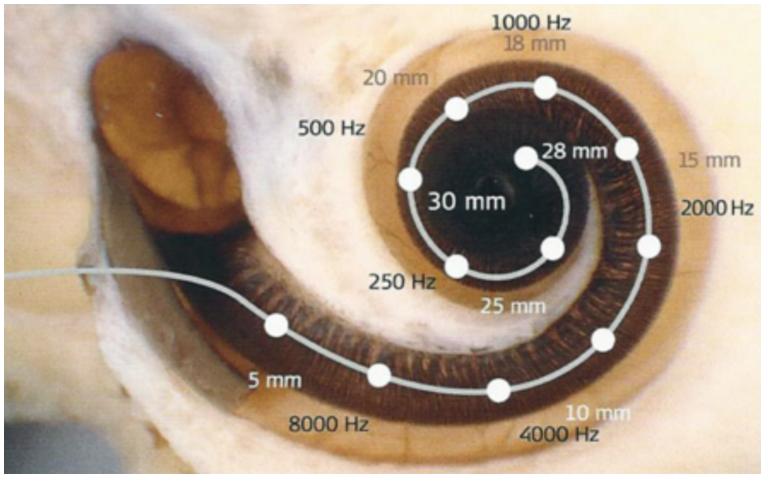

Figure 2.3: Tonotopy organization of the inner ear. [45]

a deflection of the stereocilias of each hair cells. This movement causes depolarization and hyperpolarization of the hair cells and the activation of the attached spiral ganglion neurons [40]. The spiral ganglion is formed by the gathered cell bodies of the neurons, which rotates along the modiolus for about two turns [41].

In the cochlea, different frequency components of the input sound are extracted. Two ways of encoding the frequency information are used by the cochlea: tonotopy and phase locking.

2.1.2 Tonotopy

George Von Békésy (1961 Nobel prize for physiology and medicine) first described the mechanism by which the cochlea breaks down complex sounds into their frequency components. Using cochleae taken from human cadavers and hydraulic models, he demonstrated that when the cochlea was stimulated by a sound wave, the basilar membrane motion was a wave that travelled from the base to the apex of the cochlea. In his "Theory of Location", he discovered that the amplitude of this wave increase with distance travelled, reaching maximum amplitude and afterward rapidly dropping off. The point of maximal amplitude of the travelling wave depended upon the sound frequency, see Figure 2.4. This effect is produced by the physical properties of the basilar membrane. The stiffness, width and height of the basilar membrane gradually change from the base to the apex of the cochlea. Each point of the basilar membrane has an associated characteristic frequency that is the one that produces the maximum displacement of this membrane and, therefore, the maximum deflection of the hair cells.

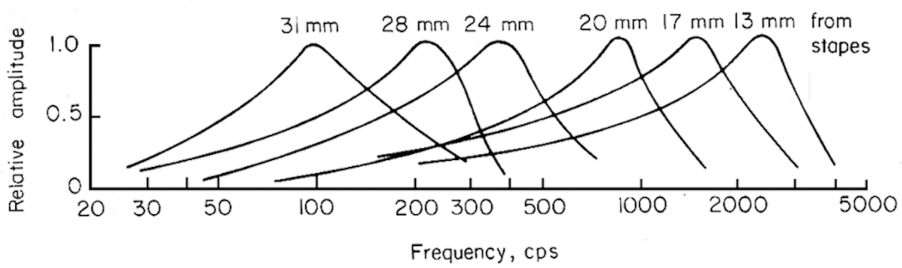

Figure 2.4: Basilar membrane displacement according to sound frequency. [5]

Thus Békésy came to the conclusion that each point of the Basilar Membrane responds to a certain frequency. Consequently, high frequencies are detected in the basal end and the low frequencies in the apical end, making the cochlea a remarkably efficient frequency analyzer [5]. As a result, the input sound is encoded into positions of the activated ANF in the cochlea.

2.1.3 Phase locking

Phase locking refers to the ability of the ANF to synchronize with a stimulus. For frequencies below 4 kHz it was observed how the nerve discharge rate and the stimulus stay in phase [30, 15]. For frequencies above 4 kHz it was observed that the ANF is unable to follow the stimulus. This, in combination with the tonotopy, provides the brain information about the pitch of the stimulus [2]. Some CI manufacturers are starting to make use of this property to adapt the electrical stimulation rate of the CI to the source.

2.2 Hearing Impairment

2.2.1 Types of hearing impairment

Hearing impairment is a partial or total inability to hear. Although it can be partial or complete, exists three classes of hearing loss, according to where the lesion is located: sensorineural, conductive or mixed. Sensorineural hearing loss is produced due to a problem in the inner ear, particularly in the functioning of the hair cells or the AN. This damage can be produced by several reasons like noise expose, ototoxicity, genetics, ageing...

On the other side conductive hearing loss is produce by a malfunction of the outer or middle ear (i.e. inflammatory process, cholesteatoma or otosclerosis) that produce a wrong sound transmission through the ear to the sensory organ, the cochlea. This damage produces a reduction of the sound intensity of the patient.

Finally, mixed hearing loss is a combination of the previous two where some frequencies have a conductive loss and other sensorineural loss.

2.2.2 Degree of hearing impairment

Another important characteristic of the hearing impairment is the degree of hearing loss. This level indicates the audible threshold of a hearing threshold patient. There are four defined degrees: mild (25-40dB HL), moderate (40-70dB HL), severe (70-90dB HL) and profound (90-120dB HL).

2.2.3 Treatment

Conductive hearing loss is generally reversible surgically or medically by restoring the conductive behavior of the outer-middle ear with a complete o partial improvement in hearing. Other alternatives are hearing aids, bone anchorage and middle ear implants. Hearing aids basically amplify the acoustic signal, middle ear implant replace the ossicle chain and bone anchorage systems produce a vibration of the temporal bone that by-pass the outter and middle ear.

For sensorineural hearing loss the use of hearing aids depend on the degree of the hearing impairment and also the speech performance of a patient. It is important to consider that this type of hearing loss is due to a loss or malfunction of hair cells or the auditory nerve. So if the acoustic receptor is lost there is no possibility to stimulate acoustically by amplification. The CI is indicated for patient that have a severe to profound hearing loss in the low frequencies and profound in the mid to high frequencies with a limited benefit from amplification in open set sentence recognition in the ear to be implanted.

Currently, the indications for CIs are expanding. Several studies has demonstrated benefit of CI in the following cases:

- Binaural hearing
  - Single-sided deafness: condition in which a person is candidacy for a CI in one ear and not in the contralateral ear [1, 37],
  - Bimodal stimulation: condition in which a person is candidacy for a CI in one ear and in the contralateral ear is needed a hearing aid, bone anchored system or middle ear implant,
  - Bilateral implantation: when a patient has a bilateral profound sensorineural deafness in both ears.
- Tinnitus is a feeling of sound without an external sound source. This pathology has a big impact in quality of life and is difficult to treat. Several studies have shown benefit of CI as tinnitus-suppression treatment [1, 37].
- Electro-acoustic stimulation is a combination of a CI and a hearing aid to treat patients with sensorineural severe-profound deafness in high frequencies by using a CI and normal-to-severe in low frequencies by using a hearing aid.

2.3 Modern multi-channel cochlear implants

Just 50 years ago, there were no effective treatments for deafness and severe losses in hearing. The development of the cochlear implant (CI) changed that completely [20].

Although is 1957 when the Djourno and Eyries the first to electrically stimulate the inner ear, in 1961, William House, from Los Angeles, and John Doyle, developed the first single-channel electrode that they placed in the round window in two patients. They reported auditory percepts, also noticing the change of loudness when the level of stimulation varied and the change of the pitch with the variation in the rate of the stimulation [29].

In the meantime, in 1967, Graeme Clark, an ENT professor from Melbourne, studied the pathophysiology of profound deafness in animals and the tolerability of implanted materials.

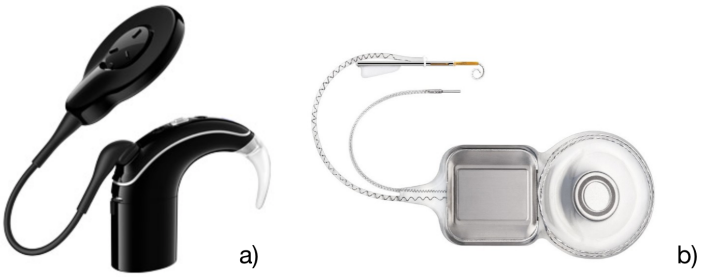

Figure 2.5: Cochlear implant system. a) External part of the system compound by the battery, the microphones, the processor and the antena; b) internal part compound by the antena/decodificator and the electrode array. Images adapted from Cochlear.

The first multichannel cochlear implant system was developed in 1984, giving place to the Cochlear Company [7].

At the same time in Europe, Kurt Burian, launched in 1975 his own research and development of a single-multichannel device. His work was continued by his pupil, Ingeborg Hochmair and her husband Erwin Hochmair, in Innsbruck. Their work culminated in 1982 with the launch of the MedEl implant [3].

This previous works show the efficacy of cochlear implant system to treat profound deafness, and also, that multi-channel prostheses are better than the previous single channel devices [43].

Modern CIs are compound by two parts: a portable external sound processor and an implanted receiver/stimulator with a set of intracochlear and extracochlear electrodes, Figure 2.5. The sound processor consists of a microphone that collects the sound; a digital electronic processor, that encodes the sound into electrical pulses and a radio frequency transmitter, which send the stimulation parameter to the receiver/stimulator through a transmitter coil. This transmission is done through inductance (magnetic field variations), which induces alternating current pulses in the receiver coil. The receiver/stimulator is a surgically implanted electronic device. It receives and decodes signals from the sound processor and generates electrical signals to selectively activate the intracochlear electrodes. Small electric current pulses are sent to these electrodes to stimulate the auditory nerve fibers in the peripheral auditory system, thereby causing auditory sensations.

CIs try to imitate the natural tonotopic encoding by using a multichannel electrode array. To take advantage of this cochlea's tonotopical organization of neurons, each electrode stimulates different subpopulations of the ANF in the inner ear and, thus, provides a different psycho-acoustic perception. The pitch perception resulting from stimulating this subpopulation depends on the electrode's location in the cochlea. Previous studies indicate that up to 7 or 8 independent electrodes can be stimulated [28, 14, 21, 22]. This is due to the channel

interaction where the electrical current spreads out widely along the cochlea, thereby exciting a wide population of ANF and consequently decreasing the selectivity and the number of effective electrodes. In some cases the best solution to reduce the channel interaction and to increase the sound quality is to disconnect some electrodes with a high channel interaction [35].

CI speech processors filters the incoming speech signal into a number of contiguous frequency channels using a bank of bandpass filters. The output of each filter is then passed through an envelope detector, which consists of a full-wave rectifier and low-pass filter. In this way, an estimation of the energy for each band is obtained. The dynamic range (DR), defined as the amplitude of currents that goes from the auditory threshold to the maximum comfortable level, is obtained by transforming the acoustic DR to the electric DR for each electrode. This transformation is specific for each patient and is different for each electrode. Finally, according to the stimulation rate, the processor generates stimulation pulses representing the current level to be sent to each electrode at each time instant. In the majority of strategies, the stimulation pulses are generated in a way such that, at each moment, there is only one channel active, to avoid overlapping sensations caused by adjacent electrodes working at the same time.

2.3.1 Surgical insertion

The surgical approach for a cochlear implant implantation has different steps : 1) retro-auricular extended incision. 2) Mastoidectomy. The mastoidectomy cavity should allow the accommodation of the redundant proximal electrode. 3) Then, following the horizontal canal and short process of the incus the facial recess is visualized and opened but taking care to not expose the facial nerver to avoid facial nerve damage. At this point the promontory and round window niche should be clearly identified. 4) A bed for the receiver/stimulator is drilled on the temporal bone surface and also a channel for the electrode guide in the direction of the facial recess.

Finally, Depending on the patient's anatomy the cochlea opening should be decided. The two main possible options are inferior cochleostomy or round window opening. In case of round window opening we guaranty that the electrode insertion achieved properly the Scala Tympani. If there is no possibility to open the round window a cochleostomy should by done by drilling anteroinferiorly to the round window niche to start in the Scala Tympani.

Finally, all the surgical approach is performed a the implant receiver/stimulator is placed on the previously drilled bed and the electrode array is inserted manually through the cochleostomy or round window opening, Figure 2.6.

2.3.2 Electrode array design

Nowadays exists many types of electrode arrays, they differ from each other in length, stiffness, diameter, number of electrodes, shape of the electrode, electrode array shape.

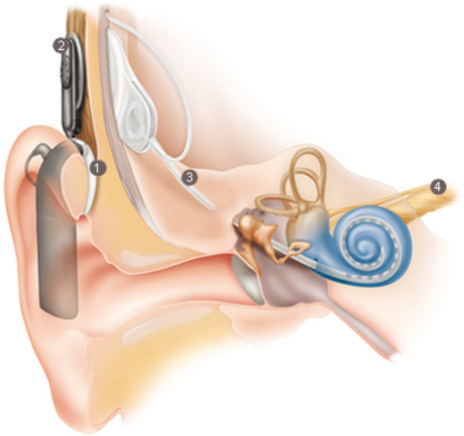

Figure 2.6: Cochlear implant position after surgery. 1) External processor, 2) Antenna, 3) Electrode array, 4) Auditory nerve. Cochlear.

Electrode array position

The electrode array position inside the Scala Tympani is divided in two main categories. These two categories are: perimodiolar and straight electrode arrays. Perimodiolar have a pre-curved shape to wrap the modiolus in such a way that, ideally, the electrodes are touching the modiolar wall. Straight electrodes follows the lateral wall of the Scala Tympani and, therefore, the electrodes are in the farthest position respect to the modiolar wall, Figure 2.7.

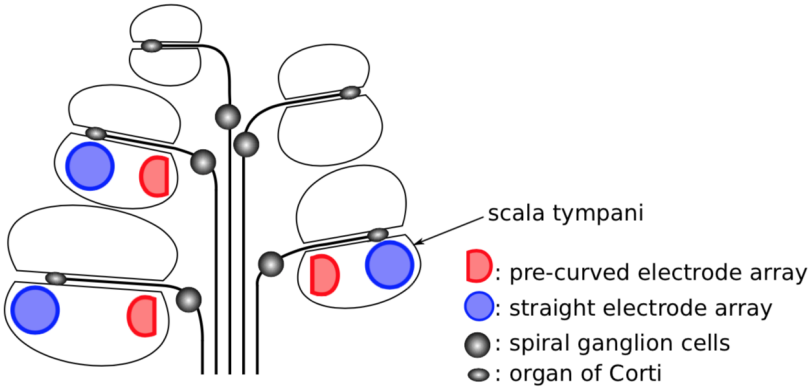

Figure 2.7: Electrode array positions in Scala Tympani [11]

Length and stiffness

The length of the electrode array depends on manufacture and CI model. Thess variations has been created to span different cochlea size and to achieve different deep of insertion (i.e. partial

insertion for electro-acoustic stimulation). The electrode array length range from 15 to 31.5 mm.

The stiffness of the CI depends in to main aspects: the manufacturing/material procedure and the use of stylet. The stiffness of the implant is chosen in terms of the patient's pathology. Patients with ossifications (i.e. meningitis) needs more rigid electrodes. In the other hand, flexible electrodes are used for patient with residual hearing.

Electrode contacts

There are two types of electrode contact, half-banded and full-banded. The half-banded cover one half of the silicone guide and the full-banded cover the totality, Figure 2.8.

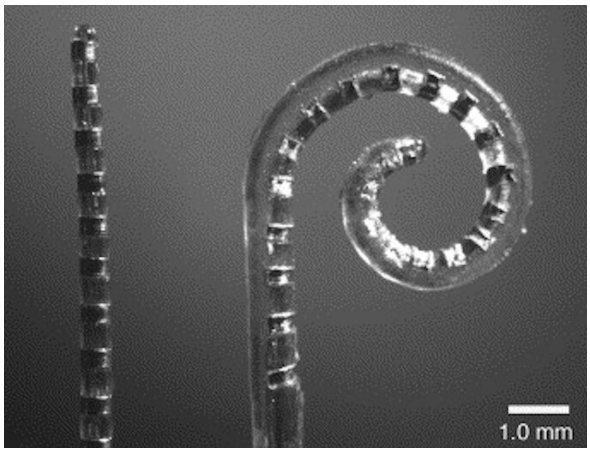

Figure 2.8: Electrode contacts: Left) Full-banded electrodes. Right) Half-banded electrodes [44]

Other electrode arrays

In some cases, when there is some malformation in the cochlea anatomy, it is not possible to insert a CI. For that cases exists some other implants like:

- Double array electrode, when the cochlea is ossified in one part of the cochlea, Figure 2.9.

Figure 2.9: Double array electrode. Cochlear

- Auditory brainstem implant, when a patient cannot make use of a cochlear implant because the cochlea is not accessible or does not exists or because the auditory nerve does not exists. This implant is placed on the cochlear nucleus, Figure 2.10.

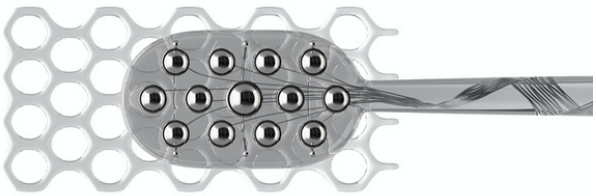

Figure 2.10: Auditory brainstem implant electrode. Medel

2.3.3 Stimulation modes

CIs are able to define the internal connections to provide different modes of stimulation. This option has been study trying to increase the focalization of the stimulus to get better electrode discrimination resulting in different stimulation modes.

Monopolar stimulation (MP) is widely used because is a relative simple stimulation mode and has good performance in power consumption. In monopolar mode the current flows from one intracochlear electrode to a reference electrode, an extracochlear electrode. The entire rest electrodes are non-active and act like floating potentials (isolated electrodes). The best characteristic of this stimulation mode is that reach the same neural activation level with lower intensity compared with other stimulation modes [4, 46]. On the other hand the cost of this power reduction leads to a wide current spread, affecting to the electrode discrimination [10], see Figure 2.11.

Bipolar stimulation mode (BP) is designed to focalize the stimulation in a narrow area of

the neural tissue. For that proposal the reference electrode is not an extracochlear electrode, instead is one of the neighbors electrode. The selection of that reference electrode depends on how far we want to have the reference electrode, so BP+1 means that the reference electrode is closest electrode to the active and BP+n means that the reference electrode is n electrodes far from the active intracochlear electrode. In the evaluation of bipolar stimulation has been observed a high consumption and little benefit in the focalization of the electrical stimulus, see Figure 2.11. Multipolar stimulation mode is a generalization of bipolar stimulation where we have one active intracochlear electrode and m intracochlear electrodes as reference.

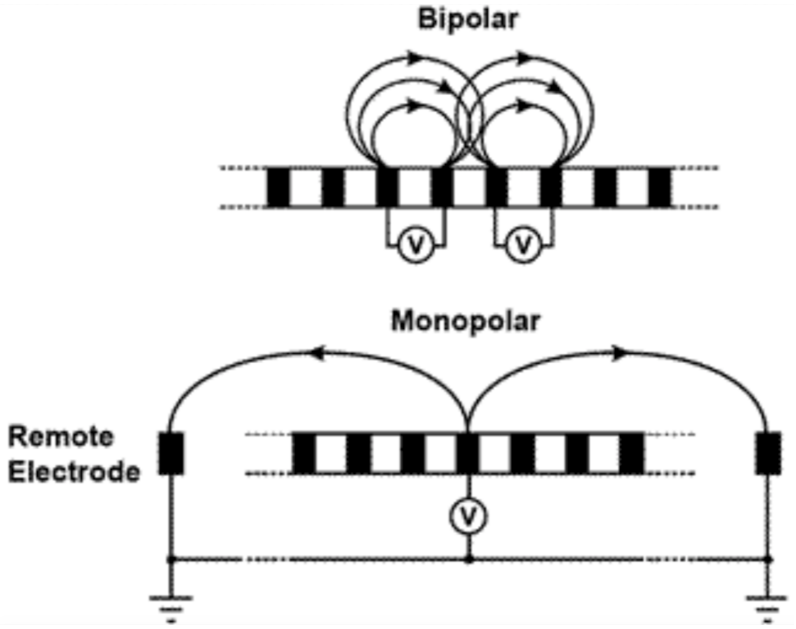

Figure 2.11: Types of stimulation modes. Top, bipolar stimulation mode. Bottom monopolar stimulation mode. [16]

Chapter 3

Objectives of the thesis

The first objective is to evaluate the best position of a cochlear implant in the Scala Tympani, regarding modiolar position, and its relation according to electrode discrimination. The second objective is to find the best electrode contact according to focalization and power consumption.

The first study aims to correlate Neural Response Telemetry (NRT), Threshold level (T), impedance and electrode-to-modiolo distance with the electrode discrimination test. We observe that perimodiolar electrodes provide significant benefits respect to straight electrodes position.

The second publication evaluates the electrode discrimination of different types of electrode arrays. For that proposal, we have used a lateral electrode array (CI522), a classical perimodiolar electrode (CI512) and a new generation of perimodiolar array (CI532). We conclude in this study that perimodiolar position has better outcomes regarding to electrode stimulation.

Attending to the previous results, the next step was to study the optimum shape of the electrodes to achieve the maximum focalization and the minimum consumption. For that proposal, and based in our experience, we use genetic algorithm [9, 26, 12, 13, 25, 42] for the electrode optimization. The electrostatic potential is calculated by using finite element method (FEM). Due this problem involves movable boundaries, and then, a modification of the FEM mesh, is crutial to apply a mesh adaption procedure to keeps constant the conectivities of the mesh [18, 17]. This question is analyzed in the third publication.

Chapter 4

Publications

4.1 First publication

4.1.1 Publication Information

Title: Importance of Perimodiolar Electrode Position for Psychoacoustic Discrimination in Cochlear Implantation.

Authors: Ángel Ramos Macias, Maria Teresa Perez Zaballos, Ángel Ramos de Miguel and Javier Cervera Paz

Journal: Otology & Neurotology

DOI: 10.1097/MAO.0000000000001594

Otology & Neurotology
38:e429–e437 © 2017, Otology & Neurotology, Inc.

Importance of Perimodiolar Electrode Position for Psychoacoustic Discrimination in Cochlear Implantation

*Angel Ramos Macias, †Maria Teresa Perez Zaballos, †Angel Ramos de Miguel, and ‡§Javier Cervera Paz

**Department of Otolaryngology Head Neck Surgery, Las Palmas University Hospital; †Department of Otolaryngology Head Neck Surgery, Psychoacoustic Laboratory, Las Palmas University, Las Palmas; ‡Department of Otolaryngolgy, Navarra University Clinic, Navarra University, Pamplona; and §Department of Statistics, Las Palmas University, Las Palmas, Spain*

Hypothesis: Modiolar proximity of the cochlear implant electrodes and low impedance values have a positive effect on electrical pitch discrimination.
Background: The proximity of the cochlear electrode to the modiolar wall can determine changes in tissue and fluid environment. With the onset of soft-surgery techniques, the trauma caused during surgery has been reduced, minimizing fibrous growth.
Methods: Computed tomography-scan measurements of electrode-inner wall distance and psychoacoustic electrode discrimination tests were done. Neural Response Telemery and impedance data were used in the study.
Results: It was found that patients fitted with perimodiolar arrays have lower impedance values and smaller electrode-inner wall distances than those fitted with straight arrays. These variables were significantly correlated to electrode discrimination. It was found that a closer distance to the modiolus also results in better electrode discrimination.
Conclusion: Perimodiolar electrodes could be a better solution in terms of pitch discrimination both because they are closer to the modiolus and because their impedance is lower. **Key Words:** Cochlear implants—Electrode discrimination—Impedance—Reimplantation.
Otol Neurotol **38:**e429–e437, 2017.

Early diagnosis of hearing loss has become very efficient in many parts of the world. This has led to early implantation in pediatric population, improving their performance making use of their early brain plasticity (1). However, as technology evolves and devices become upgraded, it is very likely that most of this implanted population will require reimplantation. Soft-surgery techniques limit the trauma caused during surgery, thus minimizing fibrous growth (2). It has been shown that, despite these efforts, impedance rises during the first months after surgery and then reaches a stable value (3). Hence, there is a great need to find ways to keep fibrous growth at a minimum to avoid such an increase in impedance.

While short electrodes used in early days of cochlear implantation via round window caused limited insertion trauma, significant intracochlear damage usually occurs at the anterior part of the basal turn when long electrodes are used (4). Insertion of the implant array beyond the so-called ''point of first resistance,'' at the lateral wall of the cochlea, results in a more extensive damage of cochlear structures (5).

In such cases, a characteristic pattern of damage to the lateral cochlear wall and basilar membrane has been identified in the upper basal turn, as well as new bone formation and perielectrode fibrosis. Other studies are now demonstrating an ability to preserve significant residual acoustic hearing with the slim straight cochlear implant (6,7)

Intracochlear fibrosis following cochlear implantation is very common (8). As the area becomes inflamed and healing after surgery occurs, scars develop in the cochlea, forming fibrotic tissue that progressively covers the electrode array (9). Such inflammatory processes may compromise the neural survival (10).

A myriad of pathological lesions have been documented in temporal bones of implanted patients. Intracochlear damage may consist of: 1) osseous lesions, i.e., osteogenesis, spiral lamina fractures, osseous dehiscence at different levels, or osteitis. 2) Membranous lesions, i.e., hydrops, injury to the stria vascularis, or fibrosis. 3) Neural lesions, i.e., necrosis of the organ of Corti, loss of dendrites, loss of neurons or intracochlear neuromas. 4) Infectious lesions, i.e., microabscesses or meningitis. 5) Other miscellaneous lesions (11,12).

It has been suggested that local tissue reaction may alter the normal anatomy and cause deleterious effects on performance after cochlear implantation (13).

Address correspondence and reprint requests to Prof. Angel Ramos Macias, Medicine, Las Palmas University, Las Palmas de gc, Spain; E-mail: angelmanuel.ramos@ulpgc.es
Á.R.d.M. and M.T.P. Z. were supported by a university grant from the Fundación Universitaria de Las Palmas.
The authors disclose no conflicts of interest.
DOI: 10.1097/MAO.0000000000001594

However, while it is true that impedance values are related to cochlear fibrosis, this is not the only reason for differences in impedances. The initial difference in impedance between perimodiolar and slim straight electrodes immediately after implantation (before fibrosis has had a chance to occur) may also be related to electrode distance from the modiolus, as opposed to cochlear trauma.

The cochlear implant electrodes are the boundary between the electrical stimulus and the auditory nerve fibers that need to be stimulated. Therefore, to ensure an optimal stimulation, electrical impedance must be minimized. This parameter depends on electrode surface area; morphological processes and electrochemical processes initiated by electrical stimulation, and is a major factor in power consumption. Moreover, electrode impedance provides an indication of the status of the electrode–tissue interface.

Hence, after surgery, changes in electrode impedance may be expected even before commencement of electrical stimulation, because morphological changes start to occur right after the surgery at the electrode–tissue interface. The formations of scars can reduce the performance of cochlear implants by increasing impedance, which raises the threshold stimulation required for sound perception and hence implant energy consumption (14).

To minimize this effect, SS techniques have been developed. These allow gentle insertion of the cochlear electrode array, and also reduce trauma to the remaining hair cells and neural tissue (2,15).

Unfortunately, no technique is able to evaluate with accuracy the extent of cochlear fibrosis, because of imaging artifacts caused by the presence of the electrode array. Therefore, measurements of electrode impedance are used as an indication of fibrotic scar tissue within the cochlea, although it is not the only factor to be considered (16).

This was followed by periods of long-term stability. Ni et al. (17) showed a steady increase in the electrical impedance over the first month postimplantation in chronically implanted, predeafened cats. Electrode impedance correlated with the degree of tissue growth observed within the scala tympani. Therefore, electrode impedance seems to be primarily related to the resistive characteristics of the fluid and tissue surrounding the electrodes (18). A study by van Wermeskerken et al. (19) demonstrated that during a period without stimulation, there is a larger increase in impedance, probably due to fibrous tissue growth. This phenomenon was more pronounced for the straight electrode arrays tested. The authors postulated that a larger tissue growth might be expected for the straight electrode because a larger volume of fluid surrounds it.

The proximity of the electrode to the modiolar wall may result in some variation in the tissue and fluid environment, and it is of interest to investigate the effect of modiolar proximity and measured impedance on pitch discrimination. The present study aims to establish the relation between these variables and establish whether perimodiolar electrode positions (not to be automatically understood as perimodiolar arrays) provide statistically significant benefits regarding improved pitch discrimination and low impedances.

Since there is a correlation between performance and electrode discrimination, it seems reasonable to suggest that fibrosis will be a factor affecting impedances. However, there has to be a connection to pitch discrimination and why it may be beneficial to deactivate electrodes in case of poor pitch discrimination (20–23).

SUBJECTS AND METHODS

Subjects

The sample comprised 10 cochlear implant recipients: 5 of them using a Cochlear Nucleus CI 422 slim straight electrode array, and 5 using Cochlear Nucleus CI 24RE contour advance (CA) perimodiolar electrode array. Of these, two were women and eight were men. The age range was 36 to 77. They were all patients of the Department of Otolaryngology, University Hospital of Las Palmas de Gran Canaria, Spain, between December 2014 and December 2015 (Table 1).

The patients met the following inclusion criteria: they were adults (older than 18); diagnosed with severe-profound postlingual progressive bilateral hearing loss (Average Pure Tone Audiometry thresholds greater than 70 dB) and unknown aetiology; they did not suffer from retrocochlear conditions, nor central auditory processing disorders. Surgery proceeded

TABLE 1. *Demographic data*

Patient	Sex	Age (yr)	Use of Implant (mo)	Duration of Profound Deafness (yr)	Electrode Array	Speech Perception (Sentences) (%)
1	Male	40	150	15	NucCI 24RE (CA)	84
2	Male	33	74	1	Nucleus CI 24RE (CA)	80
3	Male	36	72	1	Nucleus CI 24RE (CA)	84
4	Male	30	95	1	Nucleus CI 24RE (CA)	80
5	Female	38	64	5	Nucleus CI 422 slim straight	76
6	Male	33	25	1	Nucleus CI 422 slim straight	80
7	Female	22	25	5	Nucleus CI 422 slim straight	64
8	Male	11	28	3	Nucleus CI 422 slim straight	80
9	Male	48	39	1	Nucleus CI 24RE (CA)	68
10	Male	23	36	4	Nucleus CI 422 slim straight	72

without complications, and all had complete electrode insertion in all patients an Inferior Enlarged Round Window approach was used without Scala Vestibuli dislocations. The correct location was checked using Cone Beam CT (MiniCat IQ, Xoran Technologies LLC, Ann Arbor, MI); they had a stable map with 900 pps stimulation rate and 25 us pulse; a minimum of 6 months of use of their sound processor and a minimum of 18 operational channels; 50% or more of speech understanding for sentence tests in silence without lip-reading using the CI at 65 dB HL.

All subjects signed an informed consent prior to the commencement of the study. The study was approved by the Ethics Committee of our center.

Methods

The psychoacoustic study was done using a Psycoachoustic Research Platform designed in our Department. It was designed using the Nucleus Implant Communicator library for Python (Python Software Foundation, v2.3). Nucleus Implant Communicator is a research tool developed by Cochlear LTD and allows researchers to build applications to control the electrical stimuli delivered by the intracochlear electrodes of Nucleus Cochlear implants. The researcher and patient interfaces were designed using Visual Studio (Microsoft Corp. Visual Studio Community 2013) and the stimulation scripts were built in Python to control the implant receiver/transmitter by sending instructions to a supplied cochlear implant research sound processor. The supplied processor was connected to a computer via a USB port.

The subjects were instructed on what to do before commencement of each stage of the experiment, each of which took one session to complete. In turn, each session took place once a week during a 1-month period. First, C and T levels were determined for the stimuli created for this experiment. Then the electrodes were loudness balanced and, finally, an alternative forced choice experiment was completed.

Stimulus Characteristics

To minimize the effect of adaptation and learning as an obscuring factor in electrical pitch discrimination, the stimulus parameters were set so that they were those used by patients in their standard, daily maps. Accordingly, the stimulation rate used for this test was 900 pps; the pulse width was 25 us, the phase gap was 8 us and the stimulation mode was MP1+2 (meaning that both the reference electrode in the mastoid and the one embedded in the internal receiver/transmitter were used). If such parameters had been changed, the speed at which each individual adapts to a new way of stimulation could have played a major role in electrode discrimination, thus hindering the effects sought out in this experiment.

Step 0: Selection of Electrodes to Be Used

All active electrodes were used to get the data from the largest possible number of samples. Despite belonging to a perimodiolar array, some contacts were actually as far removed from the modiolus as straight ones. Those at the basal end of the cochlea might be far away because of the insertion region (cochleostomy) being at a certain distance from the modiolus. At the other end, the diameter of the Scala Vestibuli is reduced, so that it might cause both perimodiolar and lateral wall electrodes to be positioned at very similar distances to the modiolus. It is therefore interesting to contrast psychoacoustic results with the position of each electrode by means of computed tomography (CT) imaging instead of automatically classifying them as perimodiolar or lateral wall type electrodes according to the company array specifications. In all patients the same surgical cochlear approach was used (Enlarged Round Window approach).

Step 1: Determination of C and T Levels

Threshold levels for each electrode were determined using the stimuli described in step 0. The method for obtaining these levels is the classical ascending and descending methods of limits. Stimuli are sent in increasing order below threshold T until this becomes audible, at which point the same operation is performed in reverse, starting above the threshold until the patient reports no sound perception. For C levels, the one-sided method of limits is used, increasing the stimulus until it reaches the maximum comfortable level for the patient.

This procedure takes one session split into two to three parts, each lasting around 30 minutes with 10 to 15 minute breaks in between and a total test duration of 2 hours.

The tests start at the apical-most electrode and move toward the most basal one. Sometimes, when middle electrodes are reached, the first electrodes are retested if they gave anomalously small dynamic ranges, as patients tend to be scared by intense high pitch sounds first, but grow more confident after a few tests, when they realize that it is not an uncomfortable procedure.

Step 2: Loudness Balance of All Electrodes

The loudness of the electrodes was balanced to minimize interference effects. It has been shown that for a given electrode, a difference in volume can cause the illusion of a difference in electrical pitch. To avoid this, each electrode must be adjusted to sound as intense as their neighbors. A Bekesy tracking approach was used (24), which has a good compromise between speed and accuracy, given the large number of electrode samples used in this test.

The process always starts in the center of the electrode (electrode 11). This first electrode acts as the starting point. The software sets the reference electrode to an always start at a loudness level corresponding to 25% of dynamic range. Then, the neighbor is initially assigned a value of 10% above or below this level at random. The patient listened to the two sounds sequentially with a 1 second space between stimuli and indicated which sound was louder (1st or 2nd). The response was recorded using the buttons on a purpose-designed interface to lower or raise the signal electrode by one current level (Cochlear's current measuring units, CL) until the patient perceived them as equally strong. At this point, the same sound was replayed to double check and then the test was reset, but starting with the opposite situation. That is, if the target electrode had started 10% above 25%, this time it began below 10%. The equal loudness point was set as the average of both approaches. Subsequently, the target electrode served as the reference electrode for the next adjacent electrode. The same procedure was repeated until the apical end was reached and then the process started again from electrode 11 toward the basal end of the array.

The balance was set between the closest electrode pair for two reasons: 1) discrimination is most difficult at this spatial distance than any other, so their stimuli need to be as similarly intense as possible and 2) because the patients reported great difficulties and even inability to establish equal loudness between two very different electrical pitches while doing a pilot a study.

Step 3: Test Electrode Discrimination

Electrode discrimination was measured using the three-alternative-forced-choice method. After selecting the central

(reference) electrode and its two nearest neighbors on either side (signals), the number of times that each electrode was tested with the central electrode was set to three. Three electrical stimuli were sent to the implant, two of which come from the same electrode (reference) and one from the signal electrode. They were presented in random order with a 1 second gap between stimuli. The patient had to indicate the stimulus that sounded different from the other two.

The patients were presented one practise test (patients practise with a sequence of stimuli). After all the electrodes have been tested with the reference, the test is over and the researcher has to select the apical, most adjacent electrode as reference and select its two nearest neighbors on either side again. The process is repeated until all electrodes have acted as references and have been tested. This way all electrodes will be tested against four nearest neighbors, except for the apical and basal most electrodes, which can only be tested to one side and the ones before these, because they will have two electrodes on one side but only one on the other.

The results are given as percentage of correct answers.

Distance Measuring

A high-resolution cochlear imaging analysis was developed by transferring the ConeBeamCT scan data into a two-dimensional representation of the geometry. For this purpose, custom-made software was developed using MATLAB (R2008b, MathWorks, Natick, MA). To measure electrode distance to the inner wall, a script was designed to extract the inner wall and the electrode array curves and measure the distance between them at each point of the array. The inputs are two images: one was configured to observe only the electrode array and the second to analyze only the bony part of the Cochlea.

Once the images have been imported, a number of points following the inner contour of the implant are marked in the first image. After loading the points, the system generates a parametric function using the interelectrode distance to interpolate the positions of the 22 electrodes. Then a similar procedure is used to extract the inner-wall curve in the second image.

Once both the functions are generated, the distance of each electrode is calculated as the closest line between the electrode and the inner wall.

Data Analysis

Analysis of the variables under study was done using SPSS (v16) and eViews. First, descriptive statistics for the endogenous and all exogenous variables were done. Then a binomial logit model was calculated to study the correlation between the variable and its predictors.

The main shortcoming of a linear model is that its marginal effect is constant. Hence, whatever the distance of the electrode to the inner wall, a unitary increase of this distance always produces the same effect on the success rate, while in reality, as an electrode approaches 0, the increase in success rate must reach a plateau in order not to have physically unrealistic results above 1. To solve these problems, Berkson (25) proposed in 1953 the Logit Model.

This method takes the logit transformation of the endogenous variable and models it as a linear function of the predicting variable. The estimation is done using weighted least squares as follows:

$$\ln\left(\frac{p_i}{1-p_i}\right) = \beta_0 + \beta_1 x_{1i} + \beta_2 x_{2i} + \cdots + \beta_k x_{ki} + u_i \quad (1)$$

where pi is the success rate; $\{x_1,\ldots,x_k\}$ are the set of predicting variables; u_i is the random perturbation; β_i are the parameters of the model that quantify the effect of each one of the predictive variables on the success rate and I relates to each of the sampling units (patient-electrode). This transformation of the variable of interest ensures that the estimated values of the success rate are always in the interval [0.1]. Heterocedasticity problems were solved using weighted least squares (Pond2):

$$\text{Pond2} = \sqrt{N_i \cdot p_i(1-p_i)} \quad (2)$$

In the logit binomial model, the fact that the variable of interest is binomial is taken into account, while keeping the Logit transformation. Hence, the interpretation of the parameters of the model is similar to the earlier model. When working with a binomial distribution, the existence of heteroscedasticity is already considered in the inference process, which in this case is done using maximum likelihood estimation, using iterative procedures. Despite this, it incorporates the robust estimation of the variance–covariance matrix of disturbance and correction for overdispersion.

To interpret this model, the concepts of ODD and ODD ratio are often used. The ODD is the ratio between the probability of guessing right and the probability of failing for a combination of predictors.

$$ODD_0 = p_0/(1-p_0) \quad (3)$$

For two individuals, 0 and 1, the ratio of their ODDs for a variable x_i can be demonstrated to be

$$\frac{ODD_1}{ODD_0} = e^{\beta} \quad (4)$$

β being the parameter of the predictor x_i in Eq. (1). This quotient is called the ODD ratio. The conclusion is that the ODD ratio calculated between two situations that only differ in a unit of one variable is a constant value.

RESULTS

Four perimodiolar cochlear implant electrode array users (patients 2–4, and 9), and four straight array users (patients 5–8) completed the test. Patient 1 did not attend the CT scan appointment and patient 10 had undergone an inappropriate magnetic resonance imaging technique for an unrelated health issue and his array was displaced so he had to undergo reimplantation surgery and thus could not complete the test.

Upon visual inspection, scatter plots shown in Figure 1 indicate that there is a tendency toward better performance for lower impedance values, whereas the correlation between distance to the modiolus and success rate is not clear (Fig. 1).

Figure 2A and B illustrates the success rate, considered as % correct on the Alternative Force Choice test, as a function of either patient or electrode. Figure 2C shows mean impedance per patient. From these data, patients with contour arrays seem to have a tendency toward better performance, while there is great dispersion in those with straight arrays. The same happens when performance is

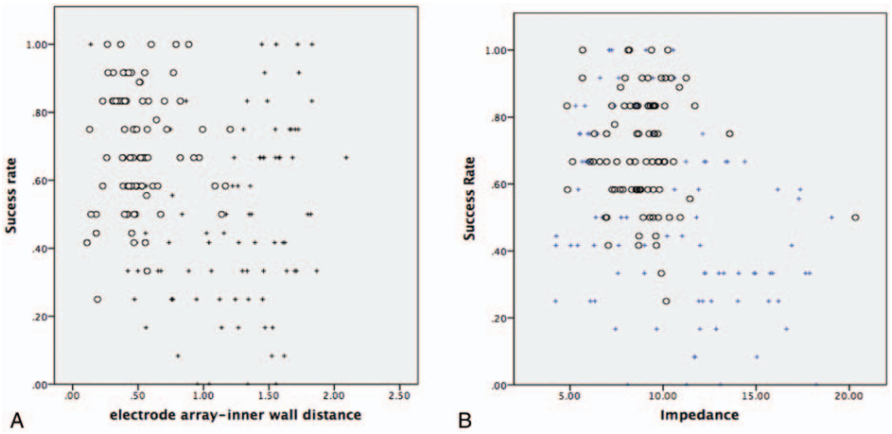

FIG. 1. Scatter plots of success rate as a function of (*A*) electrode-inner wall distance and (*B*) impedance. Crosses correspond to slim straight and circles to CA electrode arrays.

evaluated against electrode. Here we find how for high and middle frequency electrodes, contour advance arrays tend to perform better, while at the apical end this difference is not clear. The first two electrodes, however, give similar success rates for both the groups. Again, patients fitted with a straight array tend to have larger dispersions in their success rates. There does not seem to be a significant electrode effect.

Then we moved on to identify which factors have the capacity to influence and modify the success rate. We started by analyzing electrode number. A Levene test for equality of variances of the mean success rate indicates that the variance is the same for all electrodes ($p = 0.35$, the null hypothesis that states that the variances are different cannot be rejected). Consequently, an analysis of variance contrast was also done, concluding that the equality of the means of the successes for all electrodes cannot be rejected (the F statistic value had an associated $p = 0.82$).

A similar analysis of the variance was conducted for the patient factor. The result suggests the existence of statistically different results depending on the patient, both for mean and variance values (probability associated with the Levene's statistic of equality of variances $p < 0.001$, and probability associated with the F statistic of Welch of equality of variances $p < 0.001$). Accordingly, the empirical evidence supports the hypothesis that there is a patient effect that significantly affects success rate. Figure 2A shows the boxplot of the mean success rate for each patient. Patient 6 and most prominently patient 8 have a large dispersion. In addition, patient 6 also has a low mean success rate, although not as low as patient 7, which is the third patient that stands out from the sample. On the opposite end is patient 4, with the highest success rate and the smallest dispersion between electrodes.

Of these patients who have a differential behavior, three of them, patients 6, 7, and 8, have straight electrode arrays (although so does patient 5). The probability associated with the Welch's F statistic (because variances between groups were different) for the equality of the probability of success in the presence of different variances gave a value of $p < 0.001$, being the probability of success 53% for straight electrode array carriers and 70% for perimodiolar electrode array carriers. This result provides empirical evidence in favor of the hypothesis that perimodiolar electrode arrays provide better electrode discrimination.

A correlation and regression analysis was done to quantify the relationship between the distance of the electrode to the inner wall of the cochlea, impedance, patient effect, and the success rate. To this end, the following variables were incorporated: 1) neural response telemetry (NRT), which is expected that the increase in the value of this variable results in a decrease in success rate; 2) T level that, according to the literature, is expected to have a positive relationship with success rate (9); 3) impedance (in kΩ), which is expected to have a negative effect on the success rate because larger impedances result in higher currents required to reach the neural ends.

The descriptive statistics of the variables are shown in Table 2. On average, patients have been successful in 60% of the tests, have an electrode distance of 0.87 mm, a mean NRT of 183.61 CL, a T level of 126.29 CL and an impedance of 9.66 kΩ. The relative dispersion is moderate in all variables, being the variable distance the one with greater relative dispersion. Because the variable deterioration of the nerve (NRT) was not measured in 12 electrodes, the sample size had to be reduced to 158 elements (Table 2).

Table 3 contains the correlation matrix of the variables and their level of significance. It can be concluded that the success rate is significantly correlated with all explicative variables, with the expected signs. There are also significant correlations between the different explanatory variables, which make it difficult to quantify their individual effect on the mean success rate. However, their values are not high enough to produce serious problems of multicollinearity (Table 3).

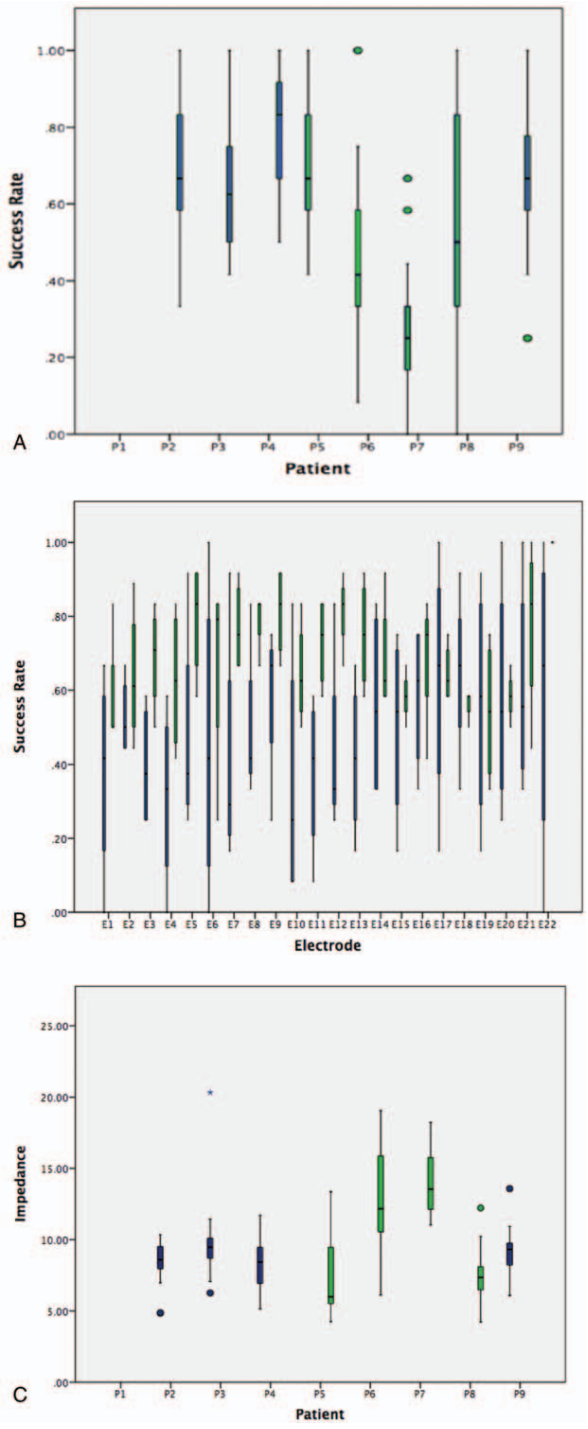

FIG. 2. Success rate (% correct on the Alternative Force Choice test) as a function of (*A*) patient and (*B*) electrode. Black boxes represent slim straight and grey boxes represent contour arrays. (*C*) Mean impedance per patient. There is a correlation between pitch discrimination and impedance.

The determining factor when modeling the endogenous variable is the very nature of the variable itself. Success rate is bounded between 0 and 1 and its theoretical behavior corresponds to a Bernouilli distribution. Let us remember that the success rate has been obtained as the quotient between the number of right answers divided by the number of trials per electrode pairs for a given reference electrode (6, 9, or 12). When calculated in this way the variable has a binomial behavior. Therefore, the assumption of linear relationship with the explanatory variables, which implies a constant linear effect, is not strictly valid because linear models give values below zero and above one. Moreover, the variance of the success rate is not constant and so there is heterocedasticity. These properties limit the use of the standard method of multiple linear regression and its estimation by ordinary least squares and thus we need to turn to a Binomial Logit model.

The parameters estimated using this method are shown in Table 4. All variables are statistically significant at 5%, and so is the model in global terms (Omnibus contrast yielded an associated probability $p < 0.001$). To obtain the goodness of the fit, the probability of success with this model and then its correlation with the original variable were calculated. The model explains 26.52% of the observed results (Table 4).

The interpretation of the estimated coefficient of the distance to the modiolus is done as follows. The estimated parameter of the distance is −0.314. Therefore, ceteris paribus and on average, if the distance is increased by 0.1 mm, the expression 4 takes the value −3.1. This means that due to that 0.1 mm increase in the distance, the probability to guess right against guessing wrong is reduced by 3.1%.

It should not be interpreted as a change in the success rate though. If the success rate at distance d_0 is p_0, then the ODD is $ODD_0 = p_0/(1 - p_0)$. If the distance is increased 0.1 mm then β becomes β/10. Solving for p_1 gives the result

$$\mathrm{ODD}_1 = \frac{\mathrm{p}_1}{1 - \mathrm{p}_1} = \mathrm{e}^{\beta}\mathrm{ODD}_0 \tag{5}$$

$$\mathrm{p}_i = \frac{\mathrm{e}^{\frac{\beta}{10}}\mathrm{ODD}_0}{1 + \mathrm{e}^{\frac{\beta}{10}}\mathrm{ODD}_0} = \frac{\mathrm{e}^{\frac{\beta}{10}}\frac{\mathrm{p}_0}{1-\mathrm{p}_0}}{1 + \mathrm{e}^{\frac{\beta}{10}}\frac{\mathrm{p}_0}{1-\mathrm{p}_0}} \tag{6}$$

β being the parameter of the variable electrode-inner wall distance in Eq. (1).

The last equation shows the relationship between the success rate at distance d_0 and at distance $d_1 = d_0 + 0.1$ mm. For example, if for d_0 the success rate is 0.8, a distance increase of 0.1 mm would cause the success rate to fall to 0,795, ceteris paribus and on average.

Figure 3 shows the probability of success estimated for this method. Two patients have been depicted: a patient with a good success rate, such as patient 5 (in blue) and the patient with the lowest success rate, patient 7 (in red). It can be seen how the model has the appropriate shape, showing ceiling and floor effects for perfect performance (value one) and lowest performance (value 0). This model also shows great variability in performance as

TABLE 2. *Descriptive statistics of explanatory variables*

	Success Rate	Electrode-inner Wall Distance	NRT	T Level	Impedance
Mean	0.60	0.87	183.61	126,29	9.66
Maximum	1.00	2.09	237.00	176.00	20.33
Minimum	0.00	0.11	109.00	95,00	4.23
Standard deviation	0.25	0.50	22.06	18.56	3.24
Relative dispersion	0.41	0.58	0.12	0.15	0.34
No. of observations	176	176	158	176	176

distance decreases in the case of patient 7. Thus, this patient could potentially get a 25% improvement in electrode discrimination if an electrode located at 1 mm from the inner wall would be placed in contact with it (Fig. 3).

DISCUSSION

The results provide evidence that the ability to discriminate between electrodes depends on multiple factors. In this study, NRT, T level, impedance, and distance were identified. They were all statistically significant in explaining electrode discrimination.

Pfingst demonstrated that impedance increased during the first months after implantation and then stabilized and even decreased a little in macaques (26). This was followed by periods of long-term stability.

Specifically, the statistical analysis provides empirical evidence in favor of the hypothesis that the electrode distance to the inner wall of the cochlea and impedance are both significant predicting variables for electrode discrimination ability. The results indicate that the greater the distance, the lower the success rate will be. Thus, distance to the inner wall will result in more difficulties to perceive electrode differences. The concept that perimodiolar electrodes could be a better solution in terms of pitch discrimination both because they are closer to the modiolus and because their impedance is lower has been noted previously (27,28).

The same thing applies to impedance. High impedances lead to low scores in electrode discrimination specifically (29,30).

The explanation can be found in the extensive research that has been conducted to describe current field patterns for various electrode configurations within the cochlea, as described in the introduction.

According to these, in our experiment, a patient with closer electrode-inner wall distance has a narrower excitation region per electrode, and hence perceives two adjacent stimulations as being more dissimilar than a patient with a larger distance, under the same conditions of neural survival and impedance.

Apart from the computer model results, human experiments have also found that perimodiolar placement seems to improve electrode discrimination; specifically Cohen et al. (31) measured electrode discrimination ability in three subjects implanted with a perimodiolar electrode array. Two of the three subjects had a portion of the electrode array close to the modiolus. Those subjects had smaller pitch difference limens for electrodes located in this portion than those that occupied a more lateral position.

Perimodiolar arrays therefore offer the potential for improvements in speech processing due, in particular, to narrower regions of neural excitation. It remains to be seen whether such changes would result in practical improvements to speech perception. Although such narrowing would be less important for stimulation toward the upper end of the dynamic range, it has been found that the effect is significant for the Contour array relative to the straight, even at 80% of the loudness.

In the present study, electrode discrimination also depended on T level. Studies have found that distance to the inner wall was positively correlated to lower thresholds and comfortable loudness levels. Other findings indicate that electrode discrimination improves with increasing level. There is, therefore, an unsolved contradiction between lower intensity and worse performance. If the theory developed by the models described above were true, then one would expect that, at low intensity levels, the patients would be most capable of discriminating electrodes (32).

TABLE 3. *Pearson correlation of explicative and endogenous variable*

	Success Rate	Electrode-inner Wall Distance	NRT	T Level	Variance Inflation Factor
Electrode-inner wall distance	−0.207[b]				1.23
NRT	−0.294[b]	0.421[b]			1.87
T level	0.169[a]	0.260[b]	0.521[b]		1.64
Impedance	−0.318[b]	−0.015	0.217[b]	−0.222[b]	1.27

[a] Significant at 5%.
[b] Significant at 1% for bilateral contrast.
NRT indicates neural response telemetry.

TABLE 4. *Binomial logit model coefficients*

Predictive Variables	Binomial Logit Model Estimated Coefficients (p Value)
Constant	1.884 (0.08)
NRT	−0.018 (0.001)
Impedance	−0.053 (0.041)
T level	0.021 (0.000)
Distance	−0.336 (0.03)

NRT indicates neural response telemetry.

However, the study presents several limitations that must be discussed to help push forward any further research in this line. First, it would be highly recommendable to extend the sample size, using a sample selection that fixes the patient demographics, since the N presented here does not allow the elimination of the patient effect. It is necessary to discard the possibility that correlations observed and quantified in Table 3 and in the models estimated could be due to a patient characteristic that was not controlled in the experiment. A multicenter study seems like the favorable option to consider.

Another limitation is the imaging technique. CT scan seems to have a clear advantage over the previously used plain film radiography with the standard Stenvers projection. With modern multislice CT scanning, more detailed information can be gathered on the intracochlear electrode position. However, when determining the exact position of the electrode in the cochlea, it was difficult to identify the separate electrodes in relation to the modiolus. This was mainly due to image degradation caused by partial volume effects, but metallic artifacts of the electrode array also posed a problem. The window depth in our software configuration limited us in visualizing the two extreme contrasts we wanted to investigate: the fluid compartment and the bony structures of the cochlea and modiolus; and the radiopaque electrode array. However, our software overcame this limitation by adjusting inter electrode distance to the total length of the array, which was clearly visible.

Finally, a third limitation can be due to differences in electrode design. Electrodes in the straight arrays consist of full platinum bands that encompass the entire circumference of the array. In contrast, the contour array consists of half-band electrodes located on the medial portion of the precurved carrier. Thus, orientation and spread of current fields will be different for the two electrode designs. This could not be quantized in this study, but, given the large importance that the electric field patterns have in determining auditory nerve stimulation, further studies where this variable is analyzed would be needed to further increase the model's predictive power.

There are scarce pathological reports of patients who underwent reimplantation procedures. These cannot absolutely clarify whether straight or perimodiolar electrodes behave equally in terms of trauma to the cochlea, nor in terms of residual hearing preservation, and similarly occur with the cochlear surgical approach, via cochleostomy or round window (33–35).

This study includes patients who were implanted via an enlarged round-window approach without scala vestibuli dislocation, half of them with a straight electrode, the other half with a perimodiolar. Our patients fitted with perimodiolar arrays have lower impedance values and smaller electrode-inner wall distances than those fitted with straight arrays. As higher impedances are associated with more intracochlear scar tissue, and provided the same atraumatic surgical technique used, differences observed may well be explained by the lower harm of the perimodiolar array, as recently suggested by Kamakura and Nadol (36).

A recent study shows that the inflammatory response to the electrode is significantly greater at the basal turn of cochlea due to the trauma of the cochleostomy (10). In this area a foreign body giant cell infiltration and granulomatous reaction was observed in $>95\%$ of temporal bones. Interestingly, the fibrotic local tissue reaction is not associated with electrode type, kind of tissue grafts used for sealing the cochleostomy or duration of implantation. The use of soft-surgery techniques minimizes trauma during surgery, thus minimizing possible fibrous growth due to scars (1). However, as stated earlier in the introduction, impedance values do rise regardless of the surgeon's best efforts. Previous studies suggest that straight electrode arrays lead to fibrosis between the implant and the inner wall, while perimodiolar electrodes lead to fibrosis toward the lateral wall (37,38).

CONCLUSIONS

In light of these findings, perhaps the path to substantial improvements lies in employing new speech processing algorithms that incorporate detailed knowledge of the neural response to stimulation of individual patients' arrays. A narrower excitation pattern produced by stimulation suing a perimodiolar array would provide a finer palette for the construction of desired excitation profiles, more closely related to those of normal hearing. However, a larger sample size is required as well as higher resolution imaging techniques before giving conclusive statements.

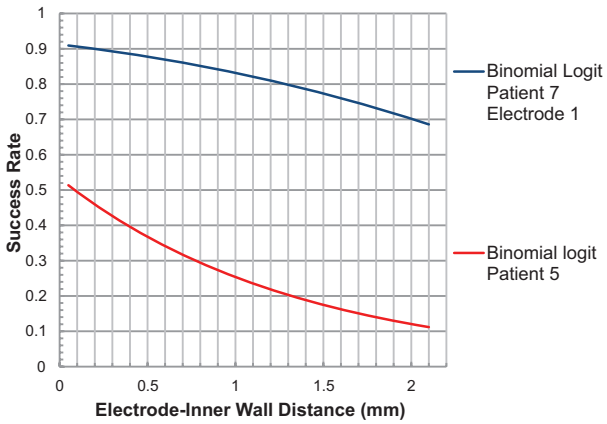

FIG. 3. Binomial Logit model predicting performance as a function of distance for patients 5 and 7.

REFERENCES

1. Garcia-Ibanez L, Macias AR, Morera C, et al. An evaluation of the preservation of residual hearing with the Nucleus Contour Advance electrode. *Acta Otolaryngol* 2009;129:651–64.
2. Jia H, Venail F, Piron JP. Effect of surgical technique on electrode impedance after cochlear implantation. *Ann Otol Rhinol Laryngol* 2011;120:529–34.
3. Fayad J, Linthicum FH Jr, Otto SR, Galey FR, House WF. Cochlear implants: histopathologic findings related to performance in 16 human temporal bones. *Ann Otol Rhinol Laryngol* 1991;100: 807–11.
4. Kennedy DW. Multichannel intracochlear electrodes: Mechanism of insertion trauma. *Laryngoscope* 1987;97:42–9.
5. Li PM, Somdas MA, Eddington DK, Nadol JB. Analysis of intracochlear new bone and fibrous tissue formation in human subjects with cochlear implants. *Ann Otol Rhinol Laryngol* 2007;116:731–8.
6. Mukherjee P, Uzun-Coruhlu H, Wong CC, Curthoys IS, Jones AS, Gibson WP. Assessment of intracochlear trauma caused by the insertion of a new straight research array. *Cochlear Implants Int* 2012;13:156–62.
7. Van Abel KM, Dunn CC, Sladen DP, et al. Hearing preservation among patients undergoing cochlear implantation. *Otol Neurotol* 2015;36:416–21.
8. Van Wermeskerken GK, van Olphen AF, Smoorenburg GF. Intra- and postoperative electrode impedance of the straight and Contour arrays of the Nucleus 24 cochlear implant: Relation to T and C levels. *Int J Audiol* 2006;45:537–44.
9. Linthicum FH Jr, Fayad J, Otto SR, Galey FR, House WF. Cochlear implant histopathology. *Am J Otol* 1991;12:245–311.
10. Abi-Hachem RN, zine A, Van De Water TR. The injured cochlea as a target for inflammatory processes, initiation of cell death pathways and application of related otoprotective strategies. *Recent Pat CNS Drug Discov* 2010;5:147–63.
11. Nadol JBJ, Shiao JY, Burgess BJ. Histopathology of cochlear implants in humans. *Ann Otol Rhinol Laryngol* 2001;110:883–91.
12. Seyyedi M, Nadol JB. Intracochlear inflammatory response to cochlear implant electrodes in the human. *Otol Neurotol* 2014;35:1545–51.
13. Kawano A, Seldon HL, Clark GM, Ramsden RT, Raine CH. Intracochlear factors contributing to psychophysical percepts following cochlear implantation. *Acta Otolaryngol* 1998;118:313–26.
14. James C, Albegger K, Battmer R, et al. Preservation of residual hearing with cochlear implantation: How and why. *Acta Otolaryngol* 2005;125:481–91.
15. Eshraghi AA, Yang NW, Balkany TJ. Comparative study of cochlear damage with three perimodiolar electrode designs. *Laryngoscope* 2003;113:415–9.
16. Vanpoucke FJ, Zarowski AJ, Peeters SA. Identification of the impedance model of an implanted cochlear prosthesis from intracochlear potential measurements. *IEEE Trans Biomed Eng* 2004;51:2174–83.
17. Ni D, Shepherd RK, Seldon HL, Xu SA, Clark GM, Millard RE. Cochlear pathology following chronic electrical stimulation of the auditory nerve. I: Normal hearing kittens. *Hear Res* 1992;62:63–81.
18. Swanson B, Seligman P, Carter P. Impedance measurement of the Nucleus 22-electrode array in patients. *Ann Otol Rhinol Laryngol* 1995;166:141–4.
19. van Wermeskerken GK, van Olphen AF, Smoorenburg GF. Intra- and postoperative electrode impedance of the straight and Contour arrays of the Nucleus 24 Cochlear Implant; relation to T and C levels. *Int J Audiol* 2006;45:537–44.
20. Finley CC, Skinner MW. Role of electrode placement as a contributor to variability in cochlear implant outcomes. *Otol Neurotol* 2008;29:920–8.
21. Henry BA, McKay CM, McDermott HJ, Clark GM. The relationship between speech perception and electrode discrimination in cochlear implantees. *J Acoust Soc Am* 2000;108:1269–80.
22. Vickers D, Degun A, Canas A, Stainsby T, Vanpoucke F. Deactivating cochlear implant electrodes based on pitch information for users of the ACE strategy. *Adv Exp Med Biol* 2016;894:115–23.
23. Zwolan TA, Collins LM, Wakefield GH. Electrode discrimination and speech recognition in postlingually deafened adult cochlear implant subjects. *J Acoust Soc Am* 1997;102:3673–85.
24. von Békésy G. A new audiometer. *Acta Otolaryngol* 1947;35: 411–22.
25. Berkson J. A statistically precise and relatively simple method of estimating the bio-assay with quantal response, based on the logistic function,. *JASA* 1953;50:529–49.
26. Pfingst BE. Changes over time in thresholds for electrical stimulation of the cochlea. *Hear Res* 1990;50:225–36.
27. Fitzgerald MB, Shapiro WH, McDonald PD, et al. The effect of perimodiolar placement on speech perception and frequency discrimination by cochlear implant users. *Acta Otolaryngol* 2007;127:378–83.
28. Hughes ML, Abbas PJ. Electrophysiologic channel interaction, electrode pitch ranking, and behavioral threshold in straight versus perimodiolar cochlear implant electrode arrays. *J Acoust Soc Am* 2006;119:1538–47.
29. Briaire JJ, Frijns JHM. Field patterns in a 3D tapered spiral model of the electrically stimulated cochlea. *Hear Res* 2000;148:18–30.
30. Kral A, Hartmann D, Mortazavi D, Klinke R. Spatial resolution of cochlear implants: The electrical field and excitation of auditory afferents. *Hear Res* 1998;121:11–28.
31. Cohen LT, Saunders E, Clark GM. Psychophysics of a perimodiolar cochlear implant electrode array. *Hear Res* 2001;155:63–81.
32. Blamey P, Arndt P, Bergeron F, et al. Factors affecting auditory performance of postlinguistically deaf adults using cochlear implants. *Audiol Neurotol* 1996;1:293–306.
33. Richard C, Fayad JN, Linthicum FH Jr. Round window versus cochleostomy in chochlear implantation: Histological findings. *Otolo Neurotol* 2012;33:1181–7.
34. Zanneti D, Nassif N, Redaelli de Zinis LO. Factors affecting residual hearing preservation in cochlear implantation. *Acta Otorhinolaryngol Ital* 2015;35:433–41.
35. Causon A, Verschuur C, Newman TA. Trends in cochlear implant complications: Implications for improving long-term outcomes. *Otol Neurotol* 2013;34:259–65.
36. Kamakura T, Nadol JB Jr. Correlation between word recognition score and intracochlear new bone and fibrous tissue after cochlear implantation in the human. *Hear Res* 2016;339:132–41.
37. Linthicum FJ, Fayad J, Otto SR, Galey FR, House WF. Cochlear implant histopathology. *Am J Otol* 1991;12:245–311.
38. Sutton D, Miller JM, Pfingst BE. Comparison of cochlear histopathology following two implant design for use in the scala timpani. *Ann Otol Rhinol Laryngol* 1980;399:19–31.

4.2 Second publication

4.2.1 Publication Information

Title: Imaging evaluation of electrode placement and effect on electrode discrimination on different cochlear implant electrode arrays.

Authors: Ángel Ramos de Miguel, Andrea A. Argudo, Silvia A. Borkoski Barreiro, Juan Carlos Falcón González and Ángel Ramos Macías

Journal: European Archives of Oto-Rhino-Laryngology

DOI: 10.1007/s00405-018-4943-2

European Archives of Oto-Rhino-Laryngology
https://doi.org/10.1007/s00405-018-4943-2

OTOLOGY

Imaging evaluation of electrode placement and effect on electrode discrimination on different cochlear implant electrode arrays

Ángel Ramos de Miguel[1] · Andrea A. Argudo[1] · Silvia A. Borkoski Barreiro[1] · Juan Carlos Falcón González[1] · Angel Ramos Macías[1]

Received: 7 August 2017 / Accepted: 19 March 2018

Abstract

Objective The aim of the present study is to evaluate the effect of electrode discrimination based on electrode to modiolus distance in different cochlear implant models, using image information to estimate the outcomes after an implantation on electrode discrimination

Methods A descriptive prospective randomized study performed during 16 months. A psychoacoustic platform was used to evaluate patients' electrode discrimination capabilities of patients. For the acquisition of the images, a cone beam computed tomography was used to assess postcochlear implantation of electrodes' position. We considered two other new measurements: the intracochlear position index, which indicates how far is the electrode from the modiolar wall, and the homogeneity factor (HF), which provides us with information about the distance between the electrodes and the modiolus

Results 21 postlingually deaf adults showing different CI models [CI522 ($n=7$), CI512 ($n=7$), and CI532 ($n=7$)] that corresponded to the lateral and perimodiolar array electrodes. The average success rate of the CI522 group was 47%, of the CI512 group was 48%, and of the CI532 group was 77%. There is statistically significant difference between groups CI532–CI522 ($p=0.0033$) and CI532–CI512 ($p=0.0027$)

Conclusion The Nucleus CI532 offers a better perimodiolar placement. HF and IPI measurements provide information about the electrodes location inside the cochlea, being related to electrode discrimination.

Keywords Cochlear implant · Electrode discrimination test · Intracochlear position index

Introduction

There is a high interest in placing the electrode array as close as possible to the modiolus wall, as this would minimize the current dissemination and the spatial overlap that would in turn result in the reduction of the interaction between channels [1–3]. Several studies have shown significant correlations between electrode discrimination and speech perception in cochlear implant (CI) holders [4, 5]. An electrode discrimination test is based on the patient's ability to distinguish the pitch generated by two electrodes located at different places. However, it has been described that the intensity of the electrical stimulus on the electrode discrimination test directly correlates with performance [6, 7]. Channel interaction is still a challenge despite significant improvements have been made by advances in hardware and signal processing [8].

The development of electrodes design has gradually increased during more than two decades. The expectation for better communication capability using these devices has increased significantly [9]. Since multichannel CIs were introduced, several studies have demonstrated that patients using these devices could discriminate speech without any visual assistance [10]. Communication skills have been considerably improved: in the first limited studies, mean PBK (Phonetically Balanced Kindergarten word lists) in-quiet scores of approximately 9% words correct for 80 children who had 1 year of multichannel cochlear implant experience were reported [11]. Currently, the CI performance has significantly improved, thus allowing the patient to reach a 95% of speech perception in quiet [12].

✉ Ángel Ramos de Miguel
aramos.gcc@gmail.com

[1] Otorhinolaryngology, Head and Neck Department, Complejo Hospitalario Universitario Insular Materno Infantil, Av. Marítima del Sur s/n, 35016 Las Palmas de Gran Canaria, Spain

Published online: 02 April 2018

Related studies evaluate the insertion properties and intracochlear trajectories of the perimodiolar Contour Advance electrode array, the Nucleus Straight array (Nucleus CI22), and the Nucleus perimodiolar electrode CI24. Their results show that perimodiolar electrode array includes both: a reduction in stimulus thresholds and an increase in dynamic range, resulting in a more localized stimulation pattern of the spiral ganglion cells, reduced power consumption, and, therefore, longer speech processor battery life [13, 14].

On the other side, imaging techniques are available to evaluate the electrode placement after the insertion in the cochlea. Although many protocols have been proposed [15–17], most of them are focussed on the position the electrode according to the insertion depth and the perimodiolar position. In this study, a radiological analysis of the electrode-to-modiolus distance (the intracochlear position of the different contacts) and the normal distribution of the electrode distance along the electrode array regarding the modiolus were introduced. First, it is essential to define the best slice plane to see the basal turn of the cochlea, which can be performed by searching the best Multi Planar Reconstruction (MPR) that is aligned with the base of the cochlea or by a plane radiograph parallel to the cochlear base [18]. From the cochlear basal turn view, a predefined cochlear coordination system based on anatomic reference points of the cochlea and the vestibule can be calculated [19]. In addition, it is interesting to obtain all the anatomical measurements of the cochlea. The relevance of these measurements is due to the possibility to evaluate the insertion using different scores, i.e., wrapping factor, insertion depth, electrode distance, insertion angle and to correlate with patient outcomes [20].

Although there are several studies focused on the relation between electrode discrimination and CI performance, the main objective of this study is to evaluate the effect of electrode discrimination based on the electrode-to-modiolus distance and to evaluate different image data to estimate the outcomes after an implantation on electrode discrimination [5, 21–24].

Materials and methods

Subjects

A descriptive prospective randomized study was performed during a 16 month period on patients accomplishing the following selection criteria: being adult (> 18 years of age); complete insertion of the electrode array. To have five or more adjacent active electrodes for the psychoacoustic test, a minimum of 20 correlatives contacts were active; being a CI holder from more than 6 months (we analysed three types of electrode arrays: CI522, CI512, and CI532). The exclusion criteria were the following: suffering from retro-cochlear pathologies, cochlear malformation, psychological disorders, and additional handicaps that would prevent participation in the study and mental disorders. Demographic details for the subjects can be observed in Table 1.

The Ethics Committee of the Clinical Assays within the University Hospital Complex Insular-Materno-Infantil of Gran Canaria approved this study.

Psychoacoustic platform

A psychoacoustic platform to evaluate the electrode discrimination capabilities of a subject [25] using the Nucleus Implant Communicator (NIC) was developed by Cochlear LTD (NIC is not a commercially available device. This was used as a research tool for this study after was approved by the Ethical Committee and after obtaining the patient's consents information. For safety reasons, every side effect was evaluated and reported). It makes possible to deliver a designed set of stimuli to the electrodes of nucleus cochlear implants.

The platform evaluates the ability of a patient to discriminate an electrode contact stimulus from the adjacent contacts using a three alternative force choice testing. Therefore, the stimulus presented in the electrode must be differentiated by the patient from the stimulus presented in the closest electrode contacts. The system reports a patient score, success rate, which range from 0 to 100%. This score measure how did the patient the test on each electrode. 100% means that in every stimulus presentation, the patient was able to differentiate the electrodes. Otherwise, 0% means that any stimulus was not correctly differentiate. The evaluation procedure consists of three main steps: dynamic range determination, loudness balance, and electrode discrimination.

The stimulus used on this experiment was set at 900 Hz (pulses per second) and applied as follows: MP1 + 2 with a pulsewidth of 25 μs, interphase gap at 8 μs, and stimulus duration of 1 s. The time lapse between stimuli was set at 1 s.

Dynamic range determination (DR)

The DR defines the current intensity span that produces auditory sensation and is determined by the Threshold (T) and Comfort (C) levels of each electrode. T is the softest sounds that can be detected by the CI patients and C is the comfortable loudness levels that are tolerated by the CI patients.

The T level is calculated using the up–down method: a stimulus is presented at a progressively increasing intensity; step size was 5 CL, until the patient reports hearing sensation. Then, it is lowered down again using a lower intensity (step size 1 CL), until it is no longer heard. For C levels, the one-sided method of limits is used, increasing the stimuli until the maximum comfortable level for the patient

Table 1 Summary of CI model data

Subject	Type of implant	Sex	Age (years)	Prosthesis use (months)	Tinnitus	Actives electrode	Deafness duration (years)	Speech perception (sentences) (%)
S1	CI 522	F	64	55	Yes	22	7	76
S2	CI 522	F	18	37	No	22	8	80
S3	CI 522	M	50	36	No	22	4	64
S4	CI 522	M	75	27	No	22	5	80
S5	CI 522	F	66	36	Yes	22	4	72
S6	CI 522	M	55	39	No	22	6	76
S7	CI 522	M	40	41	No	22	7	80
S8	CI 512	F	64	32	No	22	8	68
S9	CI 512	M	51	33	No	22	3	80
S10	CI 512	M	53	60	Yes	22	7	84
S11	CI 512	M	70	9	No	22	6	80
S12	CI 512	F	52	63	No	22	6	84
S13	CI 512	F	34	40	No	22	4	76
S14	CI 512	M	49	48	Yes	22	5	72
S15	CI 532	M	57	16	Yes	22	9	80
S16	CI 532	M	58	29	No	22	3	84
S17	CI 532	M	56	33	No	22	5	80
S18	CI 532	M	38	41	No	22	4	84
S19	CI 532	F	47	16	No	22	7	76
S20	CI 532	F	30	42	No	22	4	84
S21	CI 532	F	58	21	No	22	5	88

is reached. This procedure is repeated three times and the average of the three measurements is set as C level.

Loudness balance (LB)

The aim of this step is to produce a stimulation perceived equally loud on all electrodes, so no clues are provided to the patients, and to compare only their abilities to discriminate two electrodes by the pitch. To create a more difficult test than those performed at higher intensities [25], all the electrodes were set at 25% of the DR. Two Stimuli were presented to the subject, the first one corresponding to a baseline electrode, and the second one corresponding to a test electrode which is presented with 10% difference with respect to the DR higher or lower current level, and selected randomly to have an importance loudness difference. The patient indicates which one of the two stimuli sounds louder. Depending on the answer, the intensity of the test electrode will be lowered or raised until the patient indicates that the loudness is the same in both electrodes. The LB comparison will be repeated again but after the test electrode current level is set at 10% of the DR in the opposite sense (louder or higher) than previously. The electrode test final value is the average of the two approaches. This procedure has to be done on all the electrodes used on the experiment.

Electrode discrimination test (EDT)

This method is a procedure of a three alternative force choice test (3AFC). The tester begins with a baseline electrode (generally starts on electrode 10) and four signal electrodes adjacent (8, 9, 11, and 12). Two stimuli come from a baseline electrode selected and a third from a signal electrode adjacent. The stimulus is presented in a random order and each evaluation is presented three times randomly. A baseline electrode has a total of 12 evaluations. The patient has a user interface with four options, first, second, third, and "equal". The patient has to select the sound that is different from the others. If no sound is perceived as different, the patient selects "equal". Once we have completed the evaluation of one electrode, the test moves to evaluate another electrode. This procedure is repeated until all electrodes are evaluated. Results are given as correct percentages of the total of evaluation of a baseline electrode [25, 26].

Radiological analysis method

Images were acquired by cone beam computed tomography (CBCT). CBCT has been previously validated as a valuable tool for the assessment of electrodes postcochlear implantation [15, 27–29] as it requires less irradiation than a regular CT [30, 31] and shows less sensitivity to metal artefacts

[32]. Thus, it represents an easier identification of electrode placement in the cochlea.

Once the raw DICOM files were obtained by the imaging system, they were processed to obtain all the valuable data related to the implantation. The process steps were:

1. Identify the optimal view of the cochlea: by identifying the optimal alignment of the basal turn of the cochlea, the best multiplanar reconstruction (MPR) with the thinner available slice is identified to visualize the basal turn of the cochlea. The slice plane should be placed centred on the electrode, Fig. 1a.
2. Extract the electrode array view: while keeping the MPR position, a thicker slice (average = 3.5 mm) on average mode was set and the image was saved on DICOM format, Fig. 1b.
3. Once we have the view of the electrodes array, the signal is reduced to find the "bone view", the MPR position is set just above the electrode array. Then, with a thinner slice (average = 0.6 mm), the visualization in min mode was established and image was saved, Fig. 1c.
4. Using the two DICOM files (one with the electrode array view and another with the bone view), the electrodes coordinates, lateral and modiolus wall position, are calculated. To estimate the electrode position, a custom-made MatLab script was developed. This tool was based on a parametric function, the position of the electrode.
5. Finally, the superposition of the electrodes' location and the bone place was obtained, Fig. 1d.

From this image analysis, valuable information of the electrode position inside the cochlea can be obtained.

In this study, two new measurements are introduced: the intracochlear position index (ICPI) and the homogeneity factor (HF) of the electrode array, defined as follows.

Intracochlear position index (ICPI)

ICPI is a new measure that indicates how far is the electrode from the modiolar wall. This measurement is normalized by electrode, being zero "0" the closest position to the modiolus and one "1" the closes position to the lateral wall. The electrode diameter is also considered: the distance from the centre of the electrode to its surface is also measured considering the diameter of each type of electrode array. Considering the *i*th electrode, the line passing through this electrode that is perpendicular to the electrode array is estimated, and the Euclidean distance between the modiolus (M_i) and the lateral wall (L_{wi}) are obtained. In addition, the Euclidean distance between the modiolus (M_i) and the electrode (E_i) are extracted. The intracochlear position index measurement is defined as

$$\mathrm{ICPI}_i = \frac{\mathrm{d}M_iE_i}{\mathrm{d}M_iL_{wi}}. \tag{1}$$

From all these ICPI measurements, one per electrode, the $\overline{\mathrm{ICPI}}$ value can be calculated as follows:

$$\overline{\mathrm{ICPI}} = \frac{\sum_{i=1}^{n} \mathrm{ICPI}_i}{n}. \tag{2}$$

Homogeneity factor (HF)

HF provides information about the distance from the electrodes to the modiolus. HF value is obtained from the ICPI. This measurement indicates the electrodes array position with respect to the modiolus, Eq. (3). A HF value of 0 means that all the electrodes of the array are placed at the same distance (i.e., all the electrodes are placed on the modiolar wall or all the electrodes are placed towards the lateral wall). HF value increases when the position of the electrodes are not homogeneous, so the electrodes are placed at different positions (some of them are placed at perimodiolar positions and some others are laterally placed, Fig. 2).

HF is calculated as the square root error between the $\overline{\mathrm{ICPI}}$ value and the ICPI value of each single electrode:

$$\mathrm{HF} = \frac{\sqrt{\sum_{i=1}^{n} \left(\overline{\mathrm{ICPI}} - \mathrm{ICPI}_i\right)^2}}{n}. \tag{3}$$

In addition, the wrapping factor (WF) was also calculated.

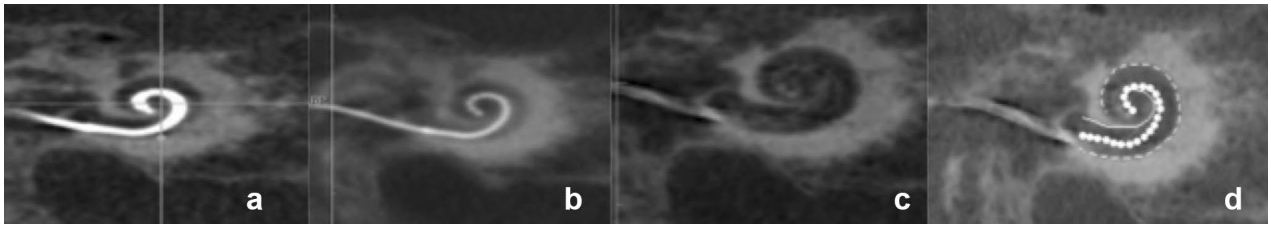

Fig. 1 **a** Best MPR to visualize the cochlear view; **b** MPR electrode view; **c** MPR bone view; **d** final structures location

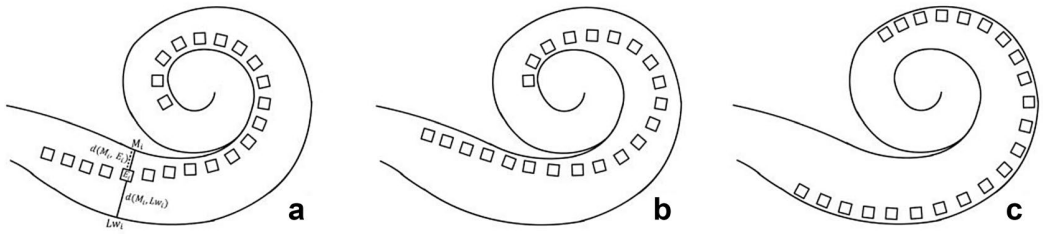

Fig. 2 HF examples. **a** Perimodiolar position with a very low HF value due to the electrodes are place at the same ICPI distance. **b** Perimodiolar position over inserted with a high HF because not all electrodes are place on the modiolar wall. **c** Lateral wall position with a very low HF value due to the electrodes are place at the same ICPI distance

Wrapping factor

One of the most valuable parameter to evaluate how perimodiolar is an inserted electrode array is the WF, which indicates that how tightly or loosely wrapped an electrode array is with respect to the modiolar wall [16]. The wrapping factor is defined as the ratio between the inserted electrode length (IEL) and the lateral wall length (LWL), Eq. (4) [16].

On one hand, the maximum WF value is 1.0. This value is obtained when the electrode array is on the lateral wall, so the IEL and LWL has the same length; therefore, the ratio is 1.0. On the other hand, WF value decreases as the array is wrapped more tightly to the modiolar wall (IEL < LWL):

$$\mathrm{WF} = \frac{\mathrm{IEL}}{\mathrm{LWL}}. \tag{4}$$

The statistical analysis of this study was done with IBM SPSS Statistics for Windows software v 24.0. A Kolmogorov–Smirnov test was performed in all cases to confirm that the data collected WF, HF, ICPI, and electrode discrimination results come from a normal distribution. Once normal distribution was confirmed, a one-way ANOVA test was used to compare the means of the three CI groups. Then, if ANOVA test reject the null hypothesis, an independent Bonferoni corrected *t* test was used to compare between pairs to identify the different cases. The hypothesis contrast will be considered statistically significant when the corresponding *p* value is lower than 0.05.

Results

21 adult patients were included in this study (12 males and 9 females) with ages ranging from 18 to 75 years (mean 51.66 years). All of them suffered from postlingual deafness and had been implanted with different CI models: CI522 ($n=7$), CI512 ($n=7$), and CI532 ($n=7$). These correspond to the lateral and perimodiolar array electrodes.

An electrode discrimination test was performed on every subject, Figs. 3 and 4. The average success rate for group CI522 was 47%, for group CI512 was 48% and for group CI532 was 77%. The percentage indicates the number of correct responses obtained during the psychoacoustic test.

In all the subjects, a postoperative image analysis was performed to obtain information about WF, $\overline{\mathrm{ICPI}}$, and HF. The average WF values were obtained from Table 2: for subjects implanted with CI522 was 0.86, for subjects implanted with CI512 was 0.68, and for subjects implanted with CI532 was 0.57. The $\overline{\mathrm{ICPI}}$ value for subjects implanted with CI522 was 0.62, for subjects implanted with CI512 was 0.26 and for subjects implanted with CI532 was 0.08. Finally, the average HF value for subjects implanted with CI522 was 0.29, for subjects implanted with CI512 was 0.16 and for subjects implanted with CI532 was 0.06, as shown in Fig. 3.

Regarding the neural response telemetry test (NRT), the results were completely normal, N1 within a time window of 0.2–0.4 ms after stimulus onset followed by P1 occurring around 0.6–0.8 ms. The average NRT threshold was 177 current level (CL) for CI522, 172 CL for CI512, and 167 CL for CI532 and there were no differences between in all groups (ANOVA $p=0.287$). The average impedance values for the different groups were the following: 10.03 kΩ for CI522, 9.66 kΩ for CI512, and 9.54 kΩ for CI532.

A statistical analysis between groups on each different imaging measurement and the electrode discrimination results was performed. The ANOVA test rejects the null hypothesis, the means of the groups are equal, in all measurements: WF ($p<0.001$), HF ($p<0.001$), $\overline{\mathrm{ICPI}}$ ($p<0.001$), and pitch discrimination ($p=0.015$). As shown in Table 3, statistical Bonferoni corrected *t* test shows significant differences in all measurements cases except one, electrode discrimination result between CI522 and CI512 ($p=0.9149$). The improvement results observed in the CI532 group over the other device models were 30% for the CI522 and 29% for the CI512.

Finally, the tendency between the imaging scores and the electrode discrimination success rate was obtained (Fig. 5). It can be observed that $\overline{\mathrm{ICPI}}$, HF, and WF values correlate inversely with the success rate on electrode discrimination test.

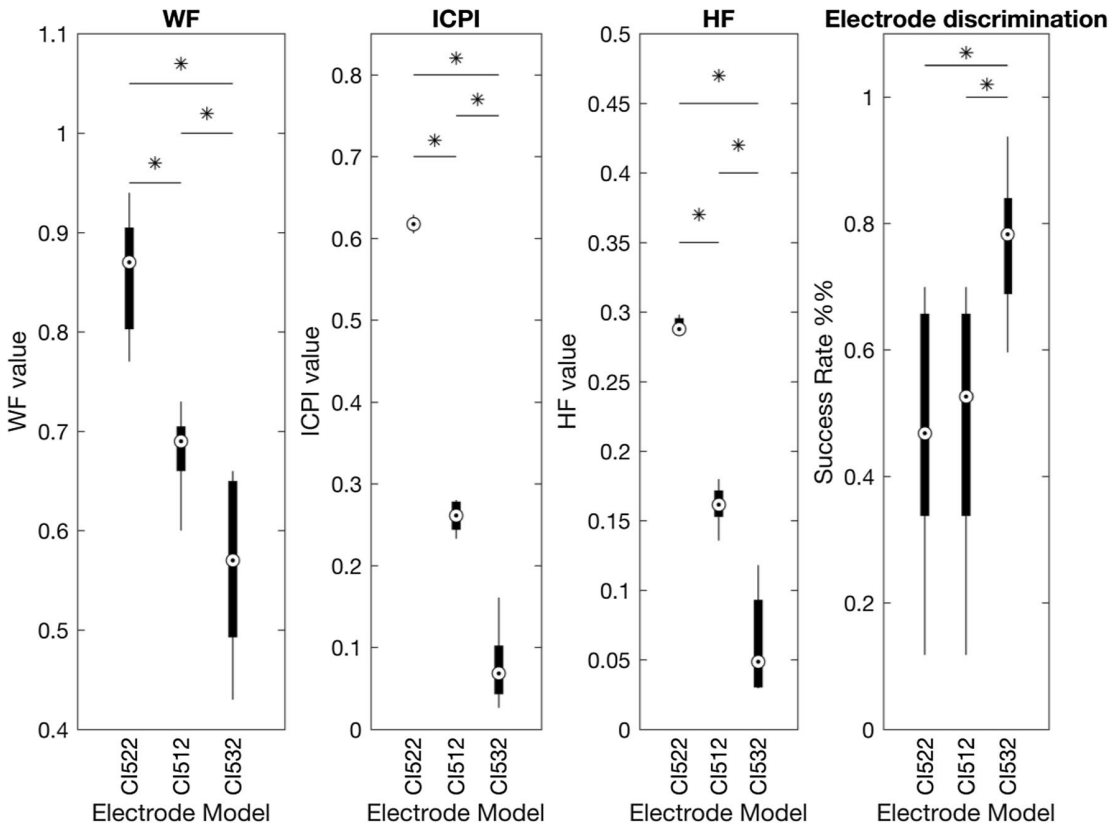

Fig. 3 Image scores by groups CI522, CI512, and CI532. On the left, it is shown the WF on each group; on the middle is plot the $\overline{\text{ICPI}}$; and on the right, the HF is shown for each group ($*p \leq 0.05$)

Discussion

Research has been conducted to describe some psychophysical reaction on intracochlear current flow for various electrode configurations within the cochlea. As it has been observed, a patient with closer electrode-inner wall distance has a narrower excitation region per electrode, and hence perceives two adjacent stimulations as being more dissimilar than a patient with a larger distance, under the same conditions of neural survival. It also considered that selectivity of the electric fields regarding neural stimulation depends on different factors in addition to the electrode-nerve proximity as patterns of neuronal survival population, stochastic variability characteristics of individual nerve fibers, cochlear anatomy, stimulus characteristics, and design features of the electrode [33, 34].

The main objective of this study was to determine the effects of electrode distance on electrode discrimination. Specifically, the statistical analysis provides empirical evidence in support of the hypothesis that the electrode distance to the inner wall of the cochlea is a significant variable for the prediction of electrode discrimination ability. Based on data from this study about WF, HF, and ICPI values, better results were obtained with the Nucleus CI532 than with the Nucleus CI522 and with the Nucleus CI512, according to modiolar proximity and better intracochlear position.

The results provide evidence that the ability to discriminate between electrodes depends on multiple factors, such as NRT, T level, or impedance. In addition, a better performance in electrode discrimination test was also obtained when those electrodes array were placed in a better position regarding the modiolus [22, 23, 35].

HF and $\overline{\text{ICPI}}$ values give more information regarding how the electrode array is placed inside the cochlea. $\overline{\text{ICPI}}$ indicates, on average, if the electrode array is placed on the modiolar wall or in the lateral wall. The ICPI value decreases to <0.2 for all electrode types at electrodes 20–22, due to the geometric configuration of the electrode arrays and the insertion dynamics in this narrow area of the cochlea. The HF value provides information about how accurate are all the averaging measurements of the contacts distance to the modiolar wall. It was also observed that the distribution widths of $\overline{\text{ICPI}}$ and HF were different between electrode types, the most important factor being not related to the insertion depth but to the over-insertion effect of the

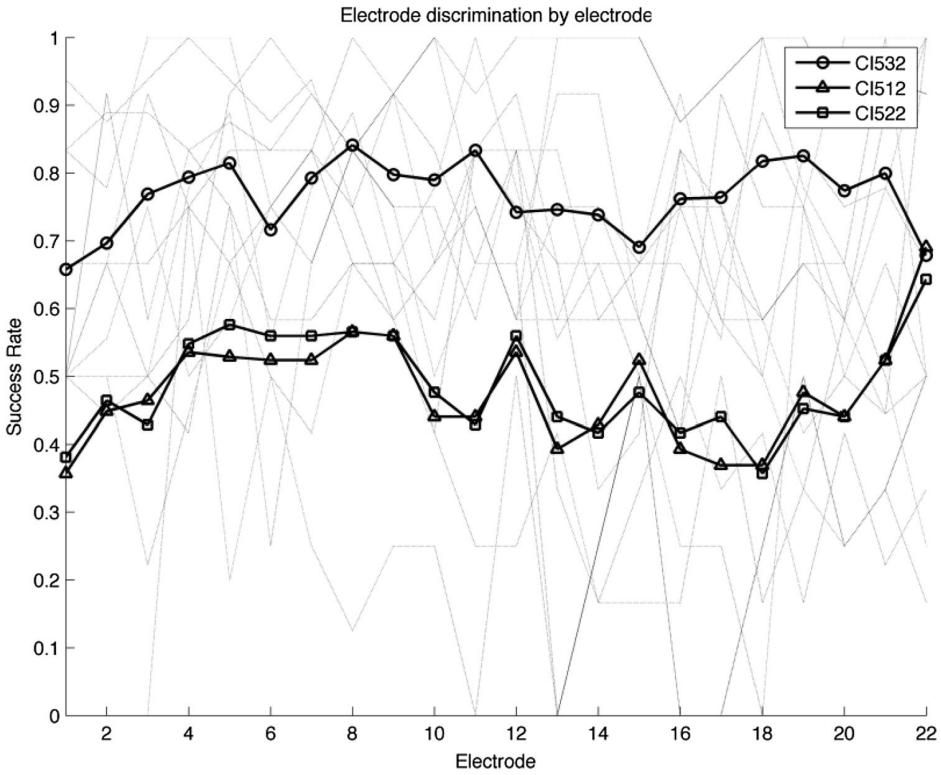

Fig. 4 Mean electrode discrimination success rate of each group by electrode. CI522–CI512 ($p=0.9149$); CI522–CI532 ($p=0.0033$), and CI512–CI532 ($p<0.0027$)

Table 2 Image analysis scores

	Type of implant	WF	$\overline{\text{ICPI}}$	HF	Electrode discrimination success rate %
S1	CI522	0.94	0.606	0.296	46.46
S2	CI522	0.77	0.623	0.284	64.39
S3	CI522	0.87	0.617	0.295	66.16
S4	CI522	0.81	0.623	0.285	69.94
S5	CI522	0.89	0.629	0.298	11.74
S6	CI522	0.80	0.617	0.283	29.50
S7	CI522	0.91	0.614	0.288	46.84
S8	CI512	0.69	0.280	0.169	46.46
S9	CI512	0.60	0.278	0.162	64.39
S10	CI512	0.71	0.261	0.180	66.16
S11	CI512	0.73	0.233	0.136	69.94
S12	CI512	0.66	0.239	0.150	11.74
S13	CI512	0.69	0.271	0.167	29.50
S14	CI512	0.66	0.259	0.173	52.65
S15	CI532	0.47	0.113	0.118	78.28
S16	CI532	0.43	0.027	0.032	67.80
S17	CI532	0.66	0.038	0.049	59.59
S18	CI532	0.57	0.068	0.030	93.75
S19	CI532	0.56	0.059	0.061	78.72
S20	CI532	0.66	0.068	0.030	71.84
S21	CI532	0.62	0.114	0.104	85.79

electrode array after the first turn, which was less frequently observed in the CI532 electrode.

Multichannel cochlear implants rely on place of electrical stimulation to encode pitch features of the acoustic signal. Thus, it is assumed that the subject's ability to discriminate stimulation of one site from another will be related to the subject's ability to understand speech and other environmental signals using the prosthesis [33, 34]. Several studies have demonstrated that removing poorly discriminated electrodes from a subject's processor map resulted in improved speech recognition scores in some subjects [21].

Our results indicate that the distance correlates inversely with the success rate. Thus, distance to the inner wall will result in more difficulties to perceive electrode differences. It is important to notice that the more apical electrodes are usually placed closest to the modiolar wall due to a reduction of the diameter of the Scala Tympani. In Fig. 4, it can be observed that the success rate is higher in all cases in the apical electrodes.

On the other hand, as proposed on the previous studies, the best way to solve channel interactions is to turn off a poor electrode [21]. For lateral wall electrode, array is important to consider reduce the amount of electrodes to avoid channel interactions [33, 34].

The final impact on word recognition of the electrode discrimination cannot be consider as the only factor. The neural population, duration of deafness, stimulation on apical area

Table 3 Image analysis scores

Statistical test	Measurement	Group	*p* value
One-way ANOVA	WF	All	< 0.001
t test Bonferoni correction	WF	CI522–CI512	< 0.001
t test Bonferoni correction	WF	CI522–CI532	0.0049
t test Bonferoni correction	WF	CI512–CI532	< 0.001
One-way ANOVA	$\overline{\text{ICPI}}$	All	< 0.001
t test Bonferoni correction	$\overline{\text{ICPI}}$	CI522–CI512	< 0.001
t test Bonferoni correction	$\overline{\text{ICPI}}$	CI522–CI532	< 0.001
t test Bonferoni correction	$\overline{\text{ICPI}}$	CI512–CI532	< 0.001
One-way ANOVA	HF	All	< 0.001
t test Bonferoni correction	HF	CI522–CI512	< 0.001
t test Bonferoni correction	HF	CI522–CI532	< 0.001
t test Bonferoni correction	HF	CI512–CI532	< 0.001
One-way ANOVA	Electrode discrimination	All	0.015
t test Bonferoni correction	Electrode discrimination	CI522–CI512	0.9149[a]
t test Bonferoni correction	Electrode discrimination	CI522–CI532	0.0033
t test Bonferoni correction	Electrode discrimination	CI512–CI532	0.0027

[a]No significant difference

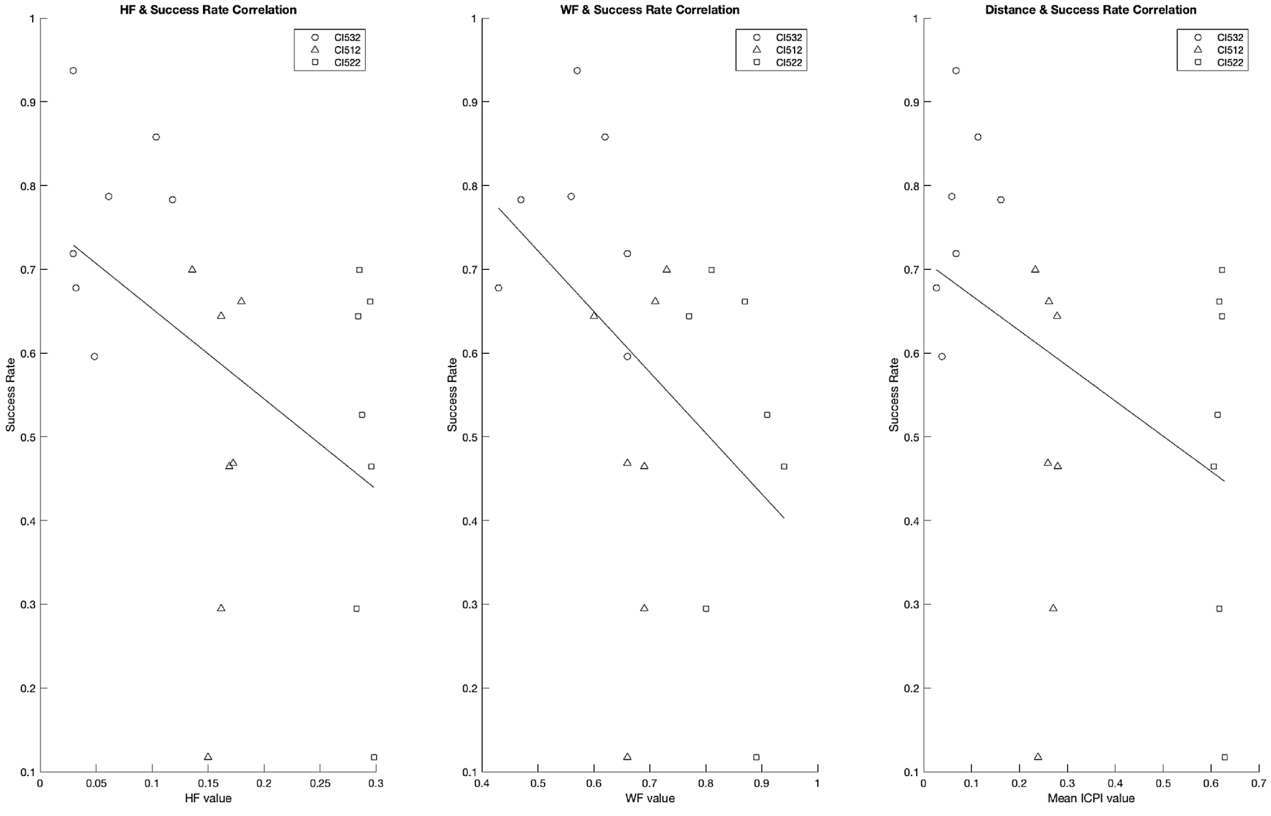

Fig. 5 Linear regression obtained between imaging scores and electrode discrimination success rate. Left, linear regression with HF ($R^2 = 0.22$), middle linear regression with WF ($R^2 = 0.20$), and right with $\overline{\text{ICPI}}$ ($R^2 = 0.19$)

of the cochlea, and the different strategies of stimulation must be consider [22, 23]. Therefore, the considerations with speech discrimination are a controversial area if we consider only the electrode discrimination [16, 35].

The final location of the CI532 and the CI512 is supposed to be both perimodiolar. However, the design of an electrode implant does not imply that after the insertion the electrode array adopt the perfect perimodiolar position. This misallocation of the electrode array can be produce due anatomy problem, smaller size of the cochlea, deformation, or due to insertion, dynamics like over-insertion. In this work, we have present that CI532 have better perimodiolar position than CI512. $\overline{\text{ICPI}}$ for CI532 is 0.08 and 0.26 for CI512 within 0.16 and 0.06 HF value, respectively. It means that the electrodes are generally place just on the modiolar wall in the CI532 electrode array.

As a weak aspect to consider in this study is, as we use different types of electrode design, we have to take into account that the different electrode surface area or half-band vs. full-band electrode might have influenced the results.

Conclusion

Nucleus CI532 offers a better perimodiolar placement than the previous multichannel cochlear implants (Nucleus CI522 and Nucleus CI512), thus affecting positively to the electrode discrimination test. The two proposed measurements, HF and ICPI, provide information about the electrode location inside the cochlea without the problems of an averaging measurement. These measurements are also related to electrode discrimination: lower $\overline{\text{ICPI}}$ values correlate with better electrode discrimination and, also, when the electrodes are placed in a more homogeneous manner, lower HF values and better electrode discrimination results are obtained.

Funding This study was not funded.

Compliance with ethical standards

Conflict of interest The Nucleus Interface Communicator (NIC) toolbox was provided by Cochlear AG for this study. No other conflict of interest or funding was used for this study.

Ethical approval All procedures performed in studies involving human participants were in accordance with the ethical standards of the institutional and/or national research committee and with the 1964 Helsinki declaration and its later amendments or comparable ethical standards.

References

1. Saunders E, Cohen L, Aschendorff A, Shapiro W, Knight M, Stecker M, Laszig R (2002) Threshold, comfortable level and impedance changes as a function of electrode-modiolar distance. Ear Hear 23(1):28S-40S
2. McKay CM, O'Brien A, James CJ (1999) Effect of current level on electrode discrimination in electrical stimulation. Hear Res 136(1–2):159–164
3. Shepherd RK, Hatsushika S, Clark GM (1993) Electrical stimulation of the auditory nerve: the effect of electrode position on neural excitation. Hear Res 66(1):108–120
4. Pfingst BE, Holloway LA, Zwolan TA, Collins LM (1993) Effects of stimulus level on electrode-place discrimination in human subjects with cochlear implants. Hear Res 66(1):108–120
5. DeVries L, Scheperle R, Bierer JA (2016) Assessing the electrode-neuron interface with the electrically evoked compound action potential, electrode position, and behavioral thresholds. J Assoc Res Otolaryngol 17(3):237–252
6. Fu QJ, Nogaki G (2005) Noise susceptibility of cochlear implant users: the role of spectral resolution and smearing. J Assoc Res Otolaryngol 6(1):19–27
7. Finley CC, Skinner MW (2008) Role of electrode placement as a contributor to variability in cochlear implant outcomes. Otol Neurotol Off Publ Am Otol Soc Am Neurotol Soc Eur Acad Otol Neurotol 29(7):920
8. Boëx C, de BalthasarC, Kós, Pelizzone MI, M (2003) Electrical field interactions in different cochlear implant systems. J Acoust Soc Am 114(4 Pt 1):2049–2057
9. Bilger RC, Black FO, Hopkinson NT (1977) Research plan for evaluating subjects presently fitted with implanted auditory prostheses. Ann Otol Rhinol Laryngol 86(3 Pt 2 Suppl 38):21–24
10. Rebscher SJ, Hetherington A, Bonham B, Wardrop P, Whinney D. Leake PA (2008) Considerations for the design of future cochlear implant electrode arrays: electrode array stiffness, size and depth of insertion. J Rehabil Res Dev 45(5):731–747
11. Staller SJ, Beiter AL, Brimacombe JA, Mecklenburg DJ, Arndt P (1991) Pediatric performance with the nucleus 22-channel cochlearimplantsystem. Am J Otol 12(Suppl):126–136
12. Ebrahimi-Madiseh A, Eikelboom RH, Jayakody DM, Atlas MD (2016) Speech perception scores in cochlear implant recipients: an analysis of ceiling effects in the CUNY sentence test (Quiet) in post-lingually deafened cochlear implant recipients. Cochlear Implants Int 17(2):75–80. https://doi.org/10.1080/14670100.2015.1114220
13. Tykocinski M, Cohen LT, Pyman BC, RolandJr T, Treaba C, Palamara J, Cohen NL (2000) Comparison of electrode position in the human cochlea using various perimodiolar electrode arrays. Am J Otol 21(2):205–511
14. Macias AR, Morera C, Manrique M, Garcia-Ibanez L, Perez D, Caballe L, Estrada E (2007) Perimodiolar electrode position: effects on thresholds, comfort levels, impedance measurements, and neural response telemetry. Mediterr J Otol 3:140–149
15. Cushing SL, Daly MJ, Treaba CG, Chan H, Irish JC, Blaser S, Papsin BC (2012) High-resolution cone-beam computed tomography: a potential tool to improve atraumatic electrode design and position.Acta Otolaryngol 132(4):361–368. https://doi.org/10.3109/00016489.2011.644805
16. Holden LK, Finley CC, Firszt JB, Holden TA, Brenner C, Potts LG, Skinner MW (2013) Factors affecting open-set word recognition in adults with cochlear implants. Ear Hear 34(3):342–360. https://doi.org/10.1097/AUD.0b013e3182741aa7
17. Iso-Mustajärvi M, Matikka H, Risi F, Sipari S, Koski T, Willberg T, Dietz A (2017) A new slim modiolar electrode array for cochlear implantation: a radiological and histological study. Otol Neurotol 38(9):e327–e334
18. Xu J, Xu SA, Cohen LT, Clark GM (2000) Cochlear view: postoperative radiography for cochlear implantation. Am J Otol 21(1):49–56

19. Cohen LT, Xu J, Xu SA, Clark GM (1996) Improved and simplified methods for specifying positions of the electrode bands of a cochlear implant array. Am J Otol 17(6):859–865
20. Ketten DR, Skinner MW, Wang G, Vannier MW, Gates GA, Neely JG (1998) In vivo measures of cochlear length and insertion depth of nucleus cochlear implant electrode arrays. Ann Otol Rhinol Laryngol 175:1–16
21. Noble JH, Labadie RF, Gifford RH, Dawant BM (2013) Image-guidance enables new methods for customizing cochlear implant stimulation strategies. IEEE Trans Neural Syst Rehabil Eng 21(5):820–829. https://doi.org/10.1109/TNSRE.2013.2253333
22. Henry BA, McKay CM, McDermott HJ, Clark GM (2000) The relationship between speech perception and electrode discrimination in cochlear implantees. J Acoust Soc Am 108(3):1269–1280
23. Vickers D, Degun A, Canas A, Stainsby T, Vanpoucke F (2016) Deactivating cochlear implant electrodes based on pitch information for users of the ACE strategy. Adv Exp Med Biol 894:115–123
24. Cosentino S, Carlyon RP, Deeks JM, Parkinson W, Bierer JA (2016) Rate discrimination, gap detection and ranking of temporal pitch in cochlear implant users. J Assoc Res Otolaryngol 17(4):371–382
25. Zaballos MP, de Miguel AR, Killian M, Macías AR (2016) A Psychophysics experimental software to evaluateelectrical pitch discrimination in Nucleuscochlearimplantedpatients. J Phys Conf Ser 689(1):012030 (**IOP Publishing**)
26. Zwolan TA, Collins LM, Wakefield GH (1997) Electrode discrimination and speech recognition in postlingually deafened adult cochlear implant subjects. J Acoust Soc Am 102(6):3673–3685
27. Marx M, Risi F, Escudé B, Durmo I, James C, Lauwers F, Fraysse B (2014) Reliability of cone beam computed tomography in scalar localization of the electrode array: a radio histological study. Eur Arch Otorhinolaryngol 71(4):673–679. https://doi.org/10.1007/s00405-013-2448-6
28. Saeed SR, Selvadurai D, Beale T, Biggs N, Murray B, Gibson P, Boyd P (2014) The use of cone-beam computed tomography to determine cochlear implant electrode position in human temporal bones. Otol Neurotol 35(8):1338–1344. https://doi.org/10.1097/MAO.0000000000000295
29. Lathuillière M, Merklen F, Piron JP, Sicard M, Villemus F, de Champfleur NM, Mondain M (2017) Cone-beam computed tomography in children with cochlear implants: the effect of electrode array position on ECAP. Int J Pediatr Otorhinolaryngol 92:27–31. https://doi.org/10.1016/j.ijporl.2016.10.033
30. Dahmani-Causse M, Marx M, Deguine O, Fraysse B, Lepage B, Escudé B (2011) Morphologic examination of the temporal bone by cone beam computed tomography: comparison with multislice helical computed tomography. Eur Ann Otorhinolaryngol Head Neck Dis 128(5):230–235. https://doi.org/10.1016/j.anorl.2011.02.016
31. Ruivo J, Mermuys K, Bacher K, Kuhweide R, Offeciers E, Casselman JW (2009) Cone beam computed tomography, a low-dose imaging technique in the postoperative assessment of cochlear implantation. Otol Neurotol 30(3):299–303. https://doi.org/10.1097/MAO.0b013e31819679f9.
32. Hodez C, Griffaton-Taillandier C, Bensimon I (2011) Cone-beam imaging: applications in ENT. Eur Ann Otorhinolaryngol Head Neck Dis 128(2):65–78. https://doi.org/10.1016/j.anorl.2010.10.008
33. Pfingst BE, Burkholder-Juhasz RA, Zwolan TA, Xu L (2008) Psychophysical assessment of stimulation sites in auditory prosthesis electrode arrays. Hear Res 242(1–2):172–183. https://doi.org/10.1016/j.heares.2007.11.007
34. Skinner MW, Holden TA, Whiting BR, Voie AH, Brunsden B, Neely JG, Finley CC (2007) In vivo estimates of the position of advanced bionics electrode arrays in the human cochlea. Ann Otol Rhinol Laryngol 197:2–24
35. Polonenko MJ, Cushing SL, Gordon KA, Allemang B, Jewell S, Papsin BC (2016) Stimulation parameters differ between current anti-modiolar and peri-modiolar electrode arrays implanted within the same child. J Laryngol Otol 130(11):1007–1021

4.3 Third publication

4.3.1 Publication Information

Title: A multiobjective optimization procedure for the electrode design of cochlear implants.
Authors: Ángel Ramos de Miguel, José M. Escobar, David Greiner and Angel Ramos Macias
Journal: International Journal for Numerical Methods in Biomedical Engineering
DOI: 10.1002/cnm.2992

Received: 29 May 2017 | Revised: 15 February 2018 | Accepted: 1 April 2018

DOI: 10.1002/cnm.2992

RESEARCH ARTICLE - APPLICATION

WILEY

A multiobjective optimization procedure for the electrode design of cochlear implants

Ángel Ramos-de-Miguel[1] | José M. Escobar[1] | David Greiner[1] | Ángel Ramos-Macías[2]

[1]University Institute of Intelligent Systems and Numerical Applications in Engineering (SIANI), University of Las Palmas de Gran Canaria, Las Palmas, Spain

[2]Otolaryngology Head and Neck Surgery, University and Children's Hospital Insular of Las Palmas, Las Palmas, Spain

Correspondence
Ángel Ramos-de-Miguel, University Institute of Intelligent Systems and Numerical Applications in Engineering (SIANI), University of Las Palmas de Gran Canaria, Las Palmas, Spain.
Email: aramos.gcc@gmail.com

Funding information
Spanish Government; "Secretaría de Estado de Universidades e Investigación,"; "Ministerio de Economía y Competitividad,"; FEDER, Grant/Award Number: CTM2014-55014-C3-1-R

Abstract

This paper presents a new procedure to design optimal electrodes for cochlear implants. The main objective of this study is to find a set of electrode designs that maximize the focalization and minimize the power consumption simultaneously. To achieve that, a criterion to measure the ability of focalization of an electrode is proposed. It is presented a procedure to determine (1) the electrical potential induced by an electrode by solving the Laplace equation through the finite element method; (2) the response of a neuron to an applied field using NEURON, a compartmentalized cell model; (3) the optimization to find the best electrode designs according to power consumption and focalization by 2 evolutionary multiobjective methods based on the non-dominated sorting genetic algorithm II: a straight multiobjective approach and a seeded multiobjective approach. An electrode design formed by 2 conductive rings with a possible difference of potential between them is proposed. It is analyzed that the response of the neuron is determined by the shape and the difference of the potential between the electrode rings. Our procedure successfully achieves a nondominated set of optimum electrode designs improving a standard electrode in both objectives, as designs with better focalization allow to include extra electrodes in the cochlear implant, and designs with lower power consumption extend the length of the battery.

KEYWORDS

cochlear implants, conduction model, FEM, multiobjective optimization, neural excitation, NSGA-II

1 | INTRODUCTION

Electrical stimulation of the auditory nerve has been used for 40 years[1] for the restoration of severe-to-profound hearing loss due to a sensorineural disease. The auditory nerve (AN) is located in the inner ear. The cochlea, found in the inner ear, is the organ where the sound, as a pressure wave, is transformed into an electrical pulse to be transmitted by the neurons to the auditory cortex.

The cochlea, found in the inner ear, is composed of the scala vestibuli, scala media, and the scala tympani , which are separated by the Reissner's membrane (between scala vestibuli and scala media), and the basilar membrane (between scala media and scala tympani). On the basilar membrane, it is located in the organ of Corti, where the inner hair cells transform the vibration of the basilar membrane into a nerve stimulus to be sent to the auditory cortex through the AN.

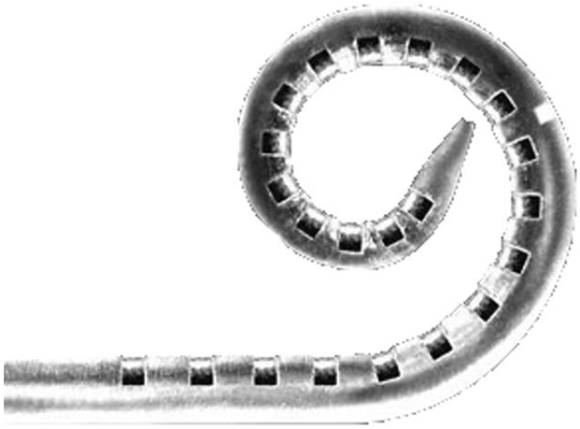

FIGURE 1 Commercially available electrode array

The cochlea acts like a mechanical Fourier transformer. This is called the tonotopic organization of the cochlea, where each part of the Basilar Membrane is tuned to one frequency to produce the maximum vibration on itself. The frequencies are distributed in the cochlea with the low frequencies on the apex and the high frequencies on the base of the cochlea. In practice, it is presumed that the frequency alignment follows the Greenwood function,[2] which assigns a characteristic frequency to an AN fiber (ANF) based on the position of its peripheral tip along the basilar membrane.[3]

Modern cochlear implants (CIs) try to imitate the natural tonotopic encoding by using a multichannel electrode array. To take advantage of this cochlea's tonotopical organization of neurons, each electrode stimulates different subpopulations of the ANF in the inner ear, and thus, provides a different psycho-acoustic perception. The pitch perception resulting from stimulating this subpopulation depends on the electrode's location in the cochlea. Previous studies indicate that up to 7 or 8 independent electrodes can be stimulated.[4-7] This is due to the channel interaction where the electrical current spreads out widely along the cochlea, thereby exciting a wide population of ANF and consequently decreasing the selectivity and the number of effective electrodes. In some cases, the best solution to reduce the channel interaction and to increase the sound quality is to disconnect some electrodes with a high channel interaction.[8]

Although these multichannel prostheses have been demonstrated to be better than the to previous single channel devices,[9] the ideal result, ie, understanding speech without the help of visual cues is only achieved in a minority of patients.[10]

All the commercially available cochlear systems present a similar electrode design: This electrode is basically a flat electrode on the surface of the silicon array as shown on Figure 1.

Currently, most patients use 2 different stimulation modes, monopolar (MP) or bipolar (BP). In the MP mode, the stimulation is produced between one intracochlear electrode and one or 2 extra-cochlear electrodes, the reference electrodes are placed under the temporal muscle. In the BP mode, the stimulation is produced between 2 intracochlear electrodes. The MP mode produces a detrimental wider channel interaction than the BP mode but requires less energy to generate an effective stimulation, producing a hearing feeling on the patient.[11] Despite the theoretical advantageous reduction of the channel interaction of the of BP mode, psychophysical and speech recognition measurements show a similar channel interaction in both stimulation modes.[12] It is important to highlight that in both stimulation modes, the inactive electrodes are isolated.

As in other electrical stimulation topics like the stimulation of central nervous system, trying to focus the stimulus without, or with a minimum, increase of the power consumption can be a problem. Modeling approaches have been used in many cases to describe and to predict the effects of electrical stimulation on neural elements.[13-18] Most of the approaches divide the model on 2 stages; in the first one, the electric field pattern produced by the electrical stimulation is calculated, and in the second one, the neural response to the electric field pattern is calculated.

In this study, the main objective is to obtain the optimum shape design of a cochlear implant electrode—within a cochlear implant system—simultaneously minimizing the power consumption and maximizing its focalization capability. The reduction of power consumption is related with a higher duration of the batteries in a cochlear implant. Maximizing the focalization capability of a single electrode is related with fewer channel interactions and with a higher number of electrodes in the implant system, as that would increase the hearing quality of the patient. Classical methods of optimization frequently need the calculation of derivatives and stagnate easily in local optima, while the use of evolutionary

algorithms (EAs) are not constrained by these limitations. Evolutionary algorithms have been demonstrated to be appropriate optimization techniques, both in single and in multiobjective optimizations in real-world engineering problems, see, eg, previous works.[19-23] Particularly in the case of evolutionary multiobjective optimization (EMO),[24] they allow to achieve a nondominated front of equally optimum solutions in one single execution. This study presents an innovative design consisting of 2 concentric rings with a dielectric material placed between them. In this design, there is an extracochlear ground electrode (0V). The optimal shape design is varied and focused towards the power consumption and focalization capability, and it is developed by using evolutionary multiobjective algorithms. More concretely, the nondominated genetic algorithm 2 (NSGA2)[25] is used in this work.

Our study proposes a methodology for the optimization of the cochlear implant electrodes centered on the electrical stimulus focalization capability and on the reduction of the energy requirements for the AN stimulation. This allows us to perform comparisons between the electrodes. It must be remarked that a simplified model is used in this study, in which the electrode—AN—interaction is evaluated without considering the rest of the cochlea.

Summarizing the contributions of this study:

1. Modeling of the electrostatic potential created by the proposed electrode is performed by the finite element method (FEM). This problem involves movable boundaries, and then, a modification of the mesh used in FEM. We opted for mesh adaption instead of remeshing, because mesh adaption keeps constant the number of elements and therefore stabilizes the discretization error. The electric potential is used to evaluate the simulation of the neuron activation pattern.
2. In the optimization procedure, 2 EMO approaches are compared: (1) a standard EMO with random initial population and (2) an EMO where the optimum solution of a weighted sum approach single-objective EAs is injected in the initial population. Both procedures maintain constant the total number of fitness evaluations as a stopping criterion.
3. The axial symmetrical electrode with dielectric material proposed in this study achieves designs with both better values of focalization and consumption than the usual cochlear implant electrode. Additionally, it is provided a well distributed nondominated front of solutions where the best value of consumption is given for each value of focalization capability; or alternatively seen, the best value of focalization capability is given for each value of consumption.

In Section 2, the modeling and simulation method applied to evaluate the fitness functions values is described. In Section 3, the optimization design procedure by using multiobjective evolutionary algorithms is described. In Section 4, the performance of EMO approaches is analyzed. In Section 5, experimental results are given. And, finally, the conclusions of this study can be consulted in Section 6.

2 | MODELING AND SIMULATION

The main objective of this study is to design an optimal electrode assembly according to the focalization and power consumption saving criteria. An electrode configuration that would maximize the focalization and minimize the power consumption is searched. An initial basic electrode is formed by 2 conductive rings separated by a dielectric material, as shown on Figure 2. In this section, the modelization and simulation procedure to evaluate consumption and focalization is described.

This section is divided into 4 subsections. In Section 2.1, the electrostatic potential is calculated by means of FEM. Section 2.2 shows the procedure to adapt the mesh to the movable boundaries. Section 2.3 describes the use of NEURON[26] to estimate the neural response. Finally, in Section 2.4, the fitness functions to achieve the mentioned objective are proposed.

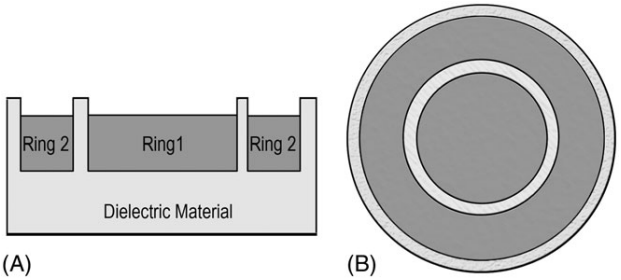

FIGURE 2 Sketch of the proposed electrode formed by 2 conductive rings. A, cross section with the current pattern and B, zenithal view

2.1 | Numerical simulations with FEM

Numerical simulations are required to calculate the electrical potential in complex domains. More concretely, FEM was used to model the electrode in a cochlea medium. The typical characteristics of a cochlear stimulus are a pulse width around 25 μS and a stimulation rate around 1 kHz. Although this is a dynamic problem, it can be solved using an electrostatic model, as shown in Bossetti et al.[27]

This electrostatic problem is determined by the Laplace equation with Dirichlet and Neumann boundary conditions

$$\Delta u = 0 \qquad in \ \ \Omega, \tag{1}$$

$$u = g \qquad on \ \ \Gamma_D, \tag{2}$$

$$\nabla u \cdot \mathbf{n} = 0 \qquad \Gamma_N, \tag{3}$$

where Ω is the domain with boundary $\partial\Omega = \Gamma = \Gamma_D \cup \Gamma_N$, being $g : \Gamma_D \to \mathbb{R}$.

Let it be

$$u_h = \sum_{i=1}^{n} u_i \phi_i + g_h \tag{4}$$

the approximation of u given by FEM, where g_h is an interpolant of the Dirichlet condition g, ϕ_i are the basis functions and u_i are the unknown potential values on the mesh nodes.

The unknowns u_i are calculated by solving the linear system of equations

$$\sum_{i=1}^{n} u_i a(\phi_i, \phi_j) + a(g_h, \phi_j) = 0 \ \forall_j = 1, \ \dots \ , n. \tag{5}$$

That is,

$$\mathbf{Ku} = \mathbf{f}, \tag{6}$$

where $\mathbf{K} = [\mathbf{K}_{j,i}]_{j,i=1}^{n}$ is the stiffness matrix, being $\mathbf{K}_{j,i} = a(\phi_i, \phi_j)$;
$\mathbf{f} = -a(g_h, \phi_j)_{j=1}^{n}$ is the load vector;
$\mathbf{u} = (u_1, u_2, \ \dots \ , u_n)^T$ is the vector of unknown coefficients; and
$a(u, v) = \int_\Omega \nabla u \cdot \nabla v \, d\Omega$ is a bilinear symmetric form.

This study focuses on the region closely located to the intracochlear electrode, where the neural tissue is placed. The numerical simulation is performed in a simplified geometry, similar to the one shown in Figure 3. A homogeneous axisymmetric domain with constant electric properties is considered. The area around the electrode is highly detailed, and the corresponding mesh is very refined, (ie, see Figure 4). FEM simulation was done by using linear Lagrange elements with three Gauss quadrature points.

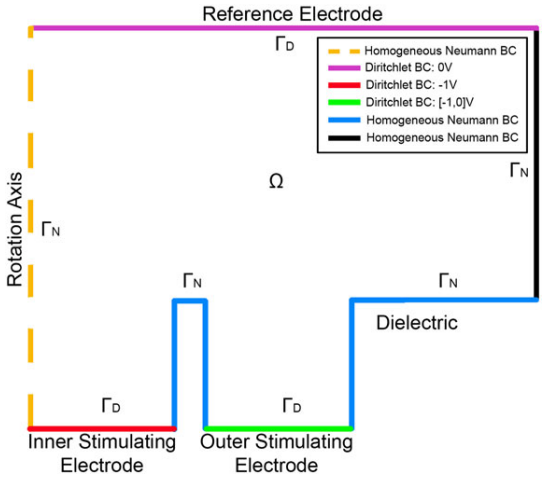

FIGURE 3 Representation of the computational domain. Rotation axis (yellow); inner stimulating ring electrode (red); outer stimulating ring electrode (green); dielectric material (blue); reference electrode (purple)

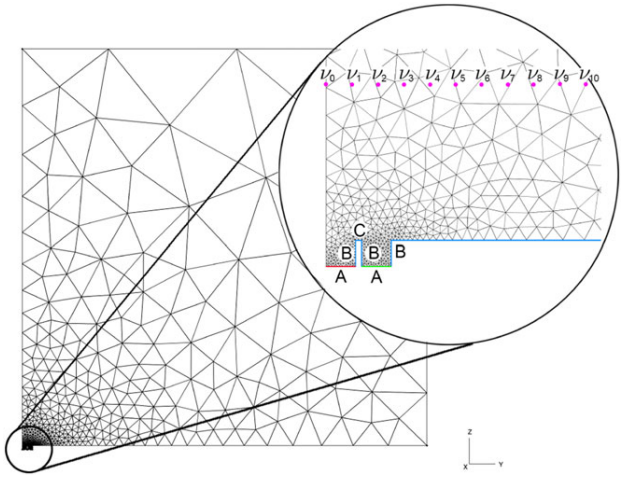

FIGURE 4 Reference mesh: Electrode size of 0.25 mm radius and 0.1 mm of height. Lengths: A=0.1125 mm, B=0.1 mm, C=0.025 mm; All mesh size: 10 mm (width) x 10.1 mm (height). On blue, we show the Neumann boundary condition which are the dielectric material and the model frontier. On red, we show the central electrode which has a fixed −1 V Dirichlet condition, and on green, we show the outer ring electrode which varies his potential from [−1,0] V. The zoom shows the region around the electrodes. The positions of the neurons are represented by pink dots. The reference electrode is set in the upper boundary of the domain

As our goal is to compare different electrode designs, only the relative values of focalization, potential, power, etc, are considered relevant. Therefore, only graphics of normalized values of power and focalization are presented. The computation of realistic values of power consumption requires anatomically accurate models, but this approach is not considered in this paper.

The geometry of the model is a cylinder of 10 mm radius and 10.1 mm height with a stimulating ring electrode in the bottom and the reference one on the top. The diameter of the outer ring of the electrode is 0.5 mm, similar to the size of the current commercially available electrodes.

In this paper, a domain with symmetry of revolution simulated as a 2D axisymmetric FEM problem is considered.

The boundary conditions applied to the model are the following:

- Dirichlet boundary conditions:

  Reference electrode: 0V
  Inner stimulating electrode: −1 V
  Outer stimulating electrode arranging the interval $[-1, 0]$V (variable to optimize)

- Homogeneous Neumann boundary conditions ($\nabla u \cdot \mathbf{n} = 0$) at the dielectric components, rotation axis, and peripheral boundary.

It is important to consider that the fitness function for the multiobjective optimization is based on power consumption (it is explained on Section 2.4). The calculation of the power consumption, being, the power consumed by an electrode assembly contained on a domain Ω, is given by $\int_\Omega \mathbf{J} \cdot \mathbf{E} d\Omega = \int_\Omega \sigma \|\mathbf{E}\|^2 d\Omega$, where $\mathbf{E}$ is the electric field, $\mathbf{J}$ is the current density, and σ the conductivity of the medium. As the electrodes assembly has an axisymmetric configuration and a constant conductivity of the medium is considered, the power consumed can be expressed as

$$P_0 = 2\pi\sigma \sum_{e=1}^{N_e} \int \int_{\Delta_e} \|\nabla u_h\|^2 r dr dz, \tag{7}$$

where Δ_e is the e-th element of $\Omega = \cup_{e=1}^{N_e} \Delta_e$ and N_e is the number of elements of the mesh.

Figure 5 shows the current lines corresponding to 2 different designs with the same geometry and different outer electrode potential. The 2D FEM simulation was done using the mesh of Figure 3, but it is only represented a zoom around the electrode. It can be observed that the current line patterns change depending on the electrode potential configuration.

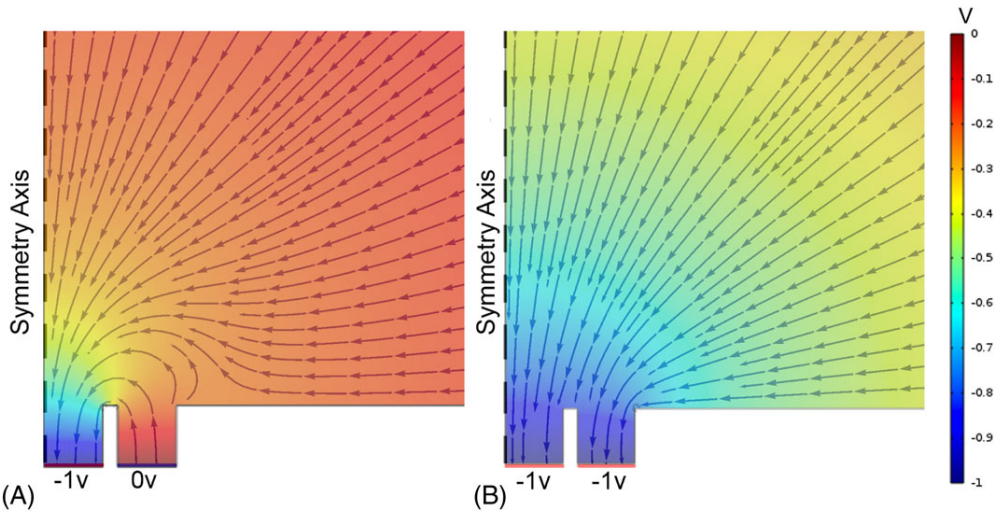

FIGURE 5 Zoom around the electrode showing current lines of two 2D simulations with the reference electrode at 0 V, the inner electrode at −1 V and the outer electrode at A, 0 V and B, −1 V

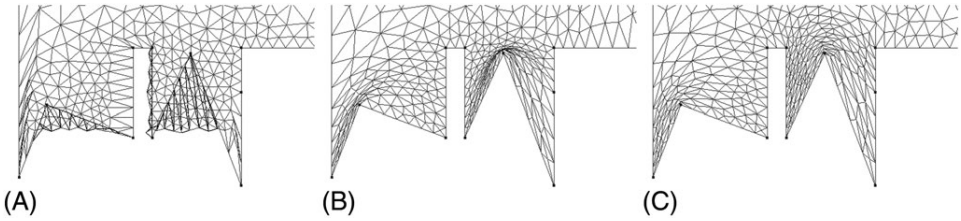

FIGURE 6 All stages of mesh generation, focused on the electrode part. A, First stage: mesh boundary deformation, B, second stage: RBF deformation to move inner nodes, C, third stage: mesh optimization

2.2 | Mesh adaptation for domains with movable boundaries

The objective is to find an optimal shape for the rings that conform the stimulating electrode. For that proposal, the profile of the conductors and dielectric rings at every optimization iteration is changed. Thus, we are involved in a FEM problem with movable boundaries. This kind of problems could be solved by remeshing the domain or by deforming the given mesh. The second option was chosen because it is less troublesome than generating a new mesh every time the boundary is changed. The main advantage of deforming the mesh is that we keep constant the number of elements and we maintain almost constant the refinement of the features of the geometry and then the discretization error.

2.2.1 | Geometry redefinition

The movable boundary, concerning to the conductors and dielectric rings of the stimulating electrode, is composed of a set of segments. The deformation of the boundary is conducted by moving the vertices, v_i, of these segments, see Figures 6 and 12. The coordinates of the vertices are considered as degrees of freedom and then replaced following the optimization procedure.

2.2.2 | Mesh adaptation

Once the vertices v_i have been placed in their new positions, the boundary nodes of the mesh are moved to define the new boundary. These movements are determined by affine transformations that preserve the straightness of the segment.

In general, the displacements of the boundary nodes produce a tangled mesh, so the inner nodes must be reallocated. This is performed using an untangling and optimization process.[28] This process is based on a quality improvement of the mesh obtained by an iterative process where each node of the mesh is moved to a new position that minimizes an objective function. The objective function is derived from a quality measure of the *local mesh*, that is, the set of triangles connected to the adjustable *free node*.

Algebraic quality and distortion measures previously proposed by Knupp[29] were used. These measures are defined in terms of the deviation from an ideal triangle that represents the desired shape to achieve.

Let τ be a triangle whose vertices are given by $\mathbf{x}_k = (x_k, y_k)^T \in \mathbb{R}^2,\ k = 0, \dots, 2$ and τ_R being the reference triangle with vertices $\mathbf{u}_0 = (0,0)^T,\ \mathbf{u}_1 = (1,0)^T$ and $\mathbf{u}_2 = (0,1)^T$. If we choose $\mathbf{x}_0$ as the translation vector, the affine map that takes τ_R to τ is $\mathbf{x} = A\mathbf{u} + \mathbf{x}_0$, where A is the Jacobian matrix of the affine map referenced to node $\mathbf{x}_0$, and expressed as $A = (\mathbf{x}_1 - \mathbf{x}_0, \mathbf{x}_2 - \mathbf{x}_0)$.

Let us consider that τ_I is our ideal or target triangle whose vertices are $\mathbf{v}_0, \mathbf{v}_1$ and $\mathbf{v}_2$. If we take $\mathbf{v}_0 = (0,0)^T$, the linear map that takes τ_R to τ_I is $\mathbf{v} = W\mathbf{u}$, where $W = (\mathbf{v}_1, \mathbf{v}_2)$ is its Jacobian matrix.

The affine map that takes τ_I to τ is given by $\mathbf{x} = AW^{-1}\mathbf{v} + \mathbf{x}_0$, and its Jacobian matrix is $S = AW^{-1}$. Quality metrics of the triangle τ can be defined in terms of the matrix S. More concretely, we have used the *mean ratio*

$$q = \frac{2s}{\|S\|^2}, \tag{8}$$

as it is an easily computable algebraic quality metric of τ, where $s = \det(S)$ and $\|S\|$ is the Frobenius norm of S. The maximum value of q is the unity, and it is reached when $A = \mu RW$, where μ is a scalar and R is a rotation matrix. In other words, q is maximum if and only if τ and τ_I are similar triangles. Additionally, any flat triangle has quality measure zero.

The distortion measure for a triangle is defined as the inverse of its quality, ie, $\eta = 1/q$. The distortion η is equal to 1 for the ideal triangle and tends to ∞ when the triangle tends to be degenerated. The objective function to be minimized is defined as $K = \sum_{i=1}^{N} \eta_i^p$, where N is the number of triangles in the local mesh and, usually, $p = 1$ or $p = 2$.

The objective function K becomes discontinuous when the volume of any triangle tends to zero. Due to these singularities, the function K improves the quality of valid elements but it does not work properly when the mesh is tangled ($s \leq 0$). Escobar et al[30] proposed a modification of K by replacing s with the positive and increasing function $h(s) = \frac{1}{2}(s + \sqrt{s^2 + 4\delta^2})$. The value of δ is selected in terms of the local mesh under consideration, reducing its value as much as possible and in such a manner to permit that the evaluation of the minimum of the modified function does not present any computational problem. For more details, see Escobar et al.[28] Then, the modified distortion becomes

$$\eta^* = \frac{\|S\|^2}{2h(s)}. \tag{9}$$

This modification eliminates the barriers associated with their singularities and the new objective function

$$K^* = \sum_{i=1}^{N} (\eta_i^*)^p \tag{10}$$

becomes smooth in $\mathbb{R}^2$. In the feasible region (subset of $\mathbb{R}^2$ where the free node could be placed for the local mesh to be valid), the modified objective function K^* approximates the original function K as $\delta \to 0$, and then, the minimum of the original and modified objective functions are nearly identical when δ is small. When this region does not exist, the minimum of the modified objective function is located so it tends to untangle the local mesh. Thus, the modified objective function allows the simultaneous untangling and smoothing of the mesh. The unconstrained optimization problem can be easily solved by using any standard method, see, for example, Dennis and Schnabel.[31]

To accelerate the optimization and untangling processes, it is convenient to reallocate the inner nodes in positions that diminish the number of tangles and the distortion of the mesh. To perform this reallocation, Radial Basic Functions (RBF) was used,[32] although other techniques based on Laplacian smoothing or Coons patches could be used. Specifically, once the boundary has been moved to its new location, the displacement $\boldsymbol{\delta}h_i$ applied to each boundary node, initially placed in h_i, was calculated. Then, a deformation function $\mathbf{d}(\mathbf{x})$ was defined. This function determines the displacement of all the nodes of the mesh enforcing the prescribed displacement of the boundary nodes, that is, $\mathbf{d}(h_i) = \boldsymbol{\delta}h_i$.

2.3 | AN simulation

To calculate the neuron response, the target neuron is segmented in compartments and the stimulation potential of each compartment is calculated by FEM. For this purpose, the NEURON software[26] provides a very suitable environment to perform these cable-equation–based calculations.

Neurons are modelized by NEURON with a set of compartment that represent the myelin sheaths and the Ranvier nodes of the neuron. The neuron stimulation is driven by the external potential on the Ranvier nodes and it is calculated by FEM.

The following subsections describe the position and the definition of neurons.

2.3.1 | Position of neurons

The cochlear nerve is the one composed by the axon fibers of neurons whose cell bodies are in the spiral ganglion of the cochlea. The CIs try to stimulate this region.

A CT to 12 patients was performed to determine the distance between the electrodes and the spiral ganglion, with a distance between slices of 0.625 mm. The selected patients were implanted with a Cochlear Nucleus CI24RE and the measurement was made in a total of 264 electrodes. For the visualization of the radiological images, OsiriX software was used.[33] From these data, a cochlear view was extracted as described by Cohen.[34] A postoperative analysis was performed to determine the average distance from the electrodes to the spiral ganglion between the electrodes. The average distance h was 0.6 mm from the electrode to the spiral ganglion (see Figure 7). The distance between electrodes depends on manufactures and the implant model. In this work, we have considered that the distance between electrodes is 1 mm, as it is a typical value.

Based on anatomical measurements, a total of 21 neurons in the complete domain was placed. As the FEM problem is modeled as an axisymmetric domain, only a central neuron over the electrode and $N = 10$ neurons along the y axis (see Figure 8) were required. The central neuron, v_0, is placed just over the electrode at a distance of $h = 0.6$ mm (z axis). The other neurons are placed at the same z position separated a distance $d = 0.1$ mm from each other (on y axis). The furthest neuron is sited at $Nd = 1$ mm.

The proposed focalization measurement is based on the neural activation. To determine whether a specific neuron is activated or not when we apply a stimulus, NEURON software was used. The neurons are defined in NEURON geometrically, electrically, and biophysically according to the first neuron of the human inner ear. The advantage of this method is that we have a simulated neuron that we can stimulate.

Alternatively, the response could be calculated by using an activating function that indicates the probability of activating a neuron. The problem of this method is that it does not consider any physical or biophysical condition, and depending on the situation, the probability of stimulating the neuron does not guarantee the activation of the neuron.

2.3.2 | Neuron definition

The neuron morphology[17] of this study is represented in Figure 9. It is characterized by a total length of 2.155 mm (x axis), a diameter of 3 μm and 10 μm at the soma.

The electrical properties of the neuron are divided in 2 main classes. In the first one, myelin parts of the neuron are defined as a passibe membrane with an equilibrium potential of −65 mV. The second class are the nodes which are defined as a Hodgkin-Huxley membrane. The maximum specific sodium channel conductance is 1.2 S/cm^2, the maximum specific potassium channel conductance is 0.09 S/cm^2, the maximum specific leakage conductance is 0.02 S/cm^2, the reversal potential for the sodium channel is 50 mV, the reversal potential for the potassium channel is −77 mV, and the reversal potential for the leakage channel is −54.3 mV. The temperature of the neuron is 37° C.

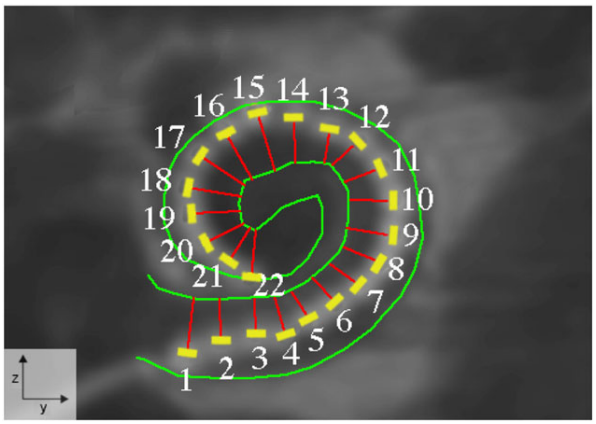

FIGURE 7 Example of the calculation to extract the distance between the electrodes, yellow marks, and the spiral ganglion, green line

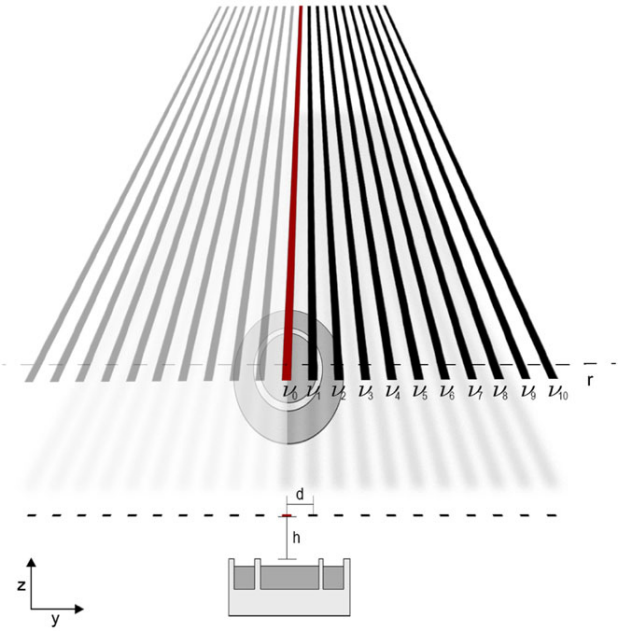

FIGURE 8 Relative position of neurons to the electrode. Neuron 0 is placed just over the electrode

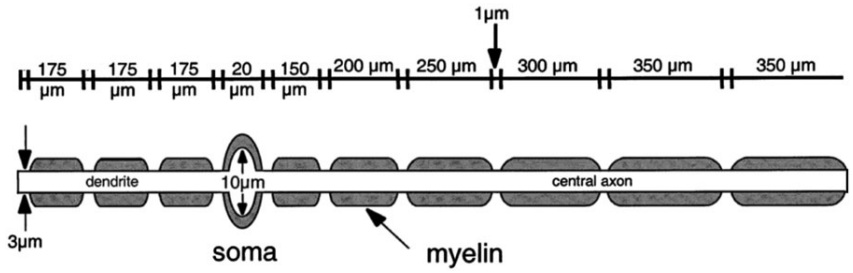

FIGURE 9 The morphology of the auditory nerve fiber model used in the calculations. The length of the myelinated internodes in the dendrite are scaled to hold the soma constant with respect to the basilar membrane[15]

Finally, the electrical stimulus was based on a biphasic stimulus with a pulse width of 25 μSec and a interphase gap of 8 μSec.

2.4 | Fitness functions evaluation

In relation with the focalization, an appropriate fitness function to compare the different electrode designs is essential. This fitness function depends on the neural activation, which is simulated by NEURON. So the power threshold needed to activate each neuron of the experiment must be obtained.

Let uh the FEM solution of a given electrode design. If ν_n is the n-th neuron of the set of neurons surrounding the electrode (see Figure 8), there is a constant g_n such that $g_n u_h$ is the threshold potential to stimulate the neuron νn. In otherwords, gn is the minimum gain that assure the stimulation of ν_n but not the farthest ν_{n+1}. As it can be expected, less power is required to activate the neuron close to the electrode than to activate other neurons. The power required to activate ν_n is

$$P_n = g_n^2 P_0, \tag{11}$$

where P_0 is given by Equation 7.

Once the threshold power of activation of each neuron, P_n, is calculated, a polynomial fit $P(r)$ of degree 4 of these values is defined.

Now, let us consider that we change the design of the electrodes and let $P^i(r)$ be the corresponding polynomial fit of the threshold power of the i-th design. Once the u_h^i solution for that design is calculated by FEM, the minimum gain such

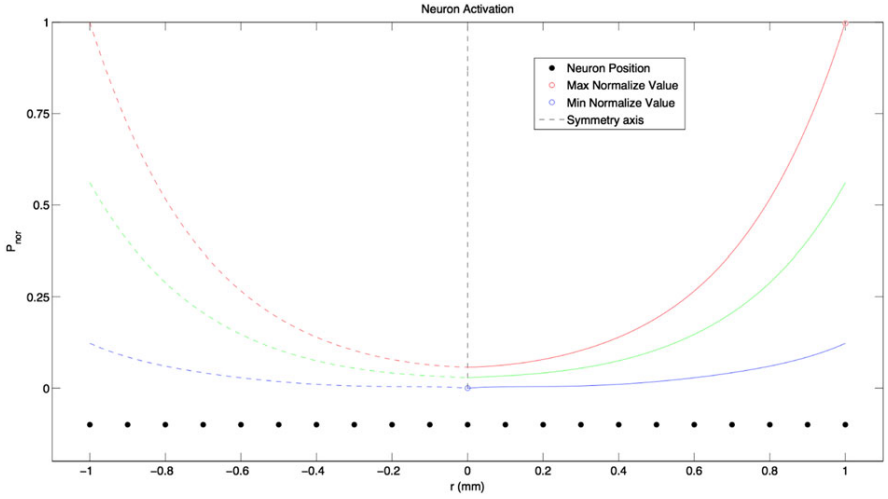

FIGURE 10 Example of focalization and power consumption of three electrode designs

that $g_n^i u_h^i$ is the minimum potential to activate the neuron n is searched. Then, the power required to activate the neuron n for the i-th design is

$$P_n^i = g_n^{i^2} P_0^i. \tag{12}$$

Therefore, $P^i(r)$ is the polynomial fit of P_n^i.

Fitness functions F_1 and F_2 that measure the focalization and power consumption are proposed. For a given design,

$$F_1^i = \int_0^{Nd} (P^i(r) - P^i(0))\, dr \tag{13}$$

represents the area under the $P^i(r)$ and measures the focalization ability, and

$$F_2^i = P^i(0) \tag{14}$$

measures the power consumption (namely, the power consumption to activate the neuron ν_0). The objectives of this procedure are the maximization of F_1 and the minimization of F_2.

To represent the different electrode designs, a power normalization of each $P^i(r)$ to the range [0,1] are performed by using the functions

$$P_{nor}^i(r) = \frac{P^i(r) - P_{thr}}{P_{max} - P_{thr}}, \tag{15}$$

where P_{thr} is the minimum threshold power for all the neurons and all the tested designs. Similarly, P_{max} is the maximum power to stimulate the farthest neuron for all the experiments. That is, $P_{thr} = \min(P^i(0))$ and $P_{max} = \max(P^i(Nd))$. With a degree 4 polynomial, $P_{nor}^i(r)$, we have obtained a maximum error of 0.0054 (0.54%) with respect to the normalized values of the power required to activate the neurons. The normalized power of three different electrode designs is shown in Figure 10. The blue curve corresponds to the design with the minimum consumption and lowest focalization and the red one is the design with the maximum consumption and highest focalization.

3 | MULTIOBJECTIVE OPTIMIZATION DESIGN PROCEDURE

The previous section has explained the way to calculate the 2 objectives involved in the optimization design procedure, which are (1) minimization of the power consumption to stimulate the first neuron, which is just over the electrode (the nearest one) and (2) maximization of the focalization behavior of the electrode design.

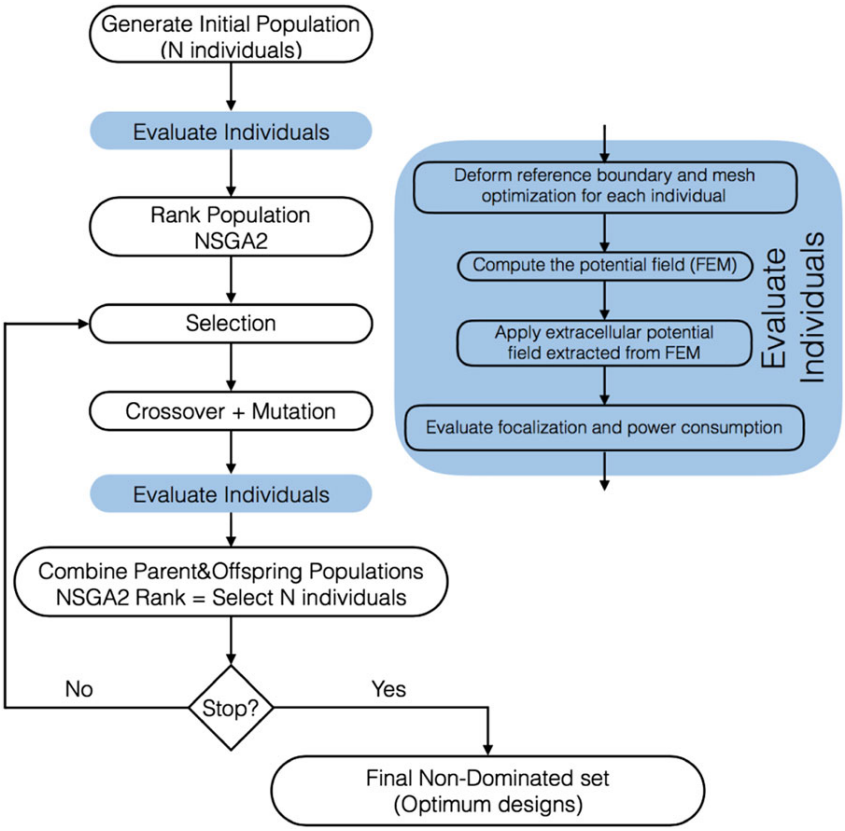

FIGURE 11 Flowchart of the automatic procedure to generate by evolutionary algorithms the desired electrodes

When solving a multiobjective optimization problem (particularly, a bi-objective optimization problem), it is essential to search for a set of equally optimum solutions among the whole set of possible solutions. This is known as the Pareto optimal set, where there is no alternative to improve one objective without worsening at least, other objective (both are conflicting objectives).[24]

To develop the multiobjective optimization, the evaluation of the 2 objectives is embedded in an automatic optimization design procedure guided through evolutionary multiobjective algorithms. Concretely, NSGA2 in this study, as shown in Figure 11. One of the higher advantages evolutionary multiobjective algorithms provided is that they are population-based global search methods, which are going to generate, in a single run, a set of optimal solutions where each electrode design gives the maximum focalization behavior, F_1, for each power consumption value, or the lowest power consumption, F_2, for each focalization value.

The following subsections describe the chromosome codification, the evolutionary algorithm operators (selection, crossover and mutation), and the compared optimization cases.

3.1 | Chromosome

A set of proposed designs is handled simultaneously with every iteration, which is equivalent to affirm that a set of individuals/chromosomes is handled simultaneously with every generation in the evolutionary algorithm terminology. Only the problem information that differentiates a proposed electrode design from another is required to be stored in every chromosome. How the chromosome is defined in our problem is described here.

Nine of 10 genes are related with the electrode shape and 1 is related with the potential difference between the 2 rings of the electrode. All of them are handled as real coded variables. The 9 genes related with the shape are shown in Figure 12. Each of these genes values has positive and negative values, which, to build the mesh, are going to be added to the value of the reference mesh. Table 1 shows maximum and minimum available values for each gene shown. The potential on the two ring electrodes are -1 V to the central electrode (green) and the value of gene 10 $[-1, 0]$V to the other electrode (blue).

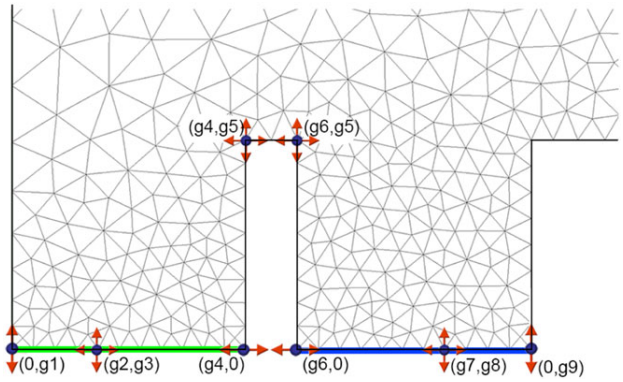

FIGURE 12 Genes of the multiobjective shape optimization (minimize power consumption and maximize focalization). Genes 1 to 9 (g1 to g9 in figure) contribute to define shape boundary of reference mesh, and gene 10 controls the potential difference between the 2 rings electrode

TABLE 1 Maximum and minimum available values for each gene

	Gene 1, mm	Gene 2, mm	Gene 3, mm	Gene 4, mm	Gene 5, mm	Gene 6, mm	Gene 7, mm	Gene 8, mm	Gene9, mm	Gene10, V
max	0.1	0.03	0.1	0.03	0	0.03	0.03	0.1	0.1	0
min	−0.1	−0.03	−0.1	−0.03	−0.2	−0.03	−0.03	−0.1	−0.1	−1

3.2 | Evolutionary algorithm

Further details of the operators of the evolutionary algorithm process as shown in Figure 11 are described in the next subsections.

3.2.1 | Selection

Evolutionary multiobjective algorithms mainly differ from single objective evolutionary algorithms in their selection method, which is focused in obtaining a wide and diverse nondominated front as close as possible to the Pareto optimal frontier. Among the state of the art evolutionary multiobjective algorithms, we will use in this study the most cited and applied to many fields of science and engineering: the NSGA2.[25] It sorts the population by successive nondominated fronts, and along each front, a crowding distance is evaluated, that gives the information if a solution is close or far to other solutions (to maintain a homogeneous density of solutions on each front). Therefore, sample individuals are ranked on the basis of the above mentioned front order first, and then, on higher to lower crowding-distance on each front.

Selection of individuals to be part of the mating pool (those set which will be later crossed) is performed by a tournament selection based on the previous ordering.

3.2.2 | Crossover and Mutation

Once the parent population has been sorted and its size has been adjusted to the maximum population size, the offspring population has to be generated from a mating pool where crossover and mutation operators are applied. For that proposal, a simulated binary crossover (SBX)[35] with a nonuniform mutation (NU-M)[36] is used. The reason by which these operators were chosen is that their simultaneous combination is the best performing variant among a set of 5 crossovers and 2 mutations EA variants in a set of 36 benchmark functions, as reported in Elsayed et al.[37]

The crossover operator SBX is widely used in practice. From parents x^1, x^2, 2 offsprings y^1, y^2 are generated as follows:

- Generate a uniform random number $rand \in [0, 1]$
- Using the previously generated $rand$, compute $\bar{\beta}$:

$$\bar{\beta} = \begin{cases} (2rand)^{\frac{1}{1+\eta}}, & rand \leq 0.5 \\ (\frac{1}{2(1-rand)})^{\frac{1}{1+\eta}}, & otherwise, \end{cases} \tag{16}$$

- Generate 2 offsprings (with $j = 1, \ldots, D$, being D the total number of genes of the chromosome):

$$y_j^1 = \frac{1}{2}[(1+\bar{\beta})x_j^1 + (1-\bar{\beta})x_j^2], \tag{17}$$

$$y_j^2 = \frac{1}{2}[(1-\bar{\beta})x_j^1 + (1+\bar{\beta})x_j^2]. \tag{18}$$

The mutation operator NU-M is a nonuniform operator where the step size is decreased as the iteration is increased, that means that the mutation in the first stages can be higher than in the last steps. Offspring $\boldsymbol{y}^z(t) = (y_1^z(t), y_2^z(t), \ldots, y_D^z(t))$ is mutated as follows:

$$y_j^z(t) = y_j^z(t) + \delta_j^z(t), \tag{19}$$

where $\delta_j^z(t)$:

$$\begin{cases} (\bar{y}_j - y_j^z(t))(1 - [rand(t)]^{(1-\frac{t}{T})^b}), & \textbf{if } rand \leq 0.5 \\ (\underline{y}_j - y_j^z(t))(1 - [rand(t)]^{(1-\frac{t}{T})^b}), & otherwise, \end{cases} \tag{20}$$

where $\bar{y}_j$ and $\underline{y}_j$ are the upper and lower boundary of individual gene y_j^z, respectively, $rand(t)$ is a random number $\in [0, 1]$, t is the generation number, T is the maximum number of generations, and b is a parameter to control the speed at which the step length decreases.[38]

3.3 | Optimization cases

In addition to the straight multiobjective optimization procedure described in the previous subsections, the insertion of a single-objective optimum design as starting seed in the multiobjective optimization will be tested. This approach works as the one described in Section 3, but including a previous application of a single-objective optimization where a weighted average fitness function with the power consumption and the focalization, as described on Section 2.4, is defined.

Once the single-objective optimization has been finished, its best individual is inserted on the initial population of a multiobjective optimization acting as a seed in the multiobjective optimization process. The use of a seed in the population of a multiobjective optimization has been demonstrated to be advantageous in some engineering design cases, eg, in Lee et al,[39] where a Nash EA optimum outcome is used as a seed of multiobjective optimization design problems in aeronautical engineering, or in Greiner et al[40] and Toledo et al,[41] where an optimization design of noise barriers using the boundary element method is enhanced in some cases with a previous single-objective optimum solution.

Both methods, the one using a single-objective weighted sum seed for multiobjective optimization (seeded MO) and the one performing a straight multiobjective optimization (straight MO), will be compared in the following section (Section 4) on the basis of an equal maximum number of total evaluations of the fitness function as stopping criterion.

4 | RESULTS AND DISCUSSION

In this section, the different nondominated optimum designs obtained by applying the modeling/simulation procedure (Section 2) are illustrated, and the outcome of the 2 optimization approaches (as described in Section 3.3), seeded MO (being 50% of fitness function evaluations allocated to the "a priori" weighted single-objective optimization, with equal weights of 0.5 assigned to each fitness function) and straight MO are compared. An additional test case of straight MO was handled, where the tenth gene corresponding to the potential value between the rings was modified from continuous values $[-1, 0]$V to the discrete values -1 or 0 V.

A total of 100 generations where evaluated on each MO scheme. The population size was 100 individuals with a generation gap of 50 individuals every generation (every generation combining 150 individuals of parent and offspring populations generate 100 new individuals of the parent population of next generation). A mutation rate of 0.1, values of ν=3 (equation 16) and b=5 (equation 20), and crossover rate of 1.0, are used.

Four independent executions have been performed for each case, taking 20 hours execution time each EA run in a MacBook Pro, Intel core i5 2.5GHz, and 8GB DDR3 RAM.

The unary metric hypervolume (HV) was used to quantify the multiobjective optimization quality (the higher the better).[42] In a bi-objective optimization, as is the case of this study, the hypervolume is the area between the nondominated

front and a dominated reference point to this front. We choose values (0,1) (according to normalized scale of Equation 15) for the reference point in our problem, as they guarantee to be dominated by any possible solution. In Figure 13, the evolution of the hypervolume average in the tested EAs is shown.

In Figure 14, a boxplot of HV final values of seeded MO and straight MO is shown. A boxplot is a graphical representation of data samples based on the minimum, first quartile, median, third quartile, and maximum. The median or second quartile is the middle red line inside box. The higher interquartile range, limited by first and third quartile, is the height of the blue box. And the higher extreme values, which extend from ends of the box to the most distant point whose value lies within 1.5 times the interquartile range, are the end of whiskers. Although no overlapping boxes are obtained, the straight MO has greater HV median, average and best, and also higher extreme values of the HV distribution. No advantages of using a seeded MO have been shown in this problem in the tested results.

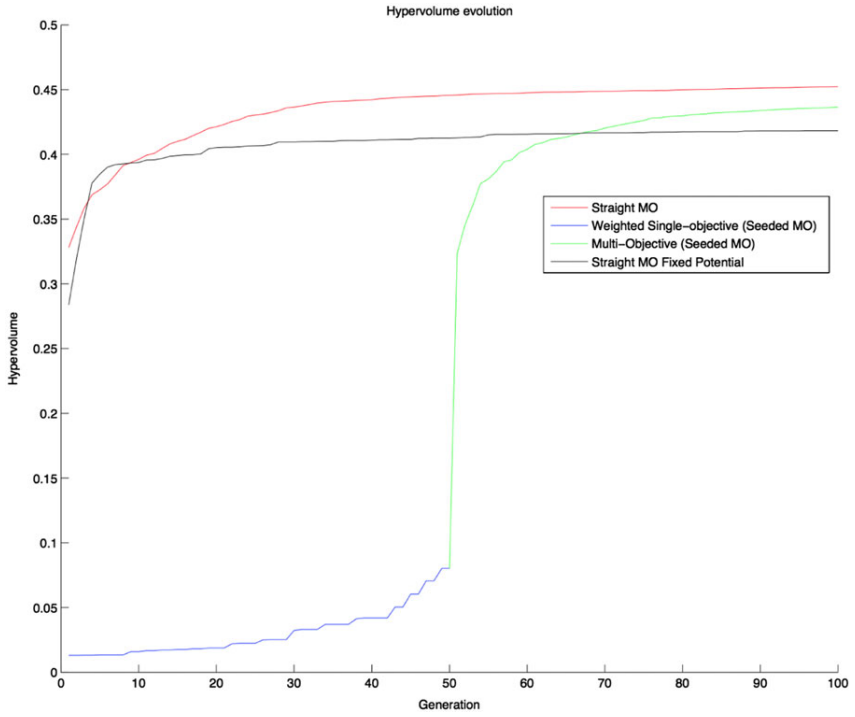

FIGURE 13 Evolution of HV average on the tested EAs schemes. The green line represents the evolution of the straight MO; the red and blue lines represent the evolution of the seeded MO: the combination of single-objective (red) on the first iterations and the multiobjective (blue) on the last iterations; and the black line represents the evolution of the 2 fixed potential multiobjective optimization

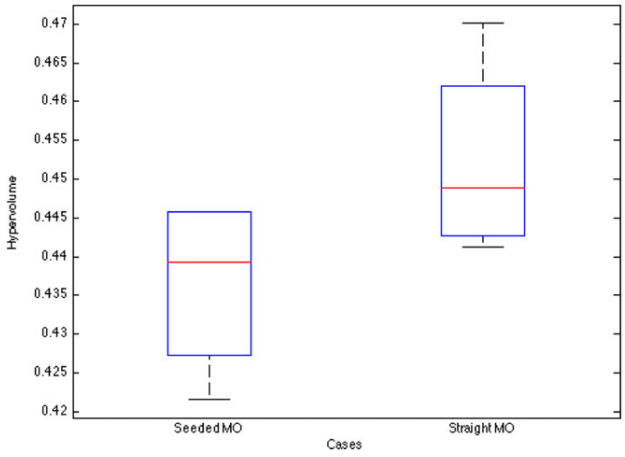

FIGURE 14 HV final values. Comparison between seeded MO and straight MO approaches

In addition, the nondominated front solutions on the last generation can be evaluated. In every cases, the 100 individuals belong to the nondominant front, so a set of the distributed individuals is represented. They range from the best focalization behavior and worst power saving to the worst focalization behavior and the best power saving.

Figure 15 shows the best accumulated nondominated fronts corresponding to different strategies. Inside the black circles, 5 representative designs are represented (A, B, C, D, and E), including the design with maximum focalization (design A) and the design with minimum consumption (design E).

A standard electrode was also tested (the black dot) to compare with nondominated optimum electrode designs. This electrode, similar to the commercially available ones, was modelized as a single disc of 0.5 mm diameter.

As it can be observed, it is a dominated design. Our procedure provides a set of electrode shapes improving both desired objectives.

Figure 16 shows the normalized power consumption corresponding to designs a,b,c,d, and e of Figure 15. The curves with higher slope correspond to better focalization designs. We observe that the power consumptions of designs with better focalization are higher than those of designs with worse focalization.

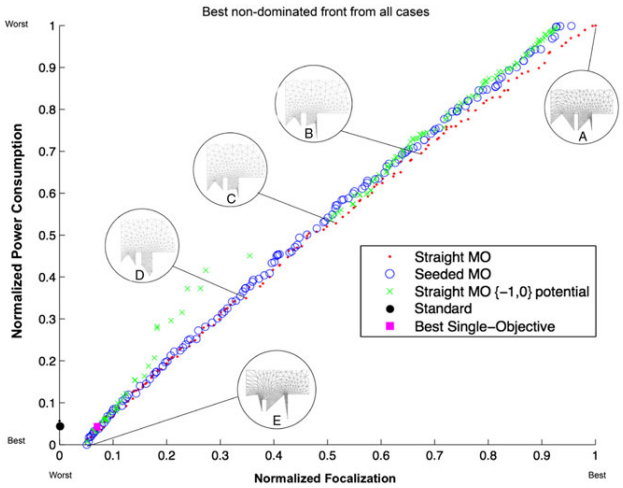

FIGURE 15 Best nondominated fronts of tested EAs. The red dots belong to straight MO, the blue circles belong to seeded MO and the green x-marks correspond to straight MO fixing the potential of the outer ring to −1 or 0 V. The black dot belongs to the standard electrode and the pink square to the best single-objective individual achieved by the first phase of seeded MO

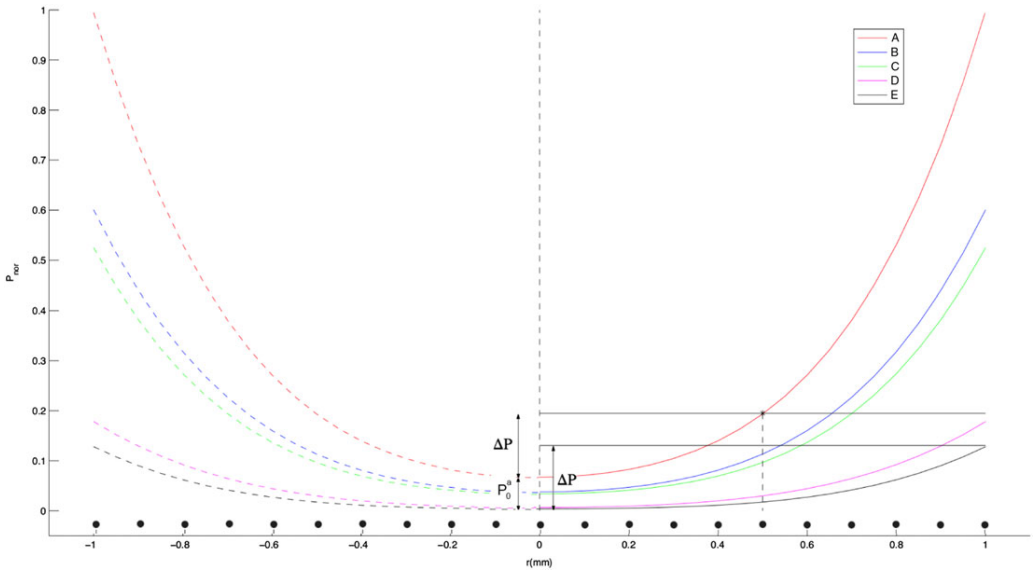

FIGURE 16 Graphics of power consumption of designs A, B, C, D, and E of Figure 15. The red curve represents the design (A) of maximum focalization and consumption. The black curve represents the design (E) of minimum focalization and consumption

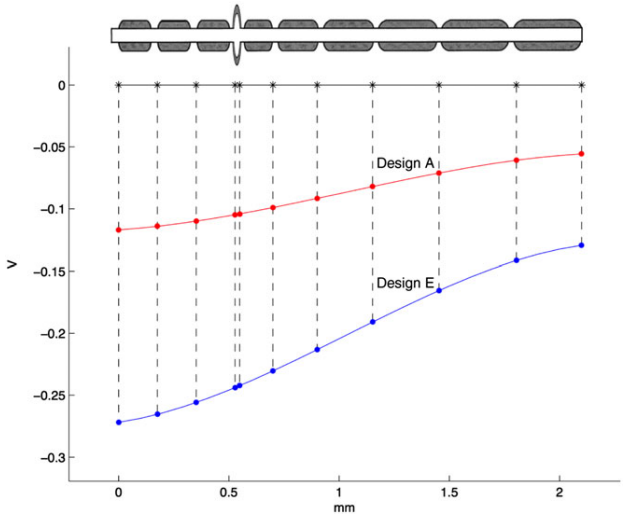

FIGURE 17 Potential along the neuron v_{10} for nonstimulated neuron (red) and activated neuron (blue) corresponding to the designs (A) and (E) of Figure 15

TABLE 2 Genes best cases a, b, c, d and e[a]

Genes	a	b	c	d	e
1 (mm)	−0.00	0.10	−0.04	−0.07	0.09
2 (mm)	0.03	−0.00	0.03	−0.00	0.03
3 (mm)	0.07	0.09	0.07	0.10	0.10
4 (mm)	0.01	0.02	0.01	0.03	−0.02
5 (mm)	−0.00	−0.00	−0.00	−0.00	−0.03
6 (mm)	0.03	0.02	0.03	0.00	−0.02
7 (mm)	0.03	−0.03	0.02	0.03	0.02
8 (mm)	0.03	−0.08	0.02	−0.05	0.098
9 (mm)	−0.08	0.02	−0.05	−0.08	−0.05
10 (V)	−0.01	−0.12	−0.15	−0.93	−0.97

[a]The genes 1 to 9 are related with the electrode shape and gene 10 with the outer ring potential.

As it can be observed in Figure 16, an increase of power of ΔP over P_0^e (the threshold power needed to excite the neuron v_0 in the design E) is able to excite the neuron v_{10} in the design (E) (black curve). The same increase of power over P_0^a (the threshold power to excite v_0 in the design A) only is able to excite the neurons from v_0 to v_5 in the design (A) (red curve). To understand why different designs need different increment of power to excite a given neuron, the potential distribution along neuron v_{10} for designs (A) and (E) were analyzed. The blue curve of Figure 17 shows the potential along neuron v_{10} when the power ΔP (as shown in Figure 16) needed to excite this neuron with the electrode of design (E) is applied. In addition, the red curve shows the potential along the same neuron when the power $P_0^a + \Delta P$ is applied, with the electrode of design (A). It was observed that the increments of potential between successive Ranvier nodes in the red curve are lower than the ones in the blue curve. The better focalization of design (A) is the reason by which this design does not excite the neuron v_{10}.

Table 2 shows the genes of the above-mentioned selected design cases, while Table 3 shows their fitness functions values and Table 4 shows their outer ring electrical potential (the inner is always at −1 V).

When considering the 2 performed approaches (seeded MO and straight MO), a total of 40 800 electrodes were designed and evaluated. A total of 200 electrode of them were finally selected (100 for each EA paradigm) to be sorted by focalization and power consumption. The best focalizing electrode shown on Figure 15 consumes 5 times more than the best power saving electrode. We have to take into account that on a CI system, the stimulation consumption is a subset of the total consumption and it takes around the 5% to 10% of the total power consumption, so this increase is affordable. In a case, in a multiobjective optimization, we can choose the desired power consumption and we get the best focalizing behavior or viceversa.

TABLE 3 Fitness functions values

Case	Focalization value	Power value
a	1.0000	1.0000
b	0.6784	0.6986
c	0.5091	0.5184
d	0.3445	0.3521
e	0.0510	0.0000

TABLE 4 Electrical potential of the outer electrode[a]

Case	Outer ring potential, V
a	−0.00889
b	−0.12001
c	−0.15104
d	−0.93785
e	−0.96791

[a]The inner ring potential is at -1V. The reference electrode is at 0 V.

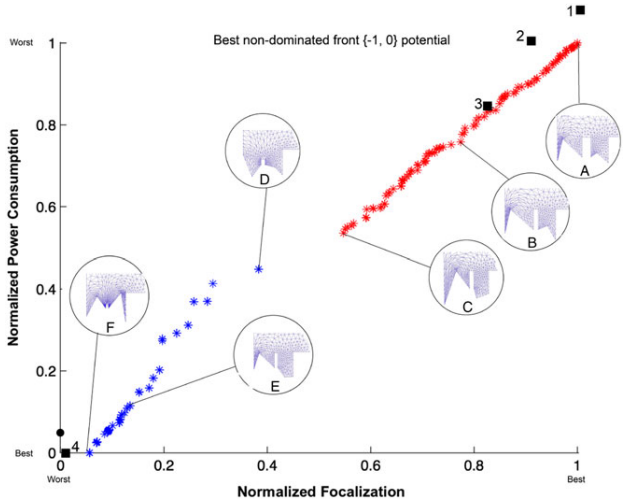

FIGURE 18 Multiobjective nondominated front keeping the potential of the outer ring in values of −1 V (blue) or 0V (red). The black squares indicates four simplified shape designs, detailed in Figure 19

As it can be observed in Table 4, designs belonging to the nondominated front have decreasing values of outer potential from right to left (or up to down) in Figure 15. Higher electrode focalization and consumption values correlated with higher values of outer ring potentials. So it must be studied the influence of the shape of the electrode on focalization and consumption. To determine that influence, we constrain the outer electrode potential values to 0 or −1 V, will leave more protagonism to shape parameters. Moreover, this constraint keeps the same electronics inside the current devices and the only variability depends on the set of the outer ring: to ground (0 V) or source (−1 V), without increasing the number of power sources or any other component. It must be remarked that the reference electrode is always set at 0 V.

We performed 4 executions of this new optimization design problem, with same optimization parameters as defined in second starting paragraph of Section 4. Figure 18 shows the nondominated solutions, where red dots correspond to optimum 0 V designs and blue dots to optimum −1 V designs. Although designs are mostly dominated by the general problem solutions (see Figures 13 and 15), they are close and still maintain the domination zone over the standard electrode.

To facilitate the manufacture of the electrode, we have analyzed 4 geometrically simplified designs. The designs 1, 2, and 3 in Figure 19 are inspired on the best focalization optimal design of Figure 18A. In this case, the inner ring potential

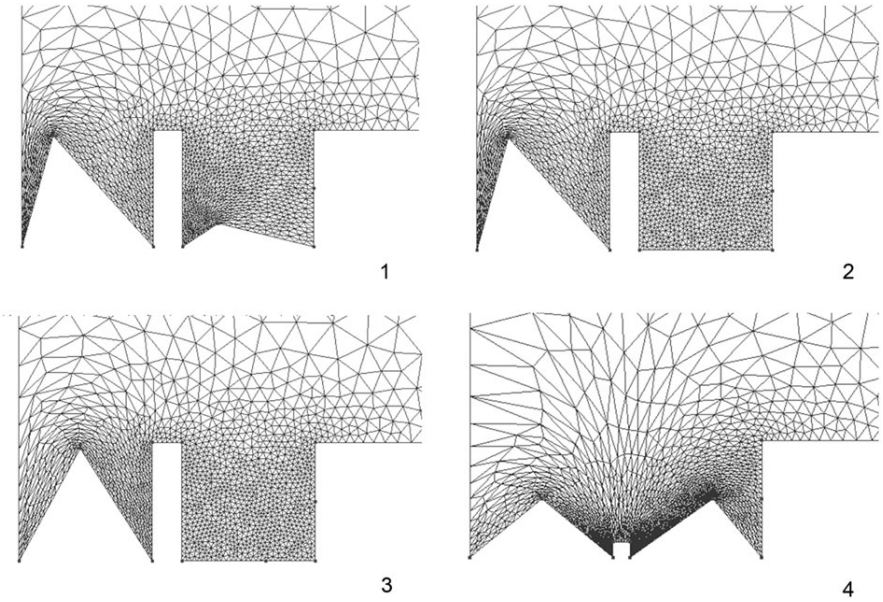

FIGURE 19 Four simplified designs. In cases 1, 2 and 3, the inner ring potential is −1 V and the outer ring potential is 0 V. In case 4, both rings potential are −1 V

is −1 V and the outer ring is 0 V. The design 4 is inspired on the lower power consumption design of Figure 18F, where the the inner and outer potential are −1 V. We can see on Figure 18 how the simplified geometric designs are dominated by the original designs, but we still have good performances (black squares); remarkably, point 4 still dominates the standard electrode. In all cases, the final results were reevaluated with higher detailed meshes (shown on Figure 19) to verify that the results are due to the geometry and not because of the element size mesh.

The methodology presented in this work is general and is prepared to include manufacturing or other type of constraints during the optimization, in terms of, eg, maximum or minimum angles of corners, ie, to attend electrochemical safety and electrode corrosion and other manufacture constraints with a penalty function or other techniques (see, eg, Coello[43]).

5 | PRACTICAL REPERCUSSIONS OF THE IMPROVEMENT OF THE ELECTRODE DESIGN

In terms of hearing quality improvement, the number of electrodes that could be added keeping the same electrode array length (22 mm), without an increase channel interaction, is a key factor (the higher the better). We calculated the number of extra electrodes in three representative nondominated designs: the same power consumption optimum design than the standard electrode, the best focalizing electrode, and the best power saving electrode. Two approaches, lowest and full interaction channel, were used to calculate the increment of number of electrodes by keeping the array length. In the first approach, we consider that only the neuron sited in the centre of 2 electrodes is excited by both electrodes. In the second approach, we admit that all the neurones placed between 2 adjacent electrodes are excited by both electrodes.

Let us consider the standard electrode placed at $r = 0$ and let $\Delta P^{std}(r) = P^{std}(r) - P^{std}(0)$ be the increment of power (over the threshold $P^{std}(0)$) to excite the neuron placed at distance r. If δ is the distance between 2 adjacent electrodes then the required power to excite the neuron in the middle of the 2 electrodes is $P^{std}(\delta/2)$, and the power to excite the farthest neuron is $P^{std}(\delta)$. Now, let us consider the i-th design electrode. We are interested in calculating the distances $\delta^i_m/2$ and δ^i_f corresponding to the excitation of middle and farthest neurons, when we increase the power in $\Delta P^{std}(\delta/2)$ and $\Delta P^{std}(\delta)$ over the threshold power $P^i(0)$, see Figures 20 and 21, respectively. That is, we have to solve the equations

$$P^i(\delta^i_m/2) = P^i(0) + \Delta P^{std}(\delta/2), \tag{21}$$

and

$$P^i(\delta^i_f) = P^i(0) + \Delta P^{std}(\delta), \tag{22}$$

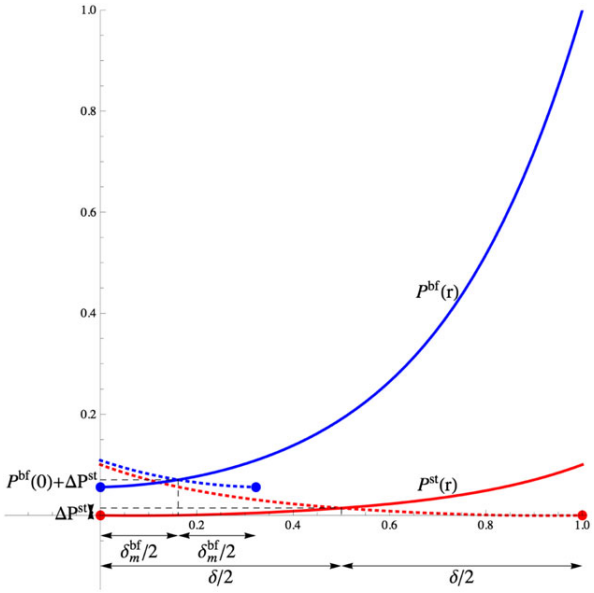

FIGURE 20 Calculation of the distance between electrodes for the lowest interaction case. In red, the channel interaction of the standard electrode; in blue, the best focalization electrode

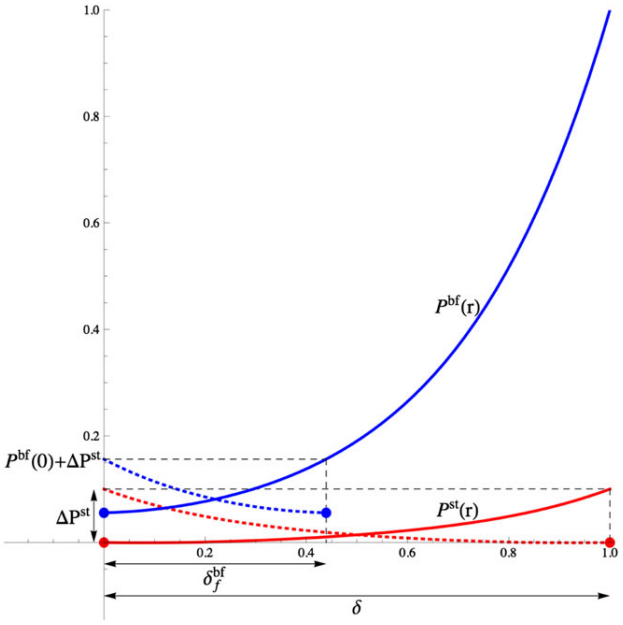

FIGURE 21 Calculation of the distance between electrodes for the full interaction case. In red, the channel interaction of the standard electrode; in blue, the best focalization electrode

TABLE 5 Increment of the number of electrodes with respect to the standard array of 22 mm length and 22 electrodes

Nondominated design	Lowest interaction	Full interaction
Best focalization	46	28
Lowest power consumption	1	1
Same power as standard	3	3

for δ_m^i and δ_f^i. These values are the distances between adjacent electrodes for each approach. They can be calculated by using a numerical procedure.

The computation of these distances allow us to calculate the number of extra electrodes that can be located in a standard array of 22 mm length. Table 5 shows these data for 3 representative designs extracted from results of Section 4. The usual number of standard electrodes in this array is 22.

6 | CONCLUSIONS

We have developed a procedure to optimize the electrode design of a cochlear implant. This procedure aims to maximize the focalization (related with increasing hearing quality when being able to increase the number of electrodes) and to save power consumption (related to increasing the battery duration).

If we analyse the nondominated results, we observe that for the best focalization designs we have a high potential difference between concentric electrodes and a great barrier. The effect of the barrier is to avoid a straight current between the rings. On the other hand, the best power saving design has a very low potential difference and the dielectric barrier has a smaller effect because the electrode works more like a monopolar stimulation mode.

The nondominated proposed designs based on a multiobjective optimization with EAs let us to improve the standard electrode in all the scenarios. Based on lowest channel interaction approach, the lowest power consumption case gives us the opportunity to include one extra electrode in a standard electrode array while reducing the power consumption in approximately 5.6%. The nondominated design with the same consumption that the standard electrode allow us to include 3 extra intracochlear electrodes. We could include 46 extra electrodes for the case of best focalization with the same spread of excitation, although in this estimation we have not taken into account the physical constraints due to the electrode size. Increasing the number of intracochlear electrodes could improve frequencial resolution and in consequence the hearing quality.

Considering that power consumption of the stimulation represents only a small percentage (about 15%) of the total consumption of CIs, even the most wasting electrode here considered (5 times more than standard electrode) could be admissible for CIs, as the total power consumption would be increased around 60%.

Moreover, we have studied simplified designs both in terms of voltage and shape achieving electrodes easy to build and keeping the current electronics without a considerable detriment in global performance.

A future step is to develop a more realistic model to take into account the anatomy of the inner ear and full electrode array. Also, an experimental research have to be done to confirm our results. Other applications of this procedure may include the design of electrode for other neural prosthesis.

ACKNOWLEDGEMENTS

This work has been supported by Spanish Government, "Secretaría de Estado de Universidades e Investigación,""Ministerio de Economía y Competitividad," and FEDER, grant contract: CTM2014-55014-C3-1-R, the first author is a beneficiary of the Predoctoral Training Program for researchers of ULPGC.

ORCID

Ángel Ramos-de-Miguel http://orcid.org/0000-0002-0528-815X

REFERENCES

1. Clark GM, Tong Y, Black R, Forster I, Patrick J, Dewhurst D. A multiple electrode cochlear implant. *J Laryngol Otol*. 1977;91(11):935-945.
2. Greenwood DD. A cochlear frequency-position function for several species–29 years later. *J Acoust Soc Am*. 1990;87(6):2592-2605.
3. Kalkman RK, Briaire JJ, Dekker DM, Frijns JH. Place pitch versus electrode location in a realistic computational model of the implanted human cochlea. *Hear Res*. 2014;315:10-4.
4. Holmes AE, Kemker EJ, Merwin GE. The effects of varying the number of cochlear implant electrodes on speech perception. *Otol Neurotol*. 1987;8(3):240-246.
5. Dorman M, Dankowski K, McCandless G, Smith L. Consonant recognition as a function of the number of channels of stimulation by patients who use the symbion cochlear implant. *Ear Hear*. 1989;10(5):288-291.

6. Fishman KE, Shannon RV, Slattery WH. Speech recognition as a function of the number of electrodes used in the speak cochlear implant speech processor. *J Speech Lang Hear Res*. 1997;40(5):1201-1215.
7. Friesen LM, Shannon RV, Baskent D, Wang X. Speech recognition in noise as a function of the number of spectral channels: comparison of acoustic hearing and cochlear implants. *J Acoust Soc Am*. 2001;110(2):1150-1163.
8. Noble JH, Labadie RF, Gifford RH, Dawant BM. Image-guidance enables new methods for customizing cochlear implant stimulation strategies. *IEEE Trans Neural Syst Rehabil Eng*. 2013;21(5):820-829.
9. Tyler RS, Abbas P, Tye-Murray N, et al. Evaluation of five different cochlear implant designs: audiologic assessment and predictors of performance. *Laryngoscope*. 1988;98(10):1100-1106.
10. Frijns J, De Snoo S, Schoonhoven R. Potential distributions and neural excitation patterns in a rotationally symmetric model of the electrically stimulated cochlea. *Hear Res*. 1995;87(1):170-186.
11. Van den Honert C, Stypulkowski P. Single fiber mapping of spatial excitation patterns in the electrically stimulated auditory nerve. *Hear res*. 1987;29(2):195-206.
12. Mens LH, Berenstein CK. Speech perception with mono-and quadrupolar electrode configurations: a crossover study. *Otol Neurotol*. 2005;26(5):957-964.
13. Joucla S, Glière A, Yvert B. Current approaches to model extracellular electrical neural microstimulation. *Front Comput Neurosci*. 2014;8:13.
14. McNeal DR. Analysis of a model for excitation of myelinated nerve. *IEEE Trans Biomed Eng*. 1976;23(4):329-337.
15. Rattay F. Analysis of models for external stimulation of axons. *IEEE Trans Biomed Eng*. 1986;33(10):974-977.
16. Rubinstein JT. Analytical theory for extracellular electrical stimulation of nerve with focal electrodes. ii. passive myelinated axon. *Biom J*. 1991;60(3):538-555.
17. Briaire JJ, Frijns JH. Field patterns in a 3D tapered spiral model of the electrically stimulated cochlea. *Hear res*. 2000;148(1):18-30.
18. Malherbe T, Hanekom T, Hanekom J. Constructing a three-dimensional electrical model of a living cochlear implant user's cochlea. *Int J Numer Methods Biomed Eng*. 2015;32(7):e02751. https://doi.org/10.1002/cnm.2751
19. Coello CAC, Lamont GB, Van Veldhuizen DA, et al. *Evolutionary Algorithms for Solving Multi-objective Problems*, Vol. 5. New York: Springer; 2007.
20. Greiner D, Galván B, Periaux J, Gauger N, Giannakoglou K, Winter G. *Advances in Evolutionary and Deterministic Methods for Design, Optimization and Control in Engineering and Sciences*. Switzerland: Springer; 2015.
21. Deb K, Bandaru S, Greiner D, Gaspar-Cunha A, Tutum CC. An integrated approach to automated innovization for discovering useful design principles: case studies from engineering. *Appl Soft Comput*. 2014;15:42-56.
22. Choi CTM, Lai WD, Chen YB. Optimization of cochlear implant electrode array using genetic algorithms and computational neuroscience models. *IEEE Trans Magn*. 2004;40(2):639-642.
23. Choi CTM, Lee SS. A new flat interface nerve electrode design scheme based on finite element method, genetic algorithm and computational neuroscience method. *IEEE Trans Magn*. 2006;42(4):1119-1122.
24. Deb K. *Multi-objective Optimization Using Evolutionary Algorithms*. New York: Wiley; 2001.
25. Deb K, Pratap A, Agarwal S, Meyarivan T. A fast and elitist multiobjective genetic algorithm: Nsga-ii. *IEEE Trans Evol Comput*. 2002;6(2):182-197.
26. Carnevale NT, Hines ML. *The NEURON Book*. Cambridge: Cambridge University Press; 2006.
27. Bossetti CA, Birdno MJ, Grill WM. Analysis of the quasi-static approximation for calculating potentials generated by neural stimulation. *J Neural Eng*. 2007;5(1):44.
28. Escobar JM, Rodrıguez E, Montenegro R, Montero G, González-Yuste J. Simultaneous untangling and smoothing of tetrahedral meshes. *Comput Meth Appl Mech Eng*. 2003;192(25):2775-2787.
29. Knupp PM. Algebraic mesh quality metrics. *SIAM J Sci Comput*. 2011;23(1):193-218.
30. Escobar JM, Montero G, Montenegro R, Rodríguez E. An algebraic method for smoothing surface triangulations on a local parametric space. *Int J Numer Methods Eng*. 2006;66(4):740-760.
31. Dennis Jr JE, Schnabel RB. *Numerical Methods for Unconstrained Optimization and Nonlinear Equations*. Philadelphia: SIAM; 1996.
32. Ruiz-Gironés E, Roca X, Sarrate J. Optimizing mesh distortion by hierarchical iteration relocation of the nodes on the cad entities. *Procedia Eng*. 2014;82:101-113.
33. Rosset A, Spadola L, Ratib O. Osirix: An open-source software for navigating in multidimensional dicom images. *J Digit Imaging*. 2004;17(3):205-16.
34. Xu J, Xu SA, Cohen LT, Clark GM. Cochlear view: postoperative radiography for cochlear implantation. *Otol Neurotol*. 2000;21(1):49-56.
35. Agrawal RB, Deb K, Agrawal R. Simulated binary crossover for continuous search space. *Complex Syst*. 1995;9(2):115-148.
36. Michalewicz Z. Gas: What are they? *Genetic algorithms+ data structures= evolution programs*. Berlin: Springer; 1994:13-30.
37. Elsayed SM, Sarker RA, Essam DL. A comparative study of different variants of genetic algorithms for constrained optimization. In: *Asia-pacific Conference on Simulated Evolution and Learning*. Springer; 2010:177-186.
38. Elsayed SM, Sarker RA, Essam DL, Hamza NM. Testing united multi-operator evolutionary algorithms on the CEC2014 real-parameter numerical optimization. In: *2014 IEEE Congress on Evolutionary Computation (CEC). IEEE*; 2014:1650-1657.
39. Lee D, Gonzalez LF, Periaux J, Srinivas K. Efficient hybrid-game strategies coupled to evolutionary algorithms for robust multidisciplinary design optimization in aerospace engineering. *IEEE Trans Evol Comput*. 2011;15(2):133-150.

40. Greiner D, Galván B, Aznárez JJ, Maeso O, Winter G. Robust design of noise attenuation barriers with evolutionary multiobjective algorithms and the boundary element method. In: Ehrgott M, Fonseca CM, Gandibleux X, Hao JK, Sevaux M, eds. *Evolutionary Multi-Criterion Optimization. EMO 2009. Lecture Notes in Computer Science*, Vol. 5467. Berlin, Heidelberg: Springer; 2009:261-274.
41. Toledo R, Aznárez J, Greiner D, Maeso O. A methodology for the multi-objective shape optimization of thin noise barriers. *Appl Math Model*. 2017;50:656-675.
42. Zitzler E, Thiele L. Multiobjective optimization using evolutionary algorithms—a comparative case study. In: *International Conference on Parallel Problem Solving from Nature*. Berlin: Springer; 1998:292-301.
43. Coello CC. Theoretical and numerical constraint-handling techniques used with evolutionary algorithms: a survey of the state of the art. *Comput Meth Appl Mech Eng*. 2002;191:1245-1287.

How to cite this article: Ramos-de-Miguel Á, Escobar JM, Greiner D, Ramos-Macías Á. A multiobjective optimization procedure for the electrode design of cochlear implants. *Int J Numer Meth Biomed Engng*. 2018;e2992. https://doi.org/10.1002/cnm.2992

Chapter 5

Conclusions and future research

5.1 Conclusions

Between the two types of electrode arrays, perimodiolar and lateral electrode arrays, the characteristics of the perimodiolar electrodes offers better performance in electrode discrimination, lower NRT threshold and lower T level. These better performances have a positive impact on sound quality, speech discrimination, battery life and quality of life.

Another factor that improves the electrode discrimination is to keep a constant distance of the electrodes respect to the modiolar wall. The new slim modiolar CI532 has a better electrode discrimination compared to previous perimodiolar electrodes due to the better positioning of the electrodes.

We have devised a new type of electrode formed by two conductive rings separated by a dielectric material. Also, we have developed a procedure to optimize the shape of the proposed electrode in terms of focalization and consumption, allowing the inclusion of more electrodes with the same spread of excitation. Increasing the number of intracochlear electrodes could improve frequencies resolution and in consequence the hearing quality.

5.2 Future Research

- Realistic simulation: Applying the procedure developed in 4.3, we plan to create a more realistic 3D model to take into account the anatomy of the inner ear. The aim of this simulation is to analyze if what extent the results obtained in 4.3 can be extrapolated to more realistic models.

  - Electrode design expanded to other prosthesis: The technics developed for cochlear implants can be transferred to other type of prosthesis where the focalization plays

also an important role. For example, in retina prosthesis the focalization is mandatory to obtain better resolution.

- Post-surgical evaluation imaging and surface reconstruction:
  - 2D imaging analysis: The most common imaging measurements to evaluate the cochlear implantation are: the deep of insertion and the wrapping factor. In this thesis we proposed the use of new metrics like the "intracochlear position index" and the "homogeneity factor" with good results. Currently, all this measurements are in validation in temporal bone. We plan to implement a system to automatically identify the cochlea and score the cochlear implantation with the new presented metrics.
  - 3D volume analysis: The objective is to automatically generate a mesh of the inner ear including the inner structures with a regular computer tomography as input data. This mesh will be useful to do anatomical measurements and to evaluate the position of an electrode array inside the cochlea.

Bibliography

[1] Arts, R. A., George, E. L., Stokroos, R. J., and Vermeire, K. cochlear implants as a treatment of tinnitus in single-sided deafness. *Current opinion in otolaryngology & head and neck surgery 20*, 5 (2012), 398–403.

[2] Bear, M. F., Connors, B. W., and Paradiso, M. A. *Neuroscience, volume 2*. Lippincott Williams & Wilkins, 2007.

[3] Burian, K. Significance of cochlear nerve electric stimulation in totally deaf patients. *Laryngologie, Rhinologie, Otologie 54*, 6 (1975), 530.

[4] Busby, P., Whitford, L., Blamey, P. J., Richardson, L., and Clark, G. M. Pitch perception for different modes of stimulation using the cochlear multiple-electrode prosthesis. *The Journal of the Acoustical Society of America 95*, 5 (1994), 2658–2669.

[5] Békésy, G. V. *Experiments in hearing*. New York: McGraw-Hill, 2006.

[6] Chittka, L., and Brockmann, A. Perception space—the final frontier. *PLoS biology 3*, 4 (2005), e137.

[7] Clark, G. Cochlear implants. In *Speech processing in the auditory system*. Springer, 2004, pp. 422–462.

[8] Clark, G. M., Tong, Y., Black, R., Forster, I., Patrick, J., and Dewhurst, D. A multiple electrode cochlear implant. *The Journal of Laryngology & Otology 91*, 11 (1977), 935–945.

[9] Coello, C. A. C., Lamont, G. B., Van Veldhuizen, D. A., et al. *Evolutionary algorithms for solving multi-objective problems*, vol. 5. Springer, 2007.

[10] Cohen, L. T., Richardson, L. M., Saunders, E., and Cowan, R. S. Spatial spread of neural excitation in cochlear implant recipients: comparison of improved ecap method and psychophysical forward masking. *Hearing research 179*, 1-2 (2003), 72–87.

[11] Dang, K. *Electrical conduction models for cochlear implant stimulation.* PhD thesis, Université Côte d'Azur, 2017.

[12] Deb, K., Bandaru, S., Greiner, D., Gaspar-Cunha, A., and Tutum, C. C. An integrated approach to automated innovization for discovering useful design principles: Case studies from engineering. *Applied Soft Computing 15* (2014), 42–56.

[13] Deb, K., Pratap, A., Agarwal, S., and Meyarivan, T. A fast and elitist multiobjective genetic algorithm: Nsga-ii. *IEEE transactions on evolutionary computation 6*, 2 (2002), 182–197.

[14] Dorman, M., Dankowski, K., McCandless, G., and Smith, L. Consonant recognition as a function of the number of channels of stimulation by patients who use the symbion cochlear implant. *Ear and hearing 10*, 5 (1989), 288–291.

[15] Dynes, S. B., and Delgutte, B. Phase-locking of auditory nerve discharges to sinusoidal electric stimulation of the cochlea. *Hearing research 58* (1992), 79–90.

[16] Emer, G. M. C. L. P., et al. Personal reflections on the multichannel cochlear implant and a view of the future. *Journal of rehabilitation research and development 45*, 5 (2008), 651.

[17] Escobar, J. M., Montero, G., Montenegro, R., and Rodríguez, E. An algebraic method for smoothing surface triangulations on a local parametric space. *International Journal for Numerical Methods in Engineering 66*, 4 (2006), 740–760.

[18] Escobar, J. M., Rodriguez, E., Montenegro, R., Montero, G., and González-Yuste, J. Simultaneous untangling and smoothing of tetrahedral meshes. *Computer Methods in Applied Mechanics and Engineering 192*, 25 (2003), 2775–2787.

[19] Escude, B., James, C., Deguine, O., Cochard, N., Eter, E., and Fraysse, B. The size of the cochlea and predictions of insertion depth angles for cochlear implant electrodes. *Audiology and Neurotology 11* (2006), 27–33.

[20] Eshraghi, A. A., Nazarian, R., Telischi, F. F., Rajguru, S. M., Truy, E., and Gupta, C. The cochlear implant: historical aspects and future prospects. *The Anatomical Record 295*, 11 (2012), 1967–1980.

[21] Fishman, K. E., Shannon, R. V., and Slattery, W. H. Speech recognition as a function of the number of electrodes used in the speak cochlear implant speech processor. *Journal of Speech, Language, and Hearing Research 40*, 5 (1997), 1201–1215.

[22] Friesen, L. M., Shannon, R. V., Baskent, D., and Wang, X. Speech recognition in noise as a function of the number of spectral channels: comparison of acoustic hearing and cochlear implants. *The Journal of the Acoustical Society of America 110*, 2 (2001), 1150–1163.

[23] Gilroy, A. M., R.MacPherson, B., and Ross, L. M. *Atlas of anatomy.* New York: Thieme, 2008.

[24] Greenwood, D. D. A cochlear frequency-position function for several species—29 years later. *The Journal of the Acoustical Society of America 87*, 6 (1990), 2592–2605.

[25] Greiner, D., Galván, B., Aznárez, J. J., Maeso, O., and Winter, G. Robust design of noise attenuation barriers with evolutionary multiobjective algorithms and the boundary element method. In *In: Ehrgott M., Fonseca C.M., Gandibleux X., Hao JK., Sevaux M. (eds) Evolutionary Multi-Criterion Optimization. EMO 2009. Lecture Notes in Computer Science* (2009), vol. 5467, Springer, Berlin, Heidelberg, pp. 261–274.

[26] Greiner, D., Galván, B., Periaux, J., Gauger, N., Giannakoglou, K., and Winter, G. *Advances in Evolutionary and Deterministic Methods for Design, Optimization and Control in Engineering and Sciences.* Springer, 2015.

[27] Henry, P. J., Rice, and Blayneyb, A. Vibro-acoustic modelling of the outer and middle ear using the finite-element method. *Audiology & Neurotology 4* (1999), 3–4.

[28] Holmes, A. E., Kemker, E. J., and Merwin, G. E. The effects of varying the number of cochlear implant electrodes on speech perception. *Otology & Neurotology 8*, 3 (1987), 240–246.

[29] House, W. F., and Urban, J. Long term results of electrode implantation and electronic stimulation of the cochlea in man. *Annals of Otology, Rhinology & Laryngology 82*, 4 (1973), 504–517.

[30] Johnson, D. H. The relationship between spike rate and synchrony in re- sponses of auditory-nerve ibers to single tones. *The Journal of the Acoustical Society of America 68* (1980), 1115–1122.

[31] Kalkman, R. K., Briaire, J. J., Dekker, D. M., and Frijns, J. H. Place pitch versus electrode location in a realistic computational model of the implanted human cochlea. *Hearing research 315* (2014), 10–24.

[32] Littler, T. S. *The Physics of the Ear: International Series of Monographs on Physics (Vol. 3).* Elsevier, 2013.

[33] Macias, A. R., Zaballos, M. T. P., de Miguel, A. R., and Paz, J. C. Importance of perimodiolar electrode position for psychoacoustic discrimination in cochlear implantation. *Otology & Neurotology 38*, 10 (2017), e429–e437.

[34] Martini, F. H., Timmons, M. J., and Tallitsch, R. B. *Human Anatomy*. Pearson, Ed. New York: Pearson Higher ed USA, 2008.

[35] Noble, J. H., Labadie, R. F., Gifford, R. H., and Dawant, B. M. Image-guidance enables new methods for customizing cochlear implant stimulation strategies. *IEEE Transactions on Neural Systems and Rehabilitation Engineering 21*, 5 (2013), 820–829.

[36] Palmers, A., and Russell, I. Phase-locking in the cochlear nerve of the guinea-pig and its relation to the receptor potential of inner hair-cells. *Hearing research 24* (1986), 1–15.

[37] Ramos, Á., Polo, R., Masgoret, E., Artiles, O., Lisner, I., Zaballos, M. L., Moreno, C., and Osorio, Á. Cochlear implant in patients with sudden unilateral sensorineural hearing loss and associated tinnitus. *Acta Otorrinolaringologica (English Edition) 63*, 1 (2012), 15–20.

[38] Ramos de Miguel, Á., Argudo, A. A., Barreiro, S. A. B., González, J. C. F., and Macías, A. R. Imaging evaluation of electrode placement and effect on electrode discrimination on different cochlear implant electrode arrays. *European Archives of Oto-Rhino-Laryngology* (2018), 1–10.

[39] Ramos-de Miguel, Á., Escobar, J. M., Greiner, D., and Ramos-Macías, Á. A multiobjective optimization procedure for the electrode design of cochlear implants. *International journal for numerical methods in biomedical engineering* (2018).

[40] Reichenbach, T., and Hudspeth, A. J. The physics of hearing: fluid mechanics and the active process of the inner ear. *Reports on Progress in Physics 77* (2014).

[41] Stakhovskaya, O., Sridhar, D., Bonham, B. H., and Leake, P. A. The physics of hearing: fluid mechanics and the active process of the inner ear. *Journal for the Association for Research in Otolaryngology 8* (2007), 220.

[42] Toledo, R., Aznárez, J., Greiner, D., and Maeso, O. A methodology for the multi-objective shape optimization of thin noise barriers. *Applied Mathematical Modelling 50* (2017), 656–675.

[43] Tyler, R. S., Abbas, P., Tye-Murray, N., Gantz, B. J., Knutson, J. F., Mccabe, B. F., Lansing, C., Brown, C., Woodworth, G., Hinrichs, J., et al. Evaluation of five different cochlear implant designs: audiologic assessment and predictors of performance. *The Laryngoscope 98*, 10 (1988), 1100–1106.

[44] Wardrop, P., Whinney, D., Rebscher, S. J., Roland Jr, J. T., Luxford, W., and Leake, P. A. A temporal bone study of insertion trauma and intracochlear position of cochlear implant electrodes. i: Comparison of nucleus banded and nucleus contour^{TM} electrodes. *Hearing research 203*, 1-2 (2005), 54–67.

[45] Wright, C. G. UT Southwestern Medical Center, Dallas.

[46] Zwolan, T. A., Kileny, P. R., Ashbaugh, C., and Telian, S. A. Patient performance with the cochlear corporation" 20+ 2" implant: bipolar versus monopolar activation. *The American journal of otology 17*, 5 (1996), 717–723.


ULPGC
UNIVERSIDAD DE LAS PALMAS
DE GRAN CANARIA